REPORT DOCUMENTATION PAGE

Form Approved
OMB No. 0704-0188

1. AGENCY USE ONLY (Leave blank)	2. REPORT DATE	3. REPORT TYPE AND DATES COVERED
	96JAN30	Final Report 92SEP1 - 95NOV30

4. TITLE AND SUBTITLE
Photorefractive Inorganic/Organic Materials Prepared by a Novel Sol-Gel Process

5. FUNDING NUMBERS
F49620-92-C-0061

6. AUTHOR(S)
Ryszard Burzynski and Martin Casstevens

7. PERFORMING ORGANIZATION NAME(S) AND ADDRESS(ES)
Laser Photonics Technology, Inc.
1576 Sweet Home Rd
Amherst, NY 14228

8. PERFORMING ORGANIZATION REPORT NUMBER
P2B-FINAL
AFOSR-TR-96-0057

9. SPONSORING/MONITORING AGENCY NAME(S) AND ADDRESS(ES)
USAF, AFMC
Air Force Office of Scientific Research
110 Duncan Avenue, Suite B115
Bolling AFB, DC 20332-0001

10. SPONSORING/MONITORING AGENCY REPORT NUMBER

11. SUPPLEMENTARY NOTES

12a. DISTRIBUTION/AVAILABILITY STATEMENT

DISTRIBUTION STATEMENT A
Approved for public release;
Distribution Unlimited

TRIBUTION CODE

13. ABSTRACT *(Maximum 200 words)*

Photorefractive materials represent an important new class of materials with the potential to (1) reversibly and holographically store digital or analog information and (2) process information in an optical format. A number of polymeric composites have been developed and evaluated in an effort to make materials that have tunable novel performance, are amenable to device construction, and are low cost. The program has culminated with a number of accomplishments including the demonstration of holographic image storage and retrieval, the first use of sol-gel processed ormosils as photorefractive media and the first demonstration that charge traps could be introduced to extend storage times, etc. A number of composites have been shown to be photorefractive using a two beam coupling experiment which distinguishes classical photorefractive processes from a variety of others. The materials developed in Phase II are clearly useful for several applications in information processing, but additional improvements will be necessary if they are to be used in long-term data storage. The development efforts have resulted in a wealth of information for the Defense Department and have enabled the company to solicit Phase III collaborators for continued work in the development of long-term storage materials.

14. SUBJECT TERMS	15. NUMBER OF PAGES
photorefractive, composite, sol-gel, ormosil, polymer, holographic memory phase grating, bi-functional, chromophore	89
	16. PRICE CODE

17. SECURITY CLASSIFICATION OF REPORT	18. SECURITY CLASSIFICATION OF THIS PAGE	19. SECURITY CLASSIFICATION OF ABSTRACT	20. LIMITATION OF ABSTRACT
Unclassified	Unclassified	Unclassified	

Final Report

Laser Photonics Technology, Inc.
1576 Sweet Home Rd.
Amherst, NY 14228

Principal Investigator: Dr. Ryszard Burzynski

Contract #: F49620-C-92-0061

January 30, 1996

1. EXECUTIVE SUMMARY

1.1. OBJECTIVES

Photorefractive media are an effective means in which to store and retrieve information optically. The physical properties of organic materials make them ideal candidates for practical, fast, high capacity optical data storage media. This report describes LPT's efforts to prepare multicomponent and multifunctional photorefractive materials. These materials are being developed to have high optical quality, controllable spectral response, enhanced figure of merit, and be capable of being implemented in practical photorefractive data storage systems.

Efforts throughout this contract were focused on deriving the most appropriate multifunctional photonics material for use in photorefractive optical devices such as holographic data storage. The staff of LPT optimized material processing conditions to achieve exceptional optical quality composite films as well as demonstrating their high second order nonlinear optical responses and efficient photocharge generation. The accomplishment of these goals involved extensive characterization of the composite materials by a thorough evaluation of their nonlinear optical (NLO) properties, dark conductivity and photoconductivity. This effort also encompassed the search for stable and efficient photosensitizers and charge transporting species, syntheses of inorganic/organic composites employing sol-gel processing techniques, and techniques for the preparation of thick films.

1.2. STATUS OF EFFORT:

This document describes LPT's efforts to design and fabricate photorefractive materials based on organic polymers and ormosils. A number of doped poly 9-vinylcarbazole based systems have been investigated. These heavily doped systems exhibit reasonable performance, but have a strong tendency to phase segregate; this leads to increased scattering losses in devices which have stringent requirements for optical quality. LPT has accomplished a great deal toward developing photorefractive materials which demonstrate diffraction efficiencies suitable for device applications and have been designed to have improved optical quality. The latter has been accomplished by the development of systems with an decreasing tendency to phase separate such as those containing bifunctional molecules which perform both photoconductive and nonlinear optical roles. Further work on a fully functional polymeric systems has also been performed. Finally, sol-gel based systems have just recently been developed that satisfy diffraction efficiency requirements and are also exhibit optical quality. These systems and their characterization are presented and discussed in this document. It is clear that current systems perform adequately for certain applications. However, continued efforts are still needed to improve the overall understanding of photorefractive processes in polymers as well as improve holographic grating lifetime for optical storage applications.

1.3. SUMMARY OF ACCOMPLISHMENTS:

The overall objective of the proposed research and development work of the Phase II effort was to produce optical quality composite photorefractive materials, i.e. possessing second order NLO properties, efficient photocharge generation and charge transporting capabilities. Optimization of the processing conditions was necessary to produce thick films in sandwiched

structures suitable for examination by holographic diffraction and two beam coupling methods.

LPT's Phase II efforts have resulted the following accomplishments:

- demonstration of high diffraction efficiency and two beam coupling gains in several polymeric composites;
- first demonstration of photorefractive responses in polymeric composites at wavelengths as short as 488 nm;
- first demonstration of photorefractivity in multifunctional sol-gel processed materials
- successful demonstration of photorefractive effect by CW four wave and two wave mixing experiments;
- first demonstration of intentionally introduced traps and their effect on photorefractive responses in polymeric blends;
- demonstration of holographic image writing and retrival;
- preparation and purification of three second order chromophores with large β value: (1). 4-(N,N-bis(β-dihydroxyethyl)amino)-4'-nitrostilbene (DHD), (2) 6-propionyl-2-dimethylaminonaphthalene (PRODAN), and (3) N-(4-nitrophenyl)-(L)-prolinol (NPP) and two bifunctional molecules: (1) N,N-diphenylamino nitrostyrene (DPANST) and (2) 4-(N,N-diphenylamino)-4'-nitrostilbene (DPANS) which exhibit second order NLO and charge transporting properties;
- preparation of a multifunctional polymer based on a methacrylate main chain containing charge transport and NLO properties;
- preparation of ormosils containing DHD as a second order NLO chromophore and N-(β-hydroxyethyl)carbazole (HCAR) as an efficient charge transporting group (CTM);
- successful preparation of high optical quality thick (100 to 300 μm) films consisting of $\chi^{(2)}$ chromophore/photosensitizer/organic polymer and sol-gel processed $\chi^{(2)}$/CTM ormosil material doped with the photosensitizer;
- measurements of the photocharge generation efficiency and the dependence of photoconductivity on an applied field;
- measurements of electrooptic responses on selected samples;

1.4. PERSONNEL SUPPORTED

Ryszard Burzynski, Martin Casstevens, Saswati Ghosal, Yue Zhang, John Wiebel, Dale Tyczka, Gen Xu, Christopher Spencer, Maciek Orczyk

1.5. PUBLICATIONS

The following is a list of papers published in refreed scientific journals. In addition, there were eight presentations on prestigious international conferences such as CLEO, SPIE, OSA and ACS.

1. "Multifunctional Photorefractive Polymer with Charge Transporting and Second-Order Side-chain Groups", Chenfang Zhao, Chi-Kyun Park, Paras N. Prasad, Yue Zhang, Saswati Ghosal and Ryszard Burzynski, *Chem. Mater.*, **7**, 1237, 1995.
2. "Bi-functional Chromophore for Photorefractive Applications", Yue Zhang, Christopher C. Spencer, Saswati Ghosal, Martin K. Casstevens and Ryszard Burzynski, *Appl. Phys. Lett.*, **66(3)**, 256, 1995.

3. "Photorefractive Composites with High-Band-Gap Second-Order Nonlinear Optical Chromophores," Ryszard Burzynski, Yue Zhang, Saswati Ghosal, Martin K. Casstevens, *J. Appl. Phys.*, **78**, 6903 (1995).
4. "Traps Controlled Photorefractive Responses in Polymeric Composites". Yue Zhang, Christopher A. Spencer, Saswati Ghosal, Martin K. Casstevens and Ryszard Burzynski, *Polym. Preprints*, **35(2)**, 233,1994.
5. "Photorefractive Properties of a Thiapyrylium Dye Sensitized Polymer Composite". Yue Zhang, Chris A. Spencer, Saswati Ghosal, Martin K. Casstevens and Ryszard Burzynski, *J. Appl. Phys.*, **76(2)**, 671,1994.
6. "Thiapyrylium Dye Sensitization of Photorefractivity in a Polymer Composite". Yue Zhang, Chris A. Spencer, Saswati Ghosal, Martin K. Casstevens and Ryszard Burzynski, *Appl. Phys. Lett.*, **64**, 1908, 1994.
7. "Novel Optical Composites:Second Order NLO materials and Polymeric Photorefarctive Materials For Optical Information Storage and Processing Applications", Ryszard Burzynski, Martin K. Casstevens, Yue Zhang and Saswati Ghosal, *Opt. Eng.*, February 1996, to appear.
8. "Photorefractive Polymers and Composite Materials," Yue Zhang, Ryszard Burzynski, Saswati Ghosal, and Martin K. Casstevens, invited review paper *Adv. Mat.*, February 1996, to appear.
9. "Photorefractive Composite Materials with Bi-Functional Charge Transporting Second-Order Nonlinear Optical Chromophores," Yue Zhang, Saswati Ghosal, Martin K. Casstevens, and Ryszard Burzynski, accepted for publication in *J. Appl. Phys.*

2. TECHNICAL REPORT

2.1. ORGNIZATION OF THIS REPORT

The following sections describe the work accomplished under contract No. F49620-C-92-0061. A brief introduction to optical storage techniques and a need for more advanced materials are presented in Sec. 2.3. A brief theoretical background is presented in Sec. 2.4. A comprehensive discussion of the materials used in this project is presented in Sec. 2.5. (Details of material syntheses and sample preparations are compiled in Sec. 4, Appendix A.) Characterization techniques are discussed in Sec. 2.6 and results on all photorefractive materials developed in this Phase II program are presented in Sec. 2.7. The report concludes with a final discussion and recommendations (Sec. 3).

2.3 WHY PHOTOREFRACTIVE MATERIALS?

Current optical memory storage devices (optical compact disc, CD) rely on Write Once, Read Many (**WORM**) technology. It provides reasonable optical data storage capabilities with high bit rate (BR) and high storage capacity (SC).

The limitations of current systems can be well understood in terms of simple commercial requirements. For example, commonly available CDs have BRs of about **1.5 Mbit/sec** and storage capacity of about **8.6 10^9 bits**. However, standard color TV displays with 30 frames/sec and 8 bits of red, green and blue colors each needs bit transfer rate of **150 Mbits/sec** to provide a reasonably good image. Applying an *image compression* technique which reduces the BR by approximately 200 times, this technology can give ca. 1 hr of NTSC video on CD.

Anticipated increases in display resolution place tremendous pressure on information storage technology. For example, a high definition television (HDTV) display that provides 10 hrs of video on CD at a BR of 6 Mbit/s requires 200 Gbit storage capacity. In addition to storing even more information in smaller volumes, it is highly desirable to develop rewritable optical memory technology.

There are several technologies which are being considered to meet these demands. The most promising techniques are not currently ready for implementation. These techniques and some reasons why they are not currently available are listed below.

1. Spectral hole burning - requires extremely *low temperatures*
2. Near-field optical techniques - bit rates are *low;* dust free environment is required since the stylus is positioned several nanometers from the disc surface.
3. Two-photon optical memory - *high power lasers* are required and high BRs are possible only in layered waveguide structures
4. Volume holography (angle or wavelength multiplexed) - the potential for *cross-talk* between the holograms may seriously affect storage capacity.

Volume holography technology based on a photorefractive effect provides a realistic approach to achieving the requirements outlined above and is compatible with inexpensive diode lasers. The ideal holographic media should possess the following characteristics:

2. exhibition of a large refractive index change (phase hologram is preferred to an amplitude one because of higher diffraction efficiency);
3. retention of the image long after a hologram is recorded and even after being read repeatedly;
4. reasonbly short writing times with low power diode lasers.

Polymers and polymeric composites are good candidates since they can be sensitized over a large range of wavelengths, give a large change of the refractive index per unit of writing radiation, are inexpensive, and easily processed. Subsequent sections address these issues in more detail.

2.4 THE PHOTOREFRACTIVE EFFECT

The photorefractive effect was accidentally discovered in 1966 in $LiNBO_3$ and $LiTaO_3$ as detrimental optically induced refractive index inhomogeneities.[1] It was referred to as "optical damage" because it caused a degradation of the performance of nonlinear optical devices based on these materials. Two years later, holographic optical storage has been demonstrated in $LiNbO_3$ using this newly discovered effect.[2] In 1969, Chen proposed a model based on the migration of photoexcited electrons which explained the main experimental observations and set the basis for the future experimental and theoretical work.[3] The term photorefractive, which literally means light induced change of the refractive index, was introduced later on and has since been reserved for this particular mechanism. In 1976, Kukhtarev et al. derived the dependence of the refractive index change on light intensity and material parameters and described the coupling of beams in thick photorefractive gratings.[4] Today, almost 30 years after its first discovery, photorefractivity is a blooming field of interdisciplinary research.

Over the years, several materials like $BaTiO_3$ $KnbO_3$ $Bi_4Ti_3O_{12}$, $Sr_{1-x}Ba_xNb_2O_6$ (SNB), $Ba_{2-x}Sr_xNa_yNb_5O_{12}$ (KNSBN), $Bi_{12}SiO_{20}$ (BSO), $Bi_{12}GeO_{20}$ (BGO), GaAs, InP, CdTe, $(Pb,La)(Zr,Ti)O_3$ and many other have been shown to exhibit the photorefractive effect [5,6], which makes it a quite general property of electrooptic crystals. Numerous applications in optical data storage, image processing and amplification, self and mutually pumped phase conjugation, photorefractive resonators, programmable optical interconnects, simulation of neural networks etc. have been proposed and demonstrated on a laboratory scale.[6,7] Apart from potential applications, intensive research has targeted the understanding of the microscopic origin of the photorefractive effect resulting in the discovery of new phenomena such as the bulk photovoltaic effect[8] and the excited state polarization.[9]

Today, the mechanism of photorefractivity is quite well, although not fully, understood. This led to the recent observation of photorefractivity in new classes of materials such as organic crystals,[10] polymers[11] and liquid crystals.[12] Figure 1 depicts the basic mechanisms. The photorefractive effect is observed in materials which are both electrooptic and photoconducting. If such a sample is illuminated with a nonuniform light intensity pattern resulting from the interference of two mutually coherent beams, charge generation will take place at the bright areas of the fringes. These photogenerated charges will migrate and eventually get trapped at the dark areas, a process which can take several cycles of photogeneration, diffusion and trapping. The resulting charge redistribution creates an internal electric field, the space charge field E_{sc}, which changes the refractive index via the electrooptic effect. The space charge field forces charges to drift in a direction opposite to that of diffusion. A dynamic equilibrium is

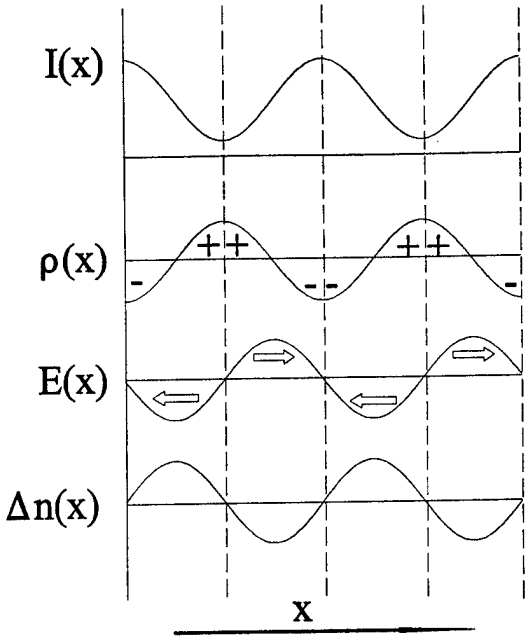

Figure 1 Photorefractive effect: formation of the space charge field and refractive index modulation.

ultimately reached when space charge filed becomes strong enough to induce a drift current of a magnitude equal and direction opposite to the diffusion current. The application of an external electric field assists charge separation through drift and generally results in a higher space charge field.

From the above description it is clear that the photorefractive effect provides a way to replicate light intensity patterns into refractive index gratings, with obvious potential applications in optical data storage. Several other mechanisms can change the refractive index upon illumination, eg., photochemical reactions, thermorefraction, formation of excited states, conventional $\chi^{(3)}$, etc.[13] The photorefractive effect, however, processes a combination of characteristics which make it unique; very high nonlinearities can be achieved even with weak laser beams as a result of the integrating nature of the effect. The resulting refractive index gratings are reversible since uniform illumination will erase the space charge field. Another very important characteristic is the existence of a spatial phase shift between the illumination pattern and the refractive index grating. This is the unique signature of the photorefractive effect; *no other mechanism can produce a phase shifted refractive index grating with respect to the space charge field pattern.* As will be discussed below, the existence of this phase shift gives rise to steady state asymmetric energy exchange between two laser beams, which is the basis for several specific applications.

In addition to being used in specific applications, the photorefractive effect provides a means to investigate material properties such as charge transport and trapping with "pure" optical techniques. Steady state and transient holographic techniques can be employed to measure small photocurrents optically, eliminating the need for sensitive electronic equipment. Moreover, the

bulk of the sample is directly probed, eliminating electrode problems. Parameters like charge diffusion lengths, mobilities, trap densities and cross sections etc. are conveniently measured in this way.[14]

2.4.1 Standard Model for Photorefractivity

The model of Kukhtarev *et al.* has been very useful in helping to understand the microscopic origin of photorefractivity in inorganic crystals. To some extent, photorefractivity in polymers can also be understood along the same lines. For this reason, a basic description of this model is presented here.

In Figure 3, the basic idea for the space charge field formation is illustrated for the case of electron transport and a single-level impurity participating in this process. Depicted are the valence (E_v) and the conduction (E_c) band, together with donor (S) and the acceptor (trap, T) impurity levels. The only role of the acceptors is to deprive some of the donors from their charge, creating an initial concentration of empty traps. Let N_s be the total donor density (in our case photocharge sensitizer molecule) and $N_s^+ = N_A$ where N_A is the density of acceptors.

If two laser beams with nonorthogonal unit polarizations, e_1 and e_2, and slowly varying electric field amplitudes, E_1 and E_2, intersect at an angle 2θ in a photorefractive material, they will create a spatially periodic intensity pattern I(x) given by:[15]

$$I(x) = I_0[1 + m\cos(k\cdot x)]e^{-\alpha x/\cos\theta} \qquad (1)$$

where $I_0 = I_1 + I_2$ is the sum of the incident laser intensities of the two intersecting beams, $m = 2E_1E_2/I_0$ is called the modulation index, $\mathbf{k} = \mathbf{k}_1 - \mathbf{k}_2$, $\mathbf{k}_1$ and $\mathbf{k}_2$ are the wave vectors of the incident beams. The amplitude $|\mathbf{k}| = 2\pi/\Lambda$ is the spatial frequency and $\Lambda = \lambda/2\sin\theta$ is the fringe spacing (see Figure 2). Attenuation is described by the absorption coefficient in Eq.(1) and can be neglected in the case of no absorption.

According to this model, the space charge field is created through the steps of photoionization of a donor in the bright areas of the fringes (step 1 in Figure 3), transport of the electron in the conduction band (step 2 in Figure 3) and subsequent trapping at an ionized donor level (step 3 in Figure 3).

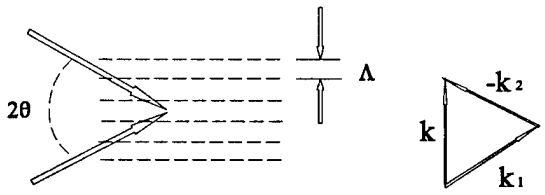

Figure 2 The interference of two beams results in periodic light intensity.

The rate of formation of ionized donors has a generation term, proportional to light intensity and the density of donors that can be ionized, plus an annihilation term proportional to the available density of electrons in the conduction band and the trap density:

$$\partial N_s^-(x)/\partial t = s_D I(x)(N_s - N_s^-(x)) - \gamma_D n(x) N_s^-(x) \qquad (2)$$

where S_D is the photogeneration rate, γ_D is the trapping rate and n is the electron density in the conduction band.

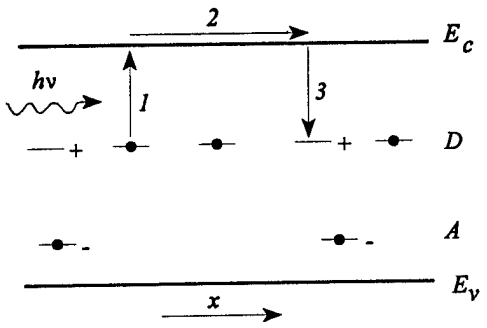

Figure 3 Band transport model for the photorefractive effect. Electrons are photoexcited (1) from donor states (D) to the conduction band (E_c), where they migrate (2), until they get trapped at ionized donor sites (3). Acceptors (A) function as charge traps.

Electrons are mobile once in the conduction band and their density changes not only due to photogeneration and trapping, but also due to transport. The continuity equation is written:

$$\partial n(x)/\partial t = \partial N_s.(x)/\partial t + \frac{1}{e}\,\partial J(x)/\partial(x) \qquad (3)$$

where e is the electron charge and J the current density, which is a result of drift and diffusion:

$$J(x) = \mu_{dr}\, e\, n(x)\, E(x) + k_B\, T\, \mu_{dr}\, \partial n(x)/\partial t \qquad (4)$$

where μ_{dr} is the electron drift mobility, E is the total electric field (space charge plus externally applied electric field), k_B is the Boltzmann constant and T the absolute temperature. The Einstein equation of diffusion has been used in equation (4).

The total electric field is calculated from Poisson's law:

$$\partial E(x)/\partial x = e\,(N_s.(x) - n(x) - N_T)/\epsilon \qquad (5)$$

where ϵ is the dc dielectric constant.

In the limit of small modulation ($m \ll 1$), the spatial variation of N_D^+, n, J and E is small and it can be represented only by the zeroth and the first harmonic in a spatial Fourier expansion. Assuming that $N_S \gg N_T \gg n$ and $S_D I \ll \gamma N_T$ which is true in the majority of photorefractive

materials, the steady state and the dynamics of the space charge field can be derived from equations (2)-(5).

In the steady state the simplex amplitude of the first Fourier component of E is:[15]

$$E^1 = E_{SC} \exp(-i\phi) = mE_s (iE_D - E_0) / (E_D + E_q + iE_0) \quad (6)$$

where E_{sc} is the space charge field, E_0 is the externally applied field, E_D is the diffusion field which is equal to:

$$E_D = k_B T K_G / e \quad (7)$$

and E_q is the saturation field, and is given as:

$$E_q = e N_T / \epsilon\epsilon_0 K_G = \frac{e N_T (N_s - N_T)}{\epsilon\epsilon_0 K_G N_s} \quad (8)$$

From equation (6) it follows that the space charge field cannot exceed mE_s, which corresponds to the limit where all the traps in the dark areas have been filled. The maximum value of the space charge field thus is set by the experimental geometry, the trap density and the dielectric constant of the material. In the absence of an external electric field, E_{SC} will be limited by the smallest of E_D and E_q (multiplied by m): Even if there are plenty of traps available, the maximum electric field that can be achieved by diffusion alone cannot exceed mE_D.

The dependence of E_{SC} on the external electric field can be understood from Figures 4 and 5, where the amplitude and the phase shift of E^1 are shown as a function of E_0 for m=0.01 and for three different values of the of the saturation field, which correspond to trap densities $3.8 \cdot 10^{15}$, $3.8 \cdot 10^{16}$ and $3.8 \cdot 10^{17}$ cm^{-3} for $\epsilon = 3.5\epsilon_0$. The grating spacing is set to 1.6 μm, which leads to a diffusion field equal to 0.1 V/μm. The space charge field increases linearly for low values of E_0. As E_0 approaches the saturation field, E_{SC} slowly saturates to a value equal to mE_S. At the same time, the phase shift, which is 90 degrees for the case of pure diffusion, reaches a minimum and asymptotically approaches back 90 degrees for electric fields higher than the saturation field.

The set of equations (2)-(5) also yields the transient behavior of the space charge field. During grating growth, the complex amplitude of the first Fourier component of E is:[15]

$$E^1(t) = E^1(0) \left(1 - \exp\left[-t/\tau \right] \right) \quad (9)$$

and during erasure:

$$E^1(t) = E^1(0) \exp[-t/\tau] \quad (10)$$

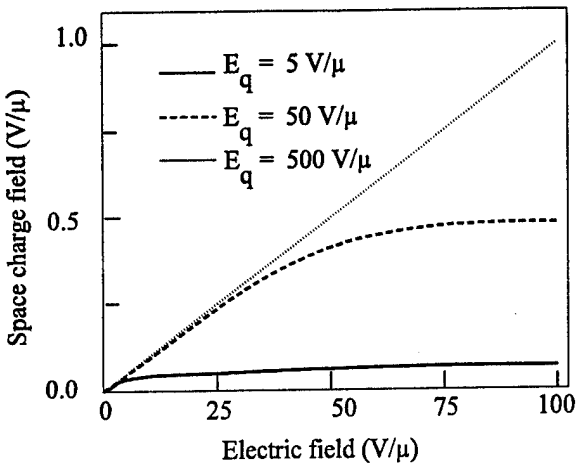

Figure 4 The space charge field as a function of an externally applied electric field, for m=0.01, $\epsilon = 3.5\epsilon_0$ and for three different values of the saturation field which correspond to trap densities of 3.8×10^{15}, 3.8×10^{16} and 3.8×10^{17} cm^{-3}. The grating spacing is set to 1.6 μm that leads to a diffusion field equal to 0.1 V/μ.

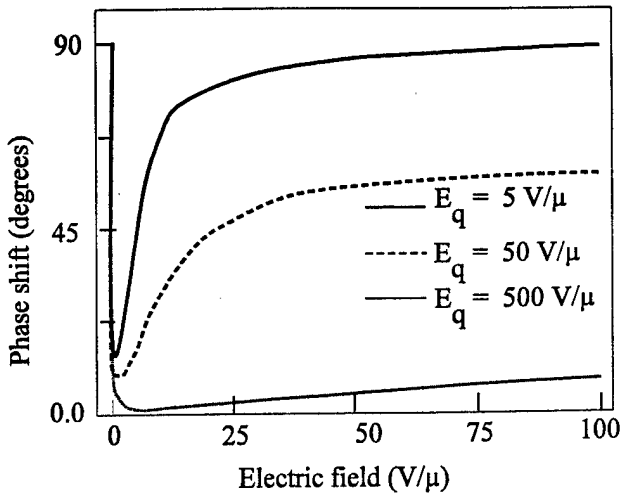

Figure 5 The phase shift of E^1 as a function of an externally applied field, for the same parameters as in Figure 4.

where E^1 (0) is the steady state value given by Eq. (6) and τ the response time. In the general case, the response time is a complex number, causing oscillatory behavior of the space charge field during grating growth. However, in the large grating spacing regime, τ is real and is inversely proportional to the photoconductivity σ_{ph} and the light intensity:[15]

$$\tau^{-1} \propto \sigma_{ph} I \qquad (11)$$

From Eqs. (6) and (11) it can be seen that although the magnitude of the effect does not depend on light intensity, the response time does.

Several extensions of this model with various degrees of complexity have been introduced, including simultaneous electron and hole transport and multiple impurity levels.[16] However, this simple picture is sufficient enough to qualitatively understand most of the results obtained during this Phase II effort.

2.4.2 Photorefractive Nonlinear Optics

Two waves that interfere inside a photorefractive material create a space charge field, which generates a refractive index grating via the electrooptic effect. In the case of a linear (Pockel's) electrooptic response, the amplitude of the first Fourier component of the refractive index grating

is given by:

$$n^1 = -\frac{1}{2} n_0^3 r_{eff} E^1 \tag{12}$$

where n_0 is the refractive index and r_{eff} the effective electrooptic coefficient, which depends on the experimental geometry. This equation can be rewritten in a form that relates refractive index change to the space charge field in a poled polymeric systems:

$$\Delta n_3 = -\frac{1}{2} n_3^3 r_{33} E_{sc} \tag{12a}$$

The fact that E^1 is complex implies the existence of a spatial phase shift ϕ between the refractive index grating and the illumination pattern. As a result of this phase shift, the two waves that interfere to write the grating couple with it, exchanging intensity and phase information. More specifically, the interference of an incident wave with its own diffracted wave (which is phase delayed by $\pi/2$), creates a new grating which adds to (or subtracts from) the initial one. Since this new grating is also phase shifted, energy transfer between the incident and the diffracted wave takes place and so on. A result of this dynamic behavior is an asymmetric energy exchange between the two initial waves and the whole process of grating formation needs to be treated in a self consistent way.

Consider a photorefractive sample which is illuminated as shown in Figure 2 resulting in the interference of two coherent beams. The application of the coupled wave theory leads to:[15]

$$\cos\theta \left(\frac{d}{dz}\right) I_1 = -\Gamma I_1 I_2 / (I_1 + I_2) - \alpha I_1 \tag{13a}$$

$$\cos\theta \left(\frac{d}{dz}\right) I_2 = +\Gamma I_1 I_2 / (I_1 + I_2) - \alpha I_2 \tag{13b}$$

where:

$$\Gamma = \frac{1}{m} \frac{\pi}{\lambda_0} n_0^3 r_{eff} E_{SC} \sin\varphi \tag{14}$$

with α being the absorption coefficients and λ_0 the wavelength of light in vacuum. The phase shift, φ, of the space charge field with respect to the interference pattern is given by:

$$\tan\varphi = \frac{E_D}{E_0}\left(1 + \frac{E_D}{E_q} + \frac{E_0^2}{E_D E_q}\right) \quad . \tag{15}$$

From the above set of equations it is clear that an asymmetric, steady state intensity exchange will take place between the two beams, which will be maximum for $\phi=\pi/2$. The direction of the energy exchange is determined by the sign of Γ and can be used to identify the type of the mobile carrier if the sign of the effective electrooptic coefficient is known.

Thus, one can use a photorefractive material transfer optical energy from a pump beam (I_1) to a probe beam (I_2). In the case where $I_1(0) >> I_2(0)$ and the pump can be considered undepleted, equations (13) yield:

$$I_1 = I_1(0)\exp[-\alpha l] \tag{16a}$$

$$I_2 = I_2(0)\exp[(\Gamma - \alpha) l] \tag{16b}$$

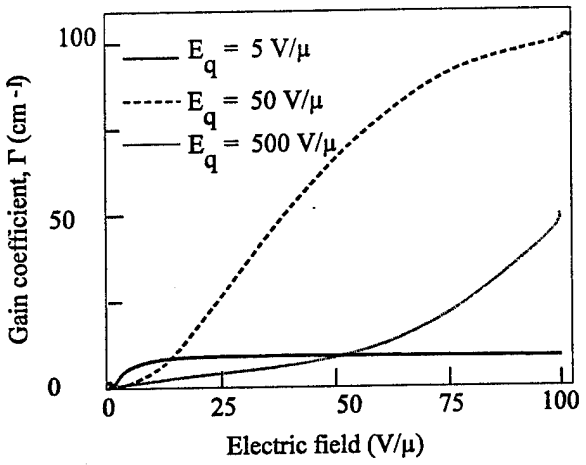

Figure 6 The gain coefficient as a function of an externally applied electric field, for m=0.01, $\epsilon = 3.5\epsilon_0$ and for three different values of the saturation field which correspond to trap densities of 3.8×10^{15}, 3.8×10^{16} and 3.8×10^{17} cm^{-3}. The grating spacing is set to 1.6 μm that leads to a diffusion field equal to 0.1 V/μ. The refractive index was taken to be 1.7 and the electrooptic coefficient 10 pm/V at 633 nm.

The definition of Γ as a gain coefficient is clear from the above equations. If $\Gamma > \alpha$, the probe beam will experience net gain of energy after a single pass from the sample. Except from the experimental geometry. Γ depends on material parameters and external electric field. In Figure 6, the dependence of Γ on electric field was calculated for the same parameters as the space charge field and the phase shift in Figures 4 and 5. The refractive index was taken to be 1.7 and the electrooptic coefficient 10 pm/V at 633 nm. A superlinear dependence at small electric fields is followed by an almost linear increase, which becomes sublinear and levels off at fields comparable to the saturation field. For the above plot, materials parameters (electrooptic coefficient, dielectric constant, refractive index, electrooptic constant etc.) that are typical for organic compounds have been used. As can be seen, gain coefficients in the order of several tens of cm^{-1} are expected

from theory for these materials.

Consider now the case of some inorganic photorefractive crystals. $BaTiO_3$ has a dielectric constant equal to $3600\epsilon_0$ and the product $n_0^3 r_{eff}$ is approximately 23000 pm/V.[6] For a geometry that yields E_D=0.1 V/μm and a trap density of 10^{16} cm^{-3}, the saturation field is an order of magnitude lower than the diffusion field and application of an external electric field will not lead to an enhancement of the gain coefficient. For the case of pure diffusion and at 633 nm, a gain coefficient of 114 cm^{-1} is expected according to theory. For $LiNbO_3$ the dielectric constant is equal to $32\epsilon_0$ and the product $n_0^3 r_{eff}$ is approximately 330 pm/V [6]. For the same parameters as in the previous example, the saturation field is equal to $1.4 \cdot 10^6$ V/μm and while for the case of pure diffusion Γ=1.4 cm^{-1}, with the application of an external electric field of 50 V/μm, a gain coefficient of 23 cm^{-1} is predicted. Experimentally, values for the gain coefficient up to a few tens of cm^{-1} are typically measured in these materials.[6]

2.4.3. Four-Wave Mixing In Photorefractive Polymers

Holographic recording in electrooptic photorefractive crystals was first proposed by Chen et al.[2] and later by Staebler *et al.*[17] Possible applications and the opportunity to explore an interesting new branch of modern optics subsequently attracted much attention. The nonlinear mixing of light beams in a photorefractive material consists of two parts: the action of light beams on the material and the action of the material back on the light beams. The first part is covered in the theory of the photorefractive effect in which light redistributes charges and therefore perturbs the refractive index of the material. The second part is described by the Maxwell's equations of electrodynamics, which describe how these variations in the refractive index scatter light passing through the material.

The theory of photorefractive degenerate four-wave mixing has been described by many authors.[6,15,18] The diffraction efficiency, defined as the ratio between the diffracted signal intensity and that of the writing beam, is given by:

$$\eta = (n^3 r_{eff} \pi LGE_{sc} /2\lambda)^2 \qquad (17)$$

where r_{eff} is the effective electrooptic coefficient which depends on the orientation of the material and the polarization of the laser beams, L the thickness of the material, λ the wavelength, and G is a polarization and geometric factor. Due to the anisotropic nature of the poled structures, the diffraction efficiency is dependent on the polarization of the reading beam. For the general case of oblique readout from tilted photorefractive phase gratings, the diffraction efficiencies for *s*- and *p*-polarized reading beams, respectively, are given by:[19]

$$\eta_s = \sin^2\left(\frac{\pi n^3 r_{13} E_{sc} L \sin\theta_g}{2\lambda\,(\cos\theta_1 \cos\theta_2)^{1/2}} \right) \qquad (18a)$$

$$\eta_p = \sin^2\left(\frac{\pi n^3 r_{eff}^p E_{sc} L \cos 2\theta_0}{2\lambda\,(\cos\theta_1 \cos\theta_2)^{1/2}} \right) \qquad (18b)$$

where θ_g is the angle between the space-charge grating wavevector and the film plane, $2\theta_0$ the angle between the two writing beams, θ_1 and θ_2 the incidence angles of beam 1 and 2, respectively. All angles here are inside the photorefractive material. The effective electrooptic coefficient for the *p*-polarized reading beam is:

$$r_{eff}^{p} = r_{13}\,[\cos\theta_1 \sin(\theta_2 + \theta_g) + \sin\theta_1\cos\theta_2\cos\theta_g] + r_{33}\sin\theta_1\sin\theta_2\sin\theta_g \qquad (19)$$

It is clear that pohotorefractivity is a combined effect of the linear electrooptic response and photoconductivity simultaneously present in a material. Photocharges generated by a spatially modulated light intensity migrate through drift and/or diffusion processes and eventually become trapped, resulting in an internal space charge field, which in turn modulates the material's refractive index via the linear electrooptic (EO) effect. In amorphous organic and polymeric composite materials, the electrooptic response arises from the alignment of the second-order nonlinear optical (NLO) chromophores induced by an external electric field.[20,21] For a composite containing a certain chromophore, the achievable EO coefficient and, thus, the photorefractive figures-of-merit increase with the chromophore concentration. Photoconductivity in organic materials consists of two processes, the photocharge generation and subsequent transport of these charges, and is usually wavelength and electric field dependent.[22] Charge transport in amorphous solids is described as a hopping process. For a given charge transporting molecule (CTM), charge mobilities increase with the decrease in the average distance between adjacent hopping sites, and therefore, with the increase in CTM number density.[23,24]

2.4.4. Photoconductivity in Polymers

Photoconductivity in amorphous organic materials consists of two processes: charge photogeneration and charge transport. The photocharge generation quantum efficiency based on the Onsager theory can be expressed as:[22,24,25]

$$\phi(r_0,E) = \phi_0\left(1 - \frac{k_BT}{eEr_0}\sum_{n=0}^{\infty} A_n(\eta)A_n(\zeta)\right) \qquad (20)$$

where

$$\eta = \frac{r_c}{r_0}, \qquad \zeta = \frac{eEr}{2k_BT} \qquad (21)$$

where e is the elementary charge, k_BT is the Boltzman energy, and $r_c = e^2/4\pi\epsilon_0\epsilon k_BT$ is the Onsager distance. The series $A_n(x)$ is given by:

$$A_0(x) = 1 - e^{-x}$$
$$A_n(x) = A_{n-1}(x) - \frac{e^{-x}x^n}{n!} \qquad (22)$$

The field dependence of the photocharge generation can be readily seen from Eq.(20).

When the photocharges are generated, they will migrate in the polymer under the influence of the electric field through the drift and/or diffusion processes. The mobility of the photocharges is both electric field and temperature dependent and can be described by the empirical expression of the form:[25]

$$\mu(E,T) = \mu_0 e^{-(T_0/T)^2} e^{E^{1/2}(\theta/T^2 - \gamma)} \qquad (23)$$

where T_0 , θ and γ are the experimentally determined constants for a certain material.

2.4.5. Practical Requirements

There are several photorefractive material properties which render their usefulness in practical applications. The most important are:[6]

1. **Photorefractive sensitivity**, **S**, which can be expressed in terms of refractive index change (Δn) per unit of absorbed energy density: $S = \Delta n/(\alpha \cdot I_0 \cdot \tau)$, where α is the material's absorption coefficient at the recording wavelength λ, and I_0 is the incident power density. τ is a material response time or material dielectric relaxation time ($1/\epsilon\epsilon_0$) modified by a function of such parameters as the applied static electric field, E_0, grating spacing, Λ and drift and diffusion of the photocarriers. A useful material must then be an efficient photoconductor at the recording wavelength with large diffusion and drift lengths of the photocarriers. This can be achieved in materials with a high (close to unity) quantum efficiency of charge generation and an absorption coefficient at the recording wavelength in the range of 1 to 3 cm^{-1}.

2. **Maximum diffraction efficiency.** The diffraction efficiency depends primarily on the magnitude of the refractive index change. High values of photoinduced index change are attained in materials possessing large electrooptic coefficients or, in case of low electrooptic coefficient, Δn may be increased by the externally applied electric field up until saturation occurs. In the saturation regime, the steady state index change is proportional to the trap density, N_t; however, if N_t is too large, the response time of the material becomes unfavorably long.

3. **Dark storage of information.** The material dielectric relaxation under no illumination and at room temperature depends on the materials dielectric constant, ϵ, and is inversely proportional to the material's *dark conductivity*, σ_0, and can be expressed as: $\tau_{diel} = \epsilon\epsilon_0/\sigma_0$. It is clear that high dark conductivity prevents many materials from being used for information storage devices. In materials with low band-gap, memory time will be considerably reduced, but a material may still be useful for *short time* photorefractive recording or erasure in *dynamic* holography.

4. **Other material requirements.** Among the other properties which determine whether a material is adaptable to photorefractive applications are: (i) Spatial frequency response (resolution) which is important for applications of high resolution imaging and signal processing. This property is strongly influenced by the material quality; granular structure or other structural inhomogeneities which will drastically limit spatial resolution (excessive scattering). (ii) Material quality and availability are very important in practical applications which determine device reliability, performance, and cost.

2.5. MATERIALS: SELECTION AND PREPARATION

During the course of this Phase II program, LPT has successfully developed a number of materials which exhibit the photorefractive effect. These materials can generally be classified into three different catagories: (1) multicomponent composites wherein each function required by photorefractivity is provided by a specific type of molecules introduced to the composite, (2) composites containing bi-functional chromophores which serve both as charge transporting and second-order NLO compounds, and (3) multifunction polymers containing both second-order NLO and charge transporting abilities. In all materials, a small amount of photocharge generation sensitizer (usually less than 0.5 wt.%) has been incorporated as a dopant.

This chapter provides a comprehensive discussion on the material components. The first part of this chapter describes the selection and general properties of the material components. For those materials which were not commercially available, their syntheses are described in Appendix 1 which also provides detailed procedures by which each photorefractive material was prepared.

A. Second-order NLO chromophores

The choice of the second order chromophores was based primarily on three factors: (1) processability (solubility) of the chromophore, (2) optical transparency in the visible and near IR wavelength regions, and (3) the value of its molecular first hyperpolarizability, β. The second-order NLO chromophores used for this Phase II program include diethylaminonitrostyrene (DEANST), 6-propionyl-2-dimethylaminonaphtalene (PRODAN), N-(4-nitrophenyl)-(L)-prolinol (NPP) and 4-(N,N-bis(β-dihydroxyethyl)amino)-4'-nitrostilbene (DHD) with chemical structures shown in Figure 7. In addition, two bifunctional chromophores which possess both second-order

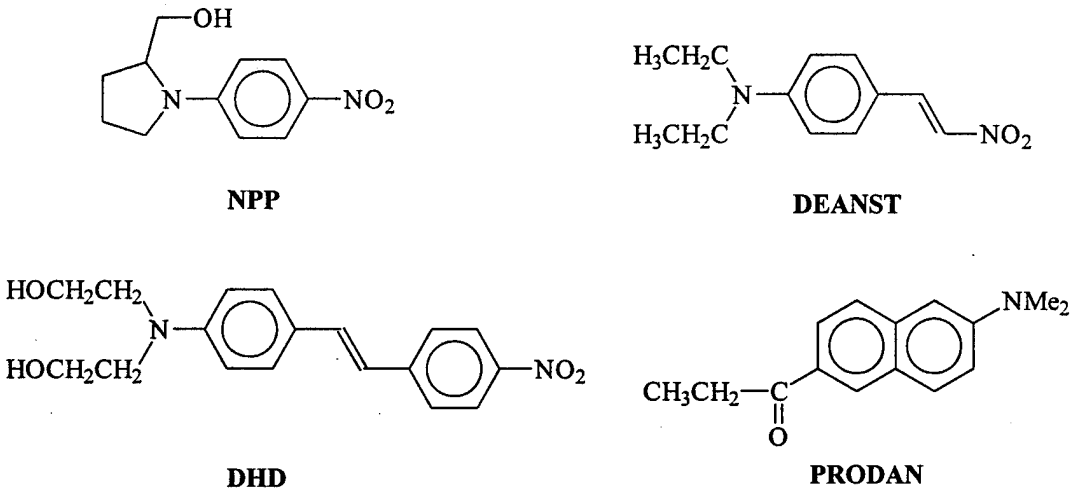

Figure 7 Chemical structures of the second-order NLO chromophores used in the photorefractive composite materials.

NLO and charge transporting properties, N,N-diphenylamino nitrostyrene (DPANST) and 4-(N,N-diphenylamino)-4'-nitrostilbene (DPANS), were also used in the preparation of PR materials (their structures are provided in Figure 8). Absorption profiles of selected chromophores are shown in Figure 9. Note that the absorption of all these chromophores above

530 nm is negligible. The properties of these molecules pertinent to their application in photorefractive materials are summarized in Appendix 1 (Table AI).

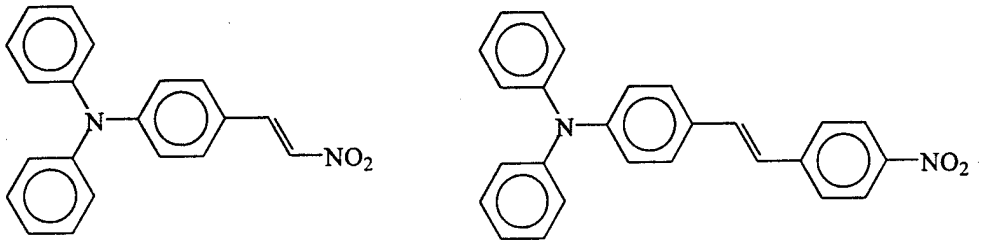

DPANST **DPANS**

Figure 8 Chemical structures of the bi-functional chromophores used in photorefractive composite materials.

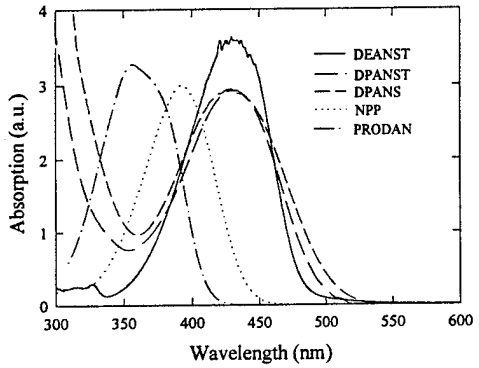

Figure 9 Absorption spectra of the second-order chromophores.

B. Charge transporting molecules

The use of charge transporting molecules is equally important since they play a crucial role in generating the space charge field in organic photorefractive materials. There is general agreement that charge transport is an electric field driven sequence of reduction-oxidation processes involving neutral molecules (M_n) or groups and their charge derivatives such as cation radicals (M_n^+) in the case of hole transport. For hole transport, it is essential that the molecules are electron donors in their neutral state, have low ionization potentials, and that redox processes (oxidation/reduction/oxidation) are completely reversible. Some of the charge transporting molecules tested in this project are presented in Figure 10.

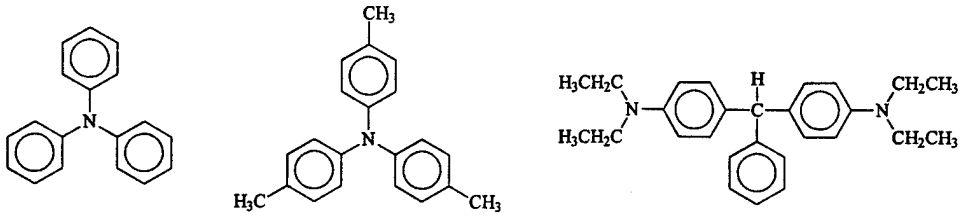

Figure 10 Chemical structures of the charge transporting agents used in the photorefractive composite materials.

C. Photocharge generation sensitizers

Photosensitive dyes have been used for a number of purposes including, but not limited to, spectral sensitizers. There are two primary characteristics for such dyes: (1) a wide operational wavelength range and (2) efficient sensitization, i.e, charge generation. Typical sensitizing dyes are characterized by high extinction transitions in the visible or infrared regions of the spectrum. In most chromophore systems, there are two extreme resonance structures where any of the formal charges tend to be located at the ends of the molecule. The important characteristics that influence the absorption wavelengths for these dyes are the length of the conjugated chain and the nature of the terminal group. Figure 11 shows molecular structures of the photosensitizers which we considered for use in photorefractive polymers. However, only thiapyrylium dye (TPY), fullerene C_{60}, and charge transfer complex of 2,4,7-Trinitrofluorenone (TNF) with carbazole (CAR) have been used, mostly due to their good solubility, compatibility with polymer matrices and high charge generation quantum efficiencies. Figure 12 shows the absorption profiles of these photosensitizers.

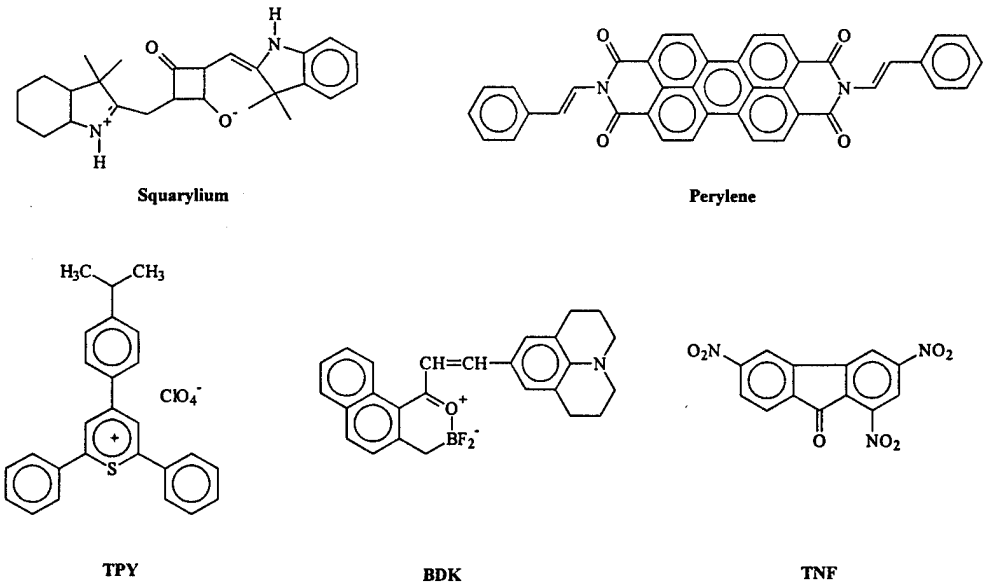

Figure 11 Chemical structures of the photocharge generation sensitizers used in the photorefractive composite materials.

It is clear that sensitizing dyes play a very important role in a photorefractive material since they define the useful wavelength regions, required light intensities and the overall

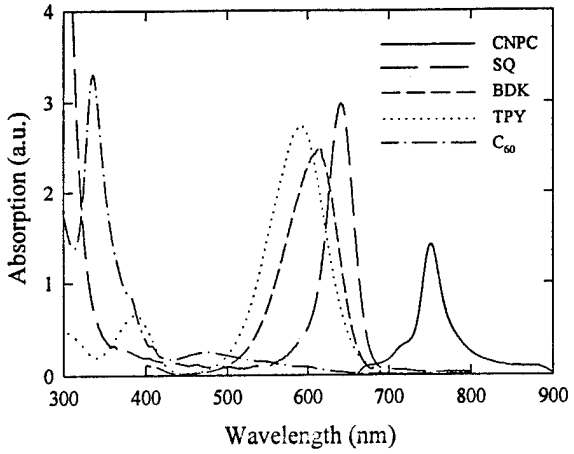

Figure 12 Absorption spectra of the sensitizers.

photorefractive efficiency. The well established properties of the thiapyrilium dye as a photosensitizer made it an obvious candidate for the photorefractive materials that LPT was developing.

D. Polymer binders

Figure 13 displays the molecular structures of polymers expolored in this effort as matrices for photorefractive materials. The choice of these polymers was based on their optical quality and processability, and to what extent they could be used to transport charges.

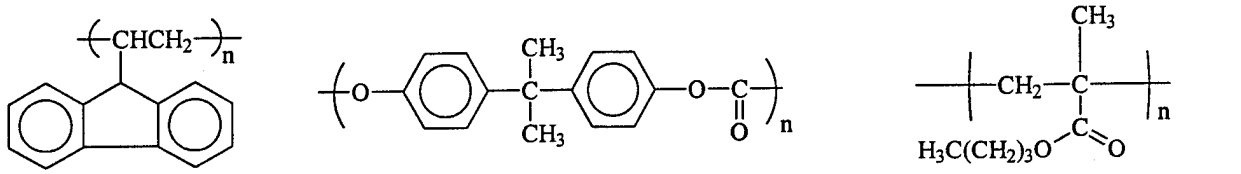

PVK **PC (Lexan)** **Poly(*n*-butyl methacrylate) (PBMA**

Figure 13 Chemical structures of the polymers used in photorefractive composite materials.

1. PVK is a polymer which, in addition to serving as a host, also provides charge transporting properties. Although it has been established that the vinyl backbone of PVK does not contribute

to charge transport, hole mobilities are in the range 10^{-6} to 10^{-7} $cm^2/Vsec$, one of the highest among organic materials.

2. Polycarbonate (Lexan) represents another approach to fabricating photoconductive matrices. Although the polymer itself is not conductive, it can be used as a host material in which charge transporting molecules are dispersed. The molecularly doped polymers are much more flexible in material design since the concentration and type of dopant molecules can be selected allowing one to optimize certain NLO, transport and charge generation properties. Lexan is optically transparent and forms a well characterized ordered composite with thiapyrylium dye. The aggregate composite formed by thiapyrylium dye and polycarbonate is one of the better organic photoconductors known today.

3. Poly (*n*-butyl methacrylate) is a low glass transition temperature, T_g, polymer of excellent optical quality. Similar to Lexan, it neither possesses conductive nor second-order NLO properties. However, it can be doped to relatively high concentrations (30 wt%) with charge transporting molecules and NLO chromophores without losing its optical transparency. Moreover, it's low T_g facilities facile reorientation of the chromophores at room temperature when an external poling field is applied. This feature enhances photorefractive responses through induced birefringence and is utilized by almost all research groups working in the field of photorefractive polymers in order to achieve a larger effective photorefractive figure-of-merit.

E. Multifunctional polymers and sol-gel processed multifunctional ormosils

Polymer and ormosil (silica based polymer containing organic functional groups) based multifunctional materials possessing charge transporting and NLO properties were also developed. Both these systems possess second-order NLO and charge transporting moieties. Molecular stuctures of methylmethacrylate based copolymer, poly{4-(N-ethyl-N-hydroxyethylamino)-4'nitrostilbenyl methacrylate}-co-[N-(2-hydroxyethyl)carbazolyl}-co-[*n*-octyl methacrylate] (PENHCOM) and the ormosils are shown in Figure 14.

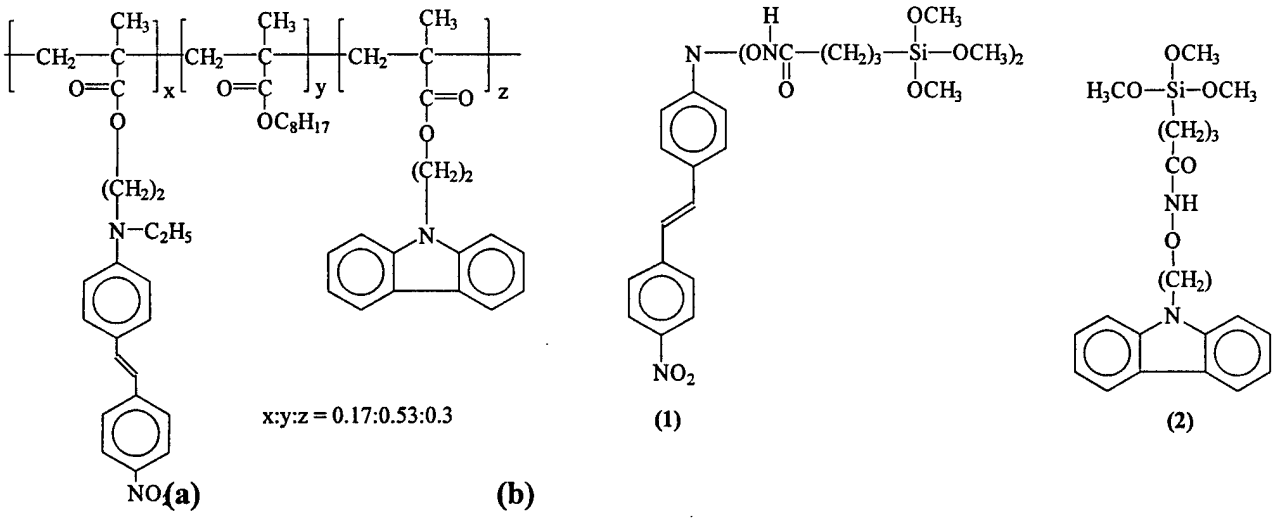

Figure 14 Molecular structure of multifunctional: (a) methacrylate copolymer PENHCOM, and (b) ormosils: DHDO (1) and HCAR (2) used as photorefractive materials.

2.6 CHARACTERIZATION TECHNIQUES

The characterization of a photorefractive material includes measurement of the absorption, electrooptic coefficient and/or second harmonic generation, photoconductivity, and observation of photorefractive grating formation, which can be usually done by wave mixing experiments. All these measurements should be performed on the same sample so that the properties of the sample are well characterized. In practice, however, it is often very difficult to perform the electrooptic (EO) modulation and second harmonic generation (SHG) on thick samples (hundreds of micrometers) required in the wave mixing experiments. It is thus important that the preparation conditions (electric field poling in particular) be almost identical for samples used for EO or SHG measurements and for samples used in wave mixing experiments. Below is a brief description of second harmonic generation, electrooptic modulation, photoconductivity measurements and degenerate wave mixing experiments used to characterize polymer/$\chi^{(2)}$ chromophore/photosensitizer composite films prepared during this development research effort.

2.6.1 Second Harmonic Generation From Poled Films

An effectively poled material possesses the ∞mm point group symmetry. This symmetry reduces the nonvanishing components of the macroscopic susceptibility to $\chi^{(2)}_{zzz}$ and $\chi^{(2)}_{zxx}$ which, to the first order of the poling electric field, are related to the microscopic hyperpolarizability, β, by:[20]

$$\chi^{(2)}_{zzz}(-2\omega;\omega;\omega) = \frac{fN\mu\beta E_p}{5kT} \tag{24}$$

and

$$\chi^{(2)}_{zzz} = 3\chi^{(2)}_{zxx} \tag{25}$$

where $f=f_{2\omega}(f_{\omega})^2 f_0$ is the local field factor, μ is the molecular dipole moment, E_p is the poling electric field and kT is the thermal energy.

The second-harmonic intensity generated from the poled film is given by:

$$I_{2\omega} = \frac{512\pi^3}{A} t_{\omega}^4 T_{2\omega} d^2 t_0^2 p^2 I_{\omega}^2 \frac{1}{(n_{2\omega}^2 - n_{\omega}^2)^2} \sin^2\psi(\theta) \tag{26}$$

where A is the area of the laser beam spot, d is the appropriate second-harmonic coefficient in the contracted notation, t_{ω}, $T_{2\omega}$ and t_0 are transmission factors, I_{ω} is the fundamental laser intensity, p is the angular factor which projects the nonlinear susceptibility tensor onto the coordinate frame defined by the propagating electric field and the n's are the refractive indices at the appropriate frequencies. The angular dependence term, $\psi(\theta)$, of the second-harmonic intensity, can be expressed as:

$$\psi(\theta) = (\pi L/2)\,(4/\lambda)\,(n_{\omega}\cos\theta_{\omega} - n_{2\omega}\cos\theta_{2\omega}) = \pi L/2l_c \qquad (27)$$

where $l_c = \lambda/4(n_{\omega}\cos\theta_{\omega} - n_{2\omega}\cos\theta_{2\omega})$ is the coherence length. At normal incidence, $l_c = \lambda/4(n_{\omega} - n_{2\omega})$.

It is apparent that when the film is rotated around an axis perpendicular to the laser beam, the second harmonic intensity changes as a function of the rotation angle. The angular dependent second harmonic curve is called a Maker fringe. Since the film thickness is usually much smaller than the coherence length (typically around 20 μm), only the envelope of the Maker fringes is observed.

The second order susceptibility of a poled material is evaluated by comparing the second harmonic intensity generated from the material to that from Y-cut quartz crystal, which has a d value of $d_{11} = 1.2 \times 10^{-9}$ esu. The material in the form of a thin film is generally mounted on a rotary stage and rotated around the axis normal to the laser beam. The obtained angular dependence curves are theoretically fitted with a computer, and the maximum SH intensities produced by the sample and the quartz reference compared.

2.6.2 Electro-Optic Modulation

The assessments of the electrooptic coefficients was done by measuring the relative amplitude and phase changes of the s- and p-polarized laser beam.[26,27] To perform the electro-optic modulation experiment, the composite film was cast on ITO coated glass substrates. A group of circular thin silver films was vacuum deposited onto the composite films to serve as electrodes and mirrors. Poling was done by applying a DC voltage of 100 V to the silver electrodes with the ITO layer connected to the ground. The experimental setup is shown in Figure 15. A He-Ne laser beam polarized 45° with respect to the plane of incidence passes through the ITO layer, traverses the sol-gel film, and is then reflected by the silver electrode. The second polarizer analyses the reflected laser beam. A half-wave plate was used to introduce a π/2 phase shift. A bipolar power supply provided the DC poling voltage as well as the modulating AC voltage by amplifying a small AC voltage from a signal generator. The modulated light signal was detected by a photodiode, amplified using a pre-amplifier (500 amplification ratio), displayed and

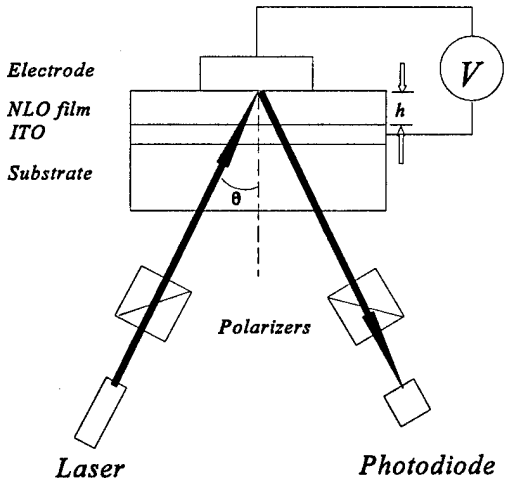

Figure 15 Schematic layout of electrooptic experimental setup.

measured with the help of a 400 MHz oscilloscope.

When an alternating voltage is applied across the poled composite film containing 2nd order NLO chromophore (NPP, DEANST, etc.), the laser beam is phase modulated due to the birefringence induced by the electric field. Because the poled film possesses an ∞mm symmetry, the only nonzero components of the electro-optic coefficients are r_{31} and r_{33} with $r_{33} = 3r_{31}$ according to Kleinman's symmetry argument. These coefficients are determined by measuring the ratio, Γ_m, between the modulated light intensity (AC) to the unmodulated light intensity using the following equations:[28]

$$\Gamma_m = \frac{2\pi}{\lambda} d\Delta n_0 \frac{\sin^2\theta}{\cos\theta} \tag{28}$$

$$\Delta n_0 = \frac{1}{2}(n_3^3 r_{33} - n_1^3 r_{31}) \frac{V}{d} \tag{29}$$

where d is the thickness of the film, Δn_0 is the birefringence one would measure if the light traversed the length of the film, λ is the laser wavelength and θ is the angle of incidence. n_1 and n_3 are the refractive indices along the directions perpendicular and parallel to the poling electric field, respectively, and r_{31} and r_{33} are the Pockels coefficients corresponding to the off-diagonal and diagonal terms. Finally, these coefficients are related to the second-order susceptibility by:

$$\chi^{(2)}_{zzz}(-\omega;\omega,0) = -n^4 r_{33}/8\pi \tag{30}$$

The electrooptic modulation experiment was usually performed on a 1μm thick poled composite films at a frequency of 1.59 KHz. The AC modulating voltage used was 100 V peak to peak.

2.6.3 Conductivity and Photoconductivity Measurements

The conductivity measurements were initially performed using the four probe method. In this method, four electrodes are placed on the sample either by vacuum deposition of a thin metal film (gold, silver, chromium etc.) through a patterned mask or by applying a conductive silver epoxy. Using a precision electrometer, one measures the current or voltage between the inner and outer pairs of electrodes, as shown below.

The four probe method is a convenient method of obtaining some preliminary results, but is not the most appropriate geometry, since it is most useful when performed with samples exhibiting minuscule conductivity and due to the fact that the measured conductivity is often affected by surface effects. For these reasons, subsequent measurements were performed by direct monitoring of current flowing through the composite film. All films subjected to conductivity measurements were deposited onto glass substrates (coated with a commercially obtained, transparent and conductive layer of indium-tin oxide (ITO)) using either the spin

coating or casting technique. Subsequent heat treatment was carried out in a temperature controlled oven under an inert atmosphere (argon or nitrogen). In this arrangement, the ITO layer deposited onto the glass substrate served as one electrode and a vacuum deposited silver film on top of composite film served as the second electrode.

The photoconductivity of the materials was measured by monitoring the photocurrent through the samples and by measuring the voltage drop on a resistor (see Figure 16). An important parameter affecting photoconductivity is the photocharge generation quantum efficiency, which is defined as the number of charges generated per photon absorbed by the material, as given by:[29]

$$\phi = \frac{n}{N} = \frac{V}{Re}\frac{hc}{\lambda}\frac{1}{P(1-e^{-\alpha})} \tag{31}$$

where n is the number of photocharges generated, N the number of photons absorbed, V the measured voltage, R the resistance, e the electron charge, h the Planck constant, c the speed of light in vacuum, λ the wavelength of the laser beam, P the laser power and α is the absorption coefficient.

The experiment was carried out with an Ar^+ laser pumped cw dye laser operating at wavelengths from 560 nm to 700 nm using different dyes as well as with Ar^+ laser pumped Ti2 sapphire laser operating at 700 nm to 1 μm. An electronic shutter controls the duration time (from 50 to 200 ms) in which the laser beam illuminates the samples. The voltage drop on the resistor was measured and displayed with the use of an oscilloscope. A typical photocurrent signal is presented in Figure 17.

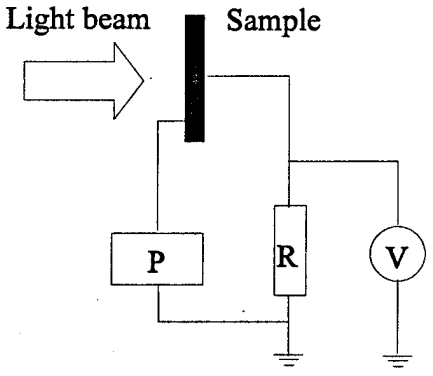

Figure 16 Photocurrent measurement

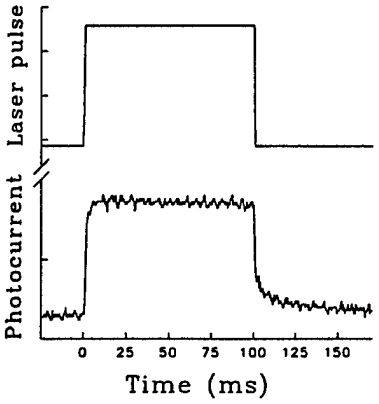

Figure 17 A typical photocurrent signal

2.6.4 Four-Wave Mixing Experiments

Backward degenerate four-wave mixing was used to study the photorefractive behavior of the material described in this research work. The setup is shown in Figure 18. A light beam delivered by Ar^+ laser pumped CW dye laser or Ti:Sapphire laser is used in all the four-wave mixing measurements. Two writing beams with nearly equal intensity are intersected in the

material, generating a spatial distribution of light intensity and, therefore, a space-charge field. The reading, or probe beam, of a much lower intensity and propagating in the direction opposite to one of the writing beams, is diffracted by the photorefractive grating formed by the writing beams. The diffracted signal is reflected by a beam splitter, detected by a photomultiplier tube and processed by a BOXCAR signal processor.

The diffraction efficiency, defined as the ratio between the diffracted signal intensity and that of the writing beam, is given by Eqs. (17)-(18). The photorefractive diffraction efficiency is highly dependent on the applied electric field. Therefore, for each material, the diffraction efficiency is measured as a function of the applied field. A high voltage power supply provides dc voltages up to 30 kV with either positive or negative polarity.

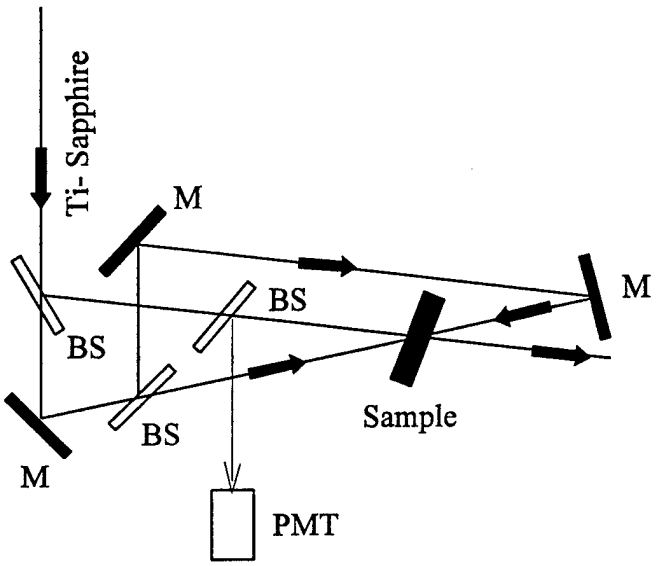

Figure 18 Experimental setup for the photorefractive degenerate four-wave mixing

2.7 EXPERIMENTAL RESULTS

2.7.1 PVK Based Photorefractive Composites

A. Electrooptic coefficient measurements

The electrooptic modulation experiment was carried out in a configuration shown in Figure 19. In the initial experiments, samples were cast on plain ITO coated glass substrates and baked at 60°C for a period of 1-2 hours. Measurement was performed on selected samples of the

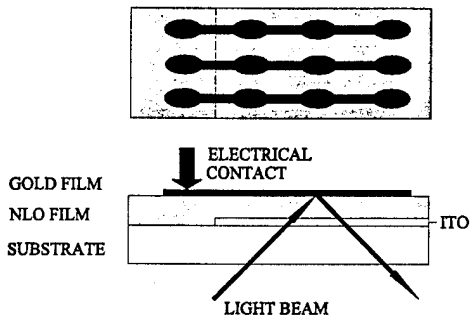

Figure 19 Modified film and electrode configuration.

titania/PVK/DEANST/fullerene composite, abbreviated here for convenience FDKT 16-19, containing different relative amounts of titania and PVK. All samples could be poled at relatively low temperatures. The electrooptic modulation signal was observed to increase as the samples were heated to higher temperatures (closer to the glass transition temperature of the composite), indicating the alignment of the NLO chromophores, DEANST, in this case. It is clear that the glass transition temperature of the composite is considerably different from that of undoped PVK, which is close to 220°C, because of the high level doping. The observed increase of the EO modulation signal reaches a maximum at around 150-160°C. However, all films were shown to suffer dielectric breakdown at temperatures higher than 140°C. The possible reasons are: (1) short baking time, which could have resulted in residual solvent inside the film; (2) hard electrode contact, imposing a high pressure on the film (this is more pronounced when the temperature of the film is close to the glass transition temperature of the material, so the film becomes softer); and (3) relatively reactive thin silver films which were used as the reflection mirrors and electrodes. Different approaches were tested to avoid the dielectric breakdown of the NLO films. These efforts included:

(1) Baking samples for longer periods of time. Sample FDKT18 was baked at 70°C for 12 hours.
(2) Using gold thin films as electrodes, instead of silver.
(3) Different electrode configuration. Long strips of electrodes instead of circular films. The ITO layer was also modified. The overall configuration is shown in Figure 17.

Using this configuration, the NLO film could be heated and poled at temperatures over 180°C without the dielectric breakdown. Poling was performed following the procedure below:
(1) Application of a dc poling field at 60 V/μm, an ac modulating field of 1.8 V/2.5μm.

Observed EO signal ~ 20mV;

(2) Heating the sample at a rate of 10°C/min to 190°C. EO signal with dc field applied ~ 600 mV.
(3) Cooling the sample to room temperature at a rate of 5°C/min.
(4) Remove the dc poling field.
(5) Measure the EO coefficient:
    AC modulating field: 80 V (p-p)
    DC signal on photodiode: 200 mV
    AC modulated signal on oscilloscope: 470 mV
    Amplification rate: 300
    Estimated EO coefficient: r_{33}=23 pm/V
    Temporal stability: After 3 hours, EO coefficient r_{33}=18 pm/V

B. Photoconductivity measurements

Several composite materials produced to this point have also been examined for their dark conductivity. This measurement ultimately determines the usefulness of a given material in applications which utilize a photorefractive effect. High dark conductivity limits material applications to, for example, short term or real-time optical memory storage devices only. Appropriately annealed composites consisting of TiO_2/PVK/DEANST/fullerene and TiO_2/PVK/NPP/fullerene showed dark conductivity of about 10^{-9} simens/cm. Such low values of dark conductivity would permit the utilization of these composite materials as a short term optical storage media. However, processing of these composites into thick films was difficult to optimize.

A very important parameter describing a photoconductive material is the photocharge generation quantum efficiency, which is defined as the number of charge carriers per absorbed photon. This quantum efficiency was studied by measuring the photocurrent through the sample when illuminated with light and calculated according to Eq. (20). In the experiment, an Ar^+ laser pumped dye laser operating at 633 nm (or Ti-Sapphire laser operating at wavelengths between 700 nm and 830 nm) illuminates the sample through the ITO glass substrate. The illumination time is controlled by a shutter resulting in 200 ms pulse duration. The photocurrent is measured by recording the voltage drop on a 1 MΩ resistor. The photocharge generation quantum efficiency is then calculated using the value of measured photocurrent and the optical density of the film. The quantum efficiency was measured as a function of the applied electric field and the field dependence of the quantum efficiency obtained from TiO_2 /PVK/DEANST/fullerene composite with a film thickness of about 3 μm; the data is presented in Figure 20.

The observed dark conductivity for a composite series containing titania samples was higher than that for composites containing silica. This is partially because of the large area of the gold electrode. Only 5% of the electrode was illuminated by the laser beam, but the whole electrode contributed to the dark current in contrast to SiO_2 composites where the entire electrode surface was illuminated. Another possible reason for the high dark conductivity is the presence of TiO_2. Since, TiO_2 by itself is known to have a higher dark conductivity than SiO_2.

Figures 21 through 23 display experimental results on electric field dependence of the quantum efficiency of charge generation in several polymer (PVK or PC)/DEANST composite films containing different photosensitizers. The experimental data for a composite film

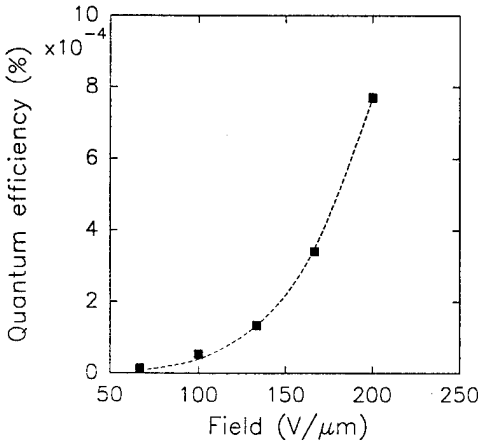

Figure 20 Electric field dependence of quantum efficiency generation for a TiO_2/PVK/DEANST/fullerenes composite

containing Co-naphthalocyanine dye which shows well defined absorption in the near IR is depicted in Figure 21. The wavelength dependence does not precisely follow the absorption profile of the dye and exhibits the highest efficiency at wavelengths shorter than the absorption maximum (750 nm). The overall efficiency of charge generation is very low, however, which is attributed to a small concentration of the dye in the composite film due to its limited solubility in the solvents used (toluene, CH_2Cl_2, cyclohexanone). The highest quantum efficiency of charge generation was obtained in PVK/DEANST films doped with BDK dye (η=0.5%, see Figure 22), and PC/DEANST films doped with TPY dye and charge transporting molecules TPY (η=0.3%, see Figure 23).

The concentration of the charge transporting molecules in a non-conducting PC polymer

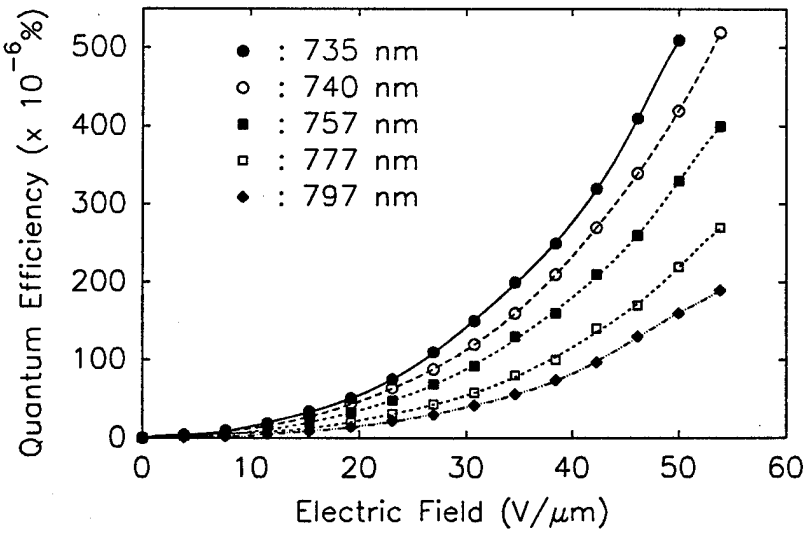

Figure 21 Electric field and wavelength dependencies of the photocharge generation quantum efficiency in Co-naphthalocyanine-doped PVK/DEANST composite

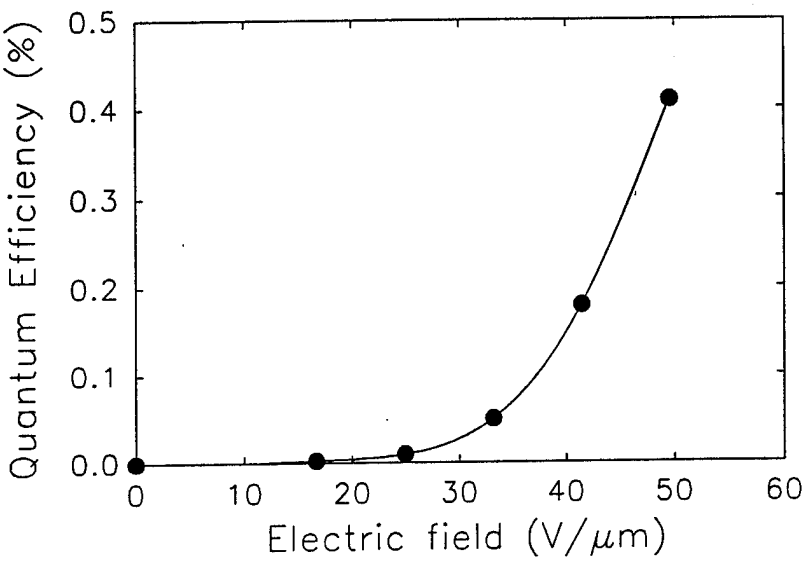

Figure 22 Quantum efficiency of photocharge generation in a BDK/DEANST/PVK composite.

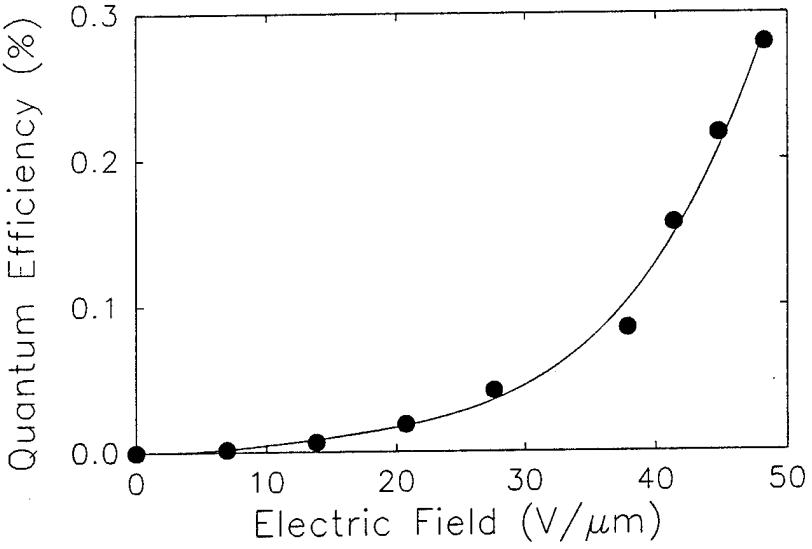

Figure 23 Quantum efficiency of photocharge generation in a TPY/TTA/DEANST/PC composite (Homogeneous phase)

matrix greatly influences charge mobilities. Such dependence is shown in Figure 24. Since the rate of the electron exchange between electron donor molecules and their cations depends on the separation distance, the mobility is a strong function of concentration. For most disordered systems (doped matrices), the empirical relation between hole mobilities, μ_H , and average intermolecular distance, R, can be expressed as follows:

$$\mu_H \approx R^2 \exp(-\frac{2R}{R_0}) \quad (32)$$

where R_0 is the localization radius of the electron. This relation fits the experimental data with the average intramolecular distance, R, being proportional to (concentration)$^{-1/3}$. This exponential dependence on the average intramolecular distance can be explained by small polaron or phono-assisted hopping mechanisms. The maximum molecular concentration in practical photoconducting media is determined by solubility and mechanical considerations.

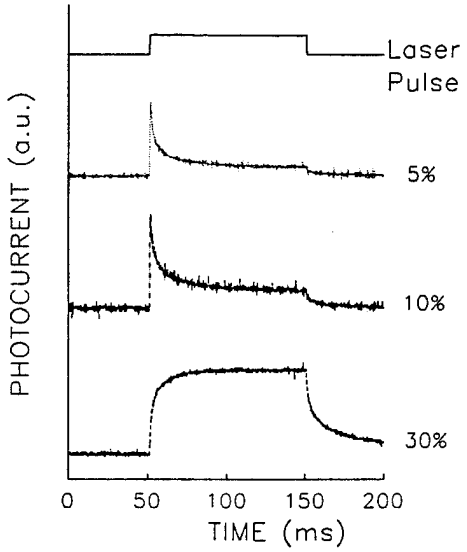

Figure 24 Dependence of the photoconductivity on the concentration of charge transporting molecules, TTA, in a TPY/TTA/DEANST/PC composite.

The staff of LPT has also explored a unique approach to forming photorefractive media by building a stratified structure in which a thin (ca. 15 μm) building block consists of two layers: NLO/charge transporting layer and a photoreceptor layer. The charge generation in such a block occurs in a photosensitizing layer. The photogenerated charges are injected subsequently into and transported through contiguous charge transport layer. The spatial distribution of the photocharges can be achieved by, for instance, introduction of photo-activated traps. This approach is very useful in cases when the photosensitizing moiety is not soluble, but can be deposited as a thin layer by vacuum evaporation.

Figures 25 and 26 depict quantum efficiency generation in bilayer structures with the perylene dye acting as charge generating medium. It can be seen that photocharge generation efficiency is close to that observed in molecularly doped polymer/DEANST/photosensitizer composite films.

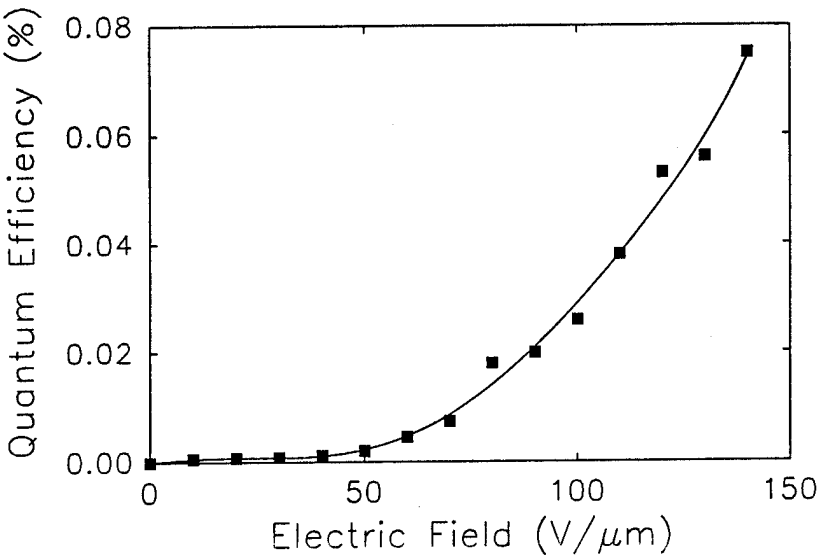

Figure 25 Electric field dependence of the photocharge generation quantum efficiency from a perylene dye / TTA-DEANST-PC bilayer composite

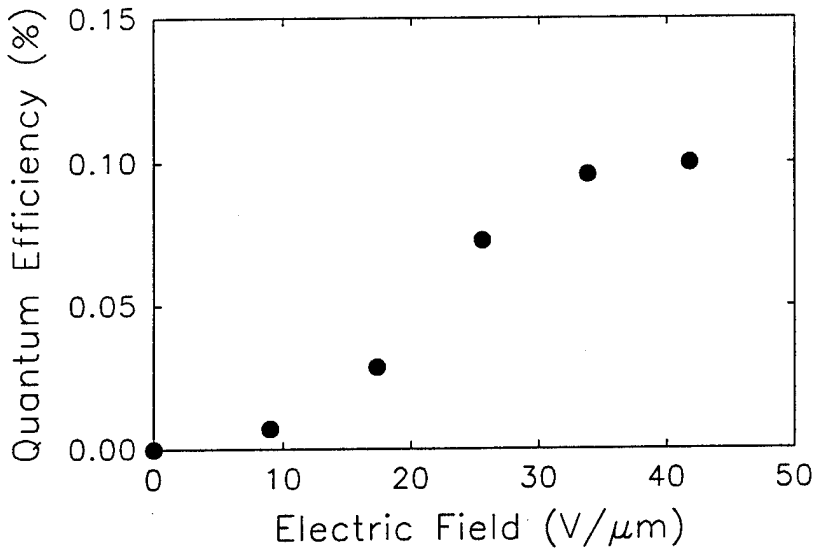

Figure 26 Quantum efficiency of photocharge generation in a bilayer structure composed of perylene sensitizer and PVK/DEANST composite.

D. Four Wave Mixing Experiments.

D.1 PVK/TiO_2/DEANST/fullerene system

The photorefractive response using a degenerate four wave mixing arrangement from the similar composite consisting of PVK, DEANST, and fullerenes, has already been observed. The appropriate parameters have been determined as described below.

The electrooptic coefficient was measured in a thin film configuration using the technique described earlier. The film of 4.87 μm thick was heated to a temperature of 70 °C followed by the application of a dc voltage of 200 V. The film was then cooled to room temperature without annealing. An electrooptic coefficient, r_{33}, of 4 pm/V was obtained. Although this coefficient is almost one order of magnitude lower than the corresponding r_{33} coefficient of TiO_2/PVK/DEANST/fullerenes composite film, the above procedure was chosen in order to perform poling under the same conditions used for the thick film wave mixing experiments. In that case, higher temperature and high poling field resulted in dielectric breakdown in the film.

The obtained r_{33} value is also considerably lower compared to the $\chi^{(2)}_{zzz}$ value obtained by second-harmonic generation, possibly owing to the lower poling temperature, lower poling electric field applied, and the dispersion of the nonlinearity. The evidence of the photorefractive effect is provided by a degenerate four-wave mixing experiment. A 88 μm thick film was sandwiched between two ITO covered glass substrates. The film was poled at 70 °C with an electric field of 250 kV/cm. Two writing beams both with *s*-polarization intersect at the sample, as shown in Figure 2. The incident angles are $\theta_1 = 37.3°$ and $\theta_2 = 30°$ and the interference fringes spacing is calculated to be Λ=5 μm and the angle θ_g to be 56.3°. The diffraction signal from the reading beam, which was also *s*-polarized and propagating opposite to the writing beam 1, was detected as the electric field was turned on and off. Figure 27 displays a typical DFWM signal obtained from the PVK/DEANST/fullerene composite. In this figure, no electric field was applied before time t_1. A dc field of 400 kV/cm was turned on at t_1 and off at t_2. It is clear that there was no DFWM signal in the absence of an external field. A DFWM signal quickly built up upon application of a dc field and decayed to zero after the field was removed. The relatively large noise observed in the DFWM signal is due to the random vibration of the experimental setup. Because of the random factor and a slow response time of the photorefractive effect, the gratings which are generated at different times will have a random spatial shift in the sample and randomly cancel or enhance each other in part, and therefore, cause the random fluctuation of the signal.

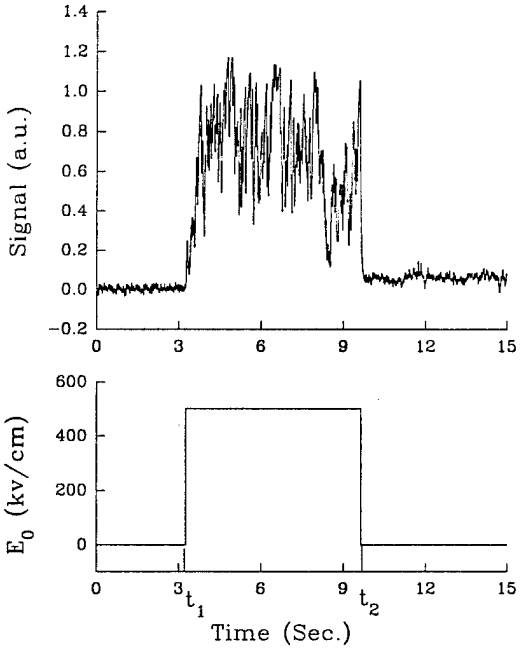

Figure 27 The electric field dependence of the four-wave mixing diffraction efficiency from a PVK/DEANST/fullerene composite

Figure 28 shows the electric field dependence of the four-wave mixing diffraction efficiency. A maximum efficiency of 2.25 x 10^{-5} was obtained at an applied field of 500 kV/cm. Also shown in the figure (solid line) is the diffraction efficiency calculated using the relation:[29] $\Delta n = -1/2\, n^3 r_{33} E_{sc}$, where it was assumed, in the calculation of the space-charge fields E_{sc}, that no traps were present in the material. The theoretical results are closest to the experimental data when an electrooptic coefficient r_{33}= 1 pm/V is used. This is lower than the r coefficient obtained in the thin films. The discrepancy can be attributed to the lower poling field used in the thick films.

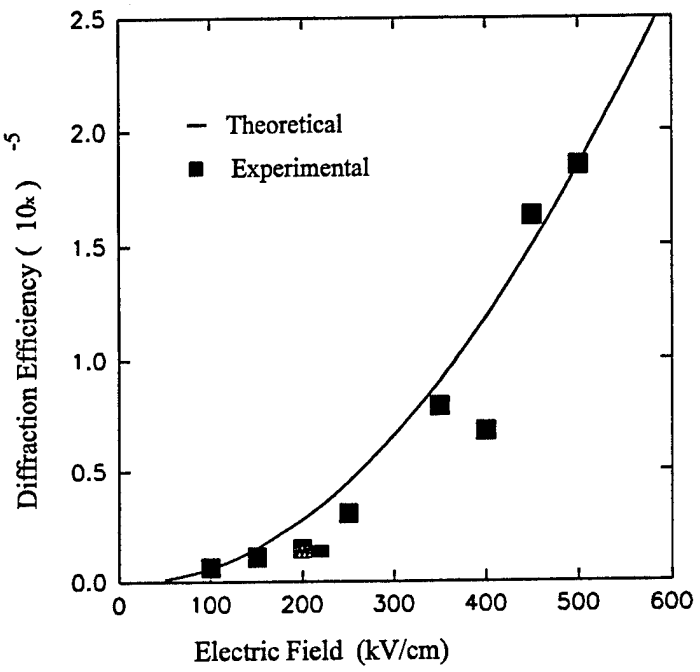

Figure 28 The electric field dependence of the four-wave mixing diffraction efficiency from a PVK/DEANST/fullerene composite

The experimental results obtained show that a photorefractive grating established by two writing beams evolves and disappears slowly most probably due to the low mobility of charge carriers. This may be caused by deep traps within the sol-gel oxide/polymer lattice and/or non-optimized concentration of the charge transporting species. The latter is currently being investigated by introducing triphenylamine, a very efficient charge transporting agent. However, optical materials with a slow decay of the photorefractive grating are very desirable for optical memory storage systems. Further optimization of photocharge generation efficiency and charge transporting processes led to a more efficient photorefractive materials with characteristics desirable for the optical memory storage devices.

D.2 The PVK/DEANST/NPP/thiapyrylium dye composite.

For the TPY/DEANST/NPP/PVK system, photorefractive degenerate four-wave mixing was carried out with an Ar^+ laser pumped Ti:Sapphire laser operating at 710 nm. A 100 μm thick sample containing 71% PVK, 15% DEANST, 14% NPP and approximately 0.1% thiapyrylium dye was sandwiched in between two ITO covered glass substrates. The use of a NPP/DEANST chromophore combination rather than a pure DEANST was dictated by the observation of strong

photo-bleaching at wavelengths coincident with the dye's absorption profile, i.e, 620 nm to 680 nm. The photo-bleaching process was not, however, observed in PVK/NPP/TPY composite films. The exact nature of the photo-bleaching has not yet been determined, but the experimental results indicate that it may be attributed to some specific interactions between the DEANST and TPY molecules. Figure 29 shows the UV-VIS spectra of the composite and its components.

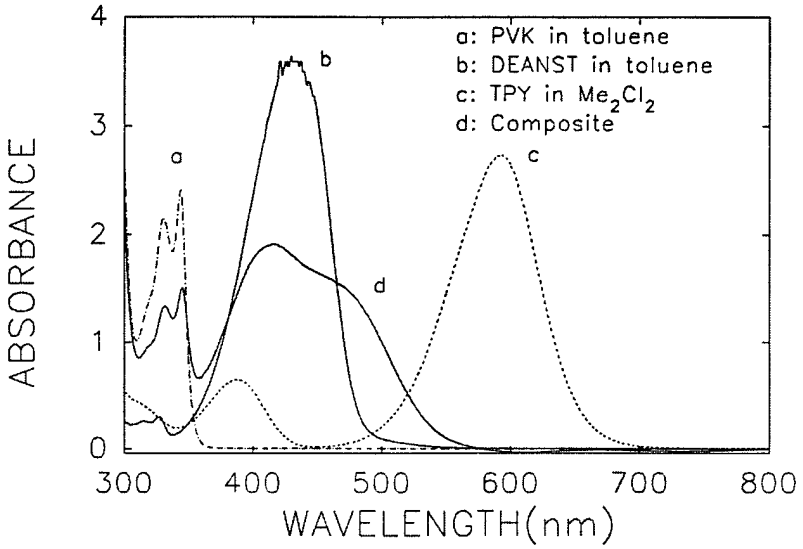

Figure 29 UV-VIS spectra of a PVK/DEANST/NPP/Thiapyrylium dye composite and components

The film was not poled prior to the four-wave mixing experiments for the reason explained earlier in the material section of this report. Two writing beams with equal intensity of 500 mW/cm^2 intersect in the sample with incidence angles of 33° and 57°, respectively, forming a grating of Λ=1.5 μm spacing and θ_g= 64°. The reading beam, from the same laser source, has an

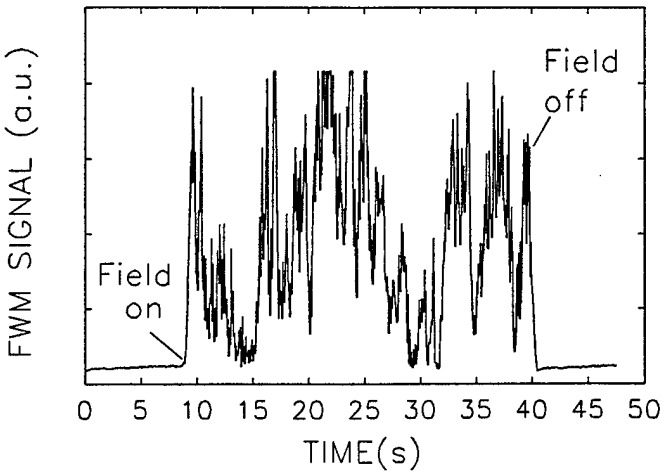

Figure 30 A typical photorefractive four-wave mixing signal from a TYP/DEANST/NPP/PVK composite

intensity of 88 mW/cm^2. Figure 30 shows a typical four-wave mixing signal from such a sample and Figure 31 displays the electric field dependence of the four-wave mixing diffraction efficiency. A maximum diffraction efficiency of 0.08 % was obtained at an electric field of 1.1 MV/cm.

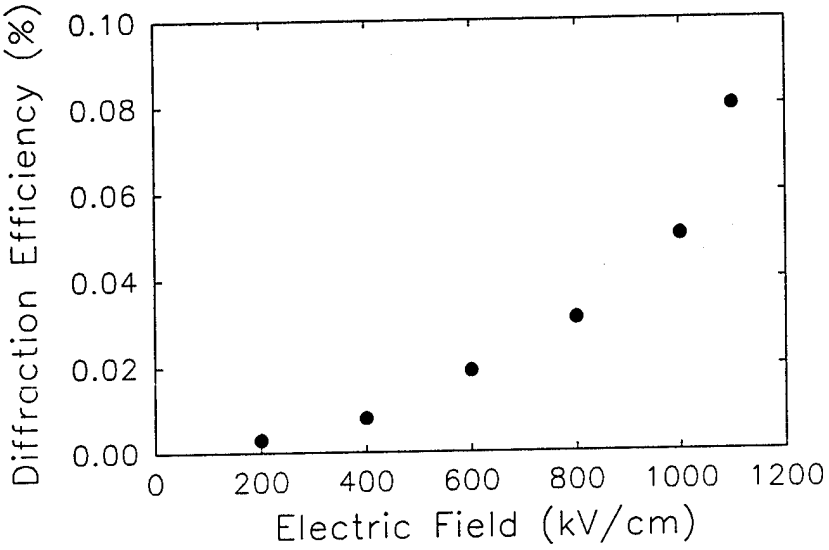

Figure 31 The electric field dependence of the photorefractive four-wave mixing diffraction efficiency from a TPY/DEANST/PVK composite

D.3 The PVK/DEANST/BDK system.

The PVK/DEANST/BDK composite investigated contains 71% of PVK, 29% of DEANST and approximately 0.1% of boron diketonate. Figure 32 displays the absorption spectra of the composite and its components. Films 300 μm thick were sandwiched between ITO covered glass substrates. The films were not poled prior to degenerate four wave mixing experiments for the reasons underlined in earlier sections of this report.

The photorefractive gratings were written using an Ar^+ laser pumped dye laser at 633 nm. Two *s*-polarized writing beams intersect at the sample, as shown in Figure 18. The incidence angles were kept at $\theta_1 = 29°$ and $\theta_2 = 53°$, giving internal angles of 18° and 30° for beams 1 and 2, respectively. Thus, the interference fringes spacing is calculated to be Λ=1.52 μm and the angle θ_g to be 66°. Both degenerate four-wave mixing and non-degenerate four-wave mixing were performed on these samples. In the case of non-degenerate four-wave mixing, a He-Ne laser with an output power of 3.2 mW at 633 nm was used as a reading beam. The writing beams have the equal intensity of 240 mW/cm^2.

The diffraction signal from the reading beam, with either *s*- or *p*- polarization and

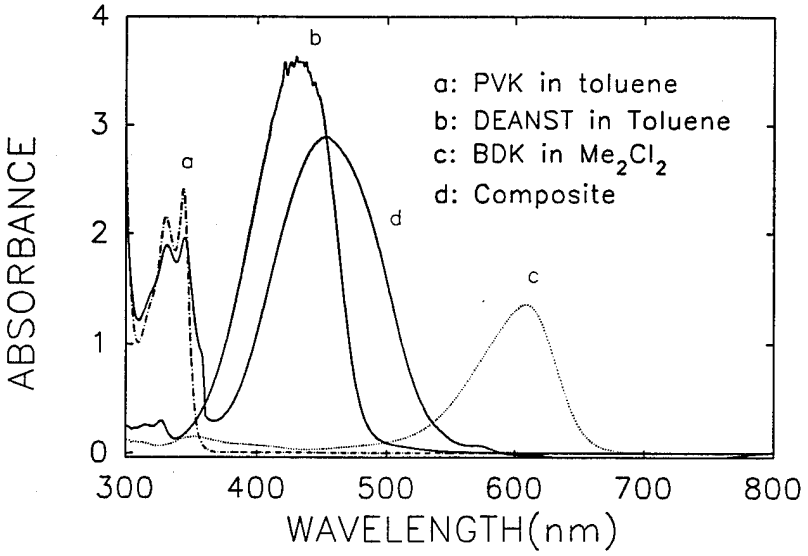

Figure 32 Absorption spectra of a PVK/DEANST/BDK composite and its components

propagating opposite to writing beam 1, was detected as the electric field was turned on and off. Figure 33 displays a typical FWM signal obtained from the BDK/DEANST/PVK composite. In the figure, no electric field was applied before time t_1. A dc field of 600 kV/cm was turned on and off at the points indicated. It is clear that there was no FWM signal in the absence of an external field. A FWM signal quickly built up upon application of a dc field and decayed to zero after the field was removed.

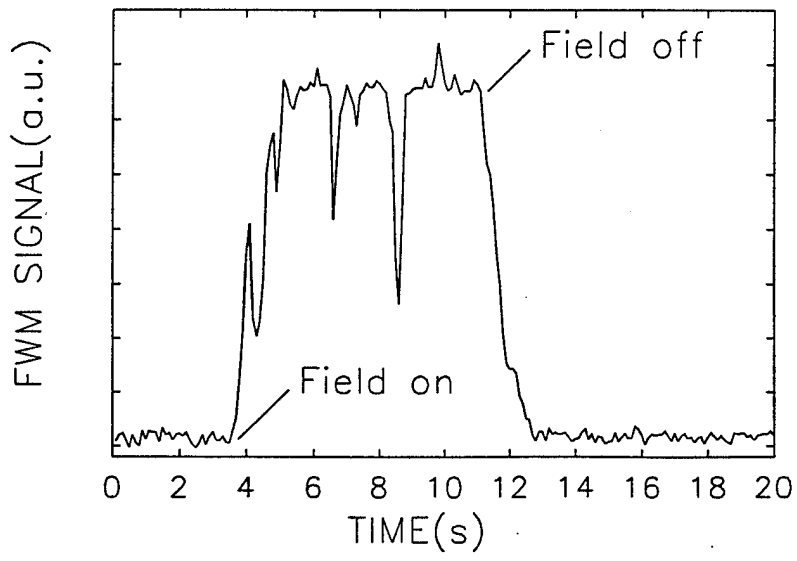

Figure 33 A typical four-wave mixing signal from a photorefractive composite of BDK/DEANST/PVK

The observed writing and erasing of the photorefractive grating is relatively fast, as can be seen from Figures 33 and 34. It should be pointed out that the sample has not been poled prior to the wave mixing experiments. This means that the rise and decay of the four-wave mixing signal involves two different processes: the electric field poling of the second-order chromophore and the buildup of a space charge field. Nevertheless, the buildup of the photorefractive gratings is in the sub-second domain. Figure 34 also shows the erasure of the

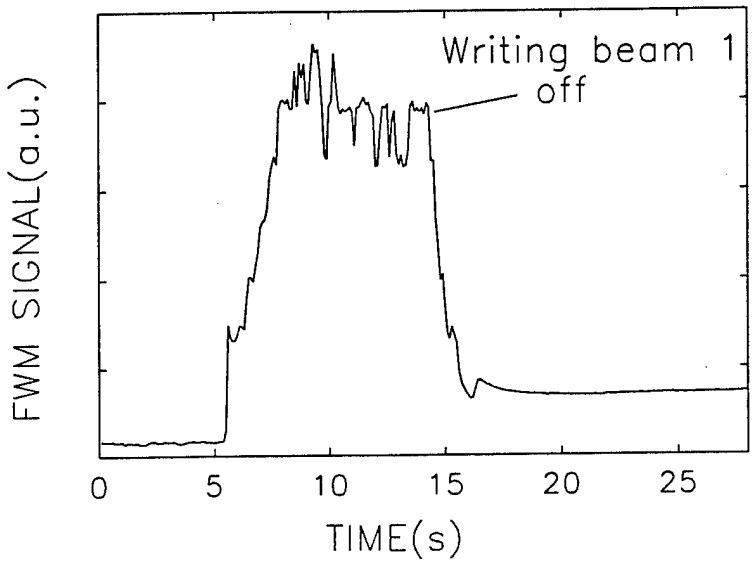

Figure 34 Erasing of a photorefractive grating

gratings by a homogeneous illumination from one of the writing beams as the second writing beam was blocked after the writing of the gratings.

The photorefractive four-wave mixing diffraction efficiency was measured as a function of the applied electric field. Figure 35 shows the electric field dependences of the four-wave mixing diffraction efficiency obtained from a 300 μm thick sample with a *p*-polarized reading beam. A maximum diffractive efficiency of 0.3 % was obtained at an electric field of 600 kV/cm. When the reading beam was *s*-polarized, the diffraction efficiency was 0.04 % at the same electric field. Theoretical calculations predict that the diffraction efficiency with *p*-polarized reading beam to be nine times that with *s*-polarized reading beam, provided that $r_{33}=3r_{31}$.

D.4 TPY/PVK/DEANST composite[30-33]

The samples used for four-wave mixing and two-beam coupling experiments were around 160 μm thick and had absorption coefficients of 14 cm^{-1} at 703 nm and 53 cm^{-1} at 633 nm. Due to the high concentration of DEANST, the composite showed a glass transition temperature (T_g) of 53 °C, considerably lower than that of PVK (T_g = 200 °C). The refractive index, measured

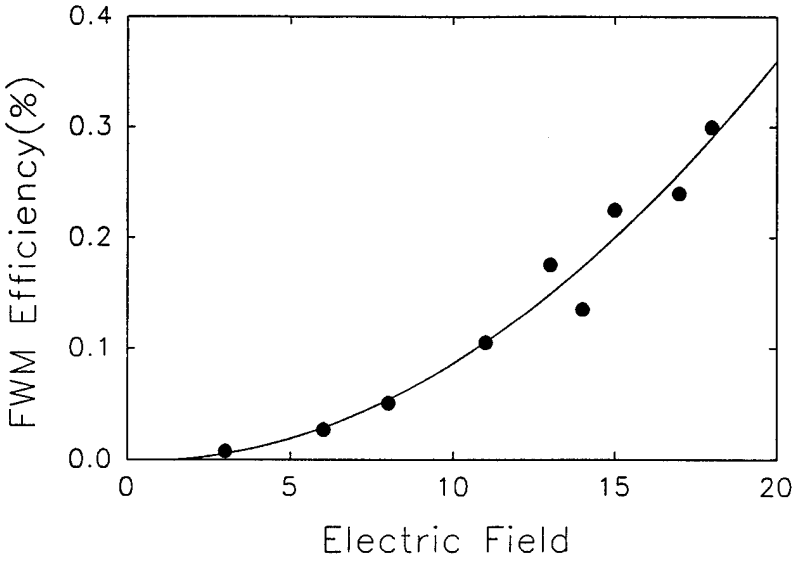

Figure 35 Electric field dependence of the four-wave mixing diffraction efficiency from a BDK/DEANST/PVK composite

using the interference method, was determined to be 1.70 at 703 nm and 1.71 at 633 nm.

A. Electrooptic and photoconductive properties

Due to the low glass transition temperature of the composite, the DEANST chromophore could be effectively aligned at room temperature by applying a strong dc electric field across the sample. This was confirmed by the observation of electrooptic modulation at room temperature when a dc electric field is applied. The EO coefficient was measured as a function of the poling electric field and a linear dependence was obtained up to 100 V/μm, after which the EO coefficient began to saturate, reaching a value of r_{33}= 9.6 pm/V at 135 V/μm, as shown in Figure 36. Dielectric breakdown was observed at fields higher than 140 V/μm. At a field of 62.5 V/μm, the maximum electric field applied in the four-wave mixing experiments, the electrooptic coefficient (r_{33}) was measured to be 4.2 pm/V. The experimentally determined electrooptic coefficient was fitted to Eq. (34) and the result is shown in Figure 36 (solid line).

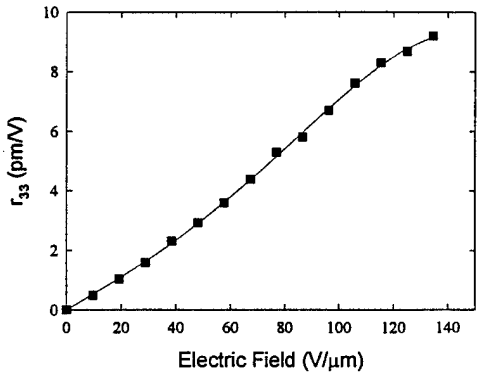

Figure 36 Electric field dependence of the electrooptic coefficient (r_{33}). Filled squares: experimental data; Solid curve: fit to Eq.(1).

The measured dependence of the photocharge generation quantum efficiency on the applied electric field is presented in Figure 37 (filled circles, right ordinate). These data were fitted to the Onsager model (Eq. 20) with a best fit parameter r_0 = 1.5 nm giving a curve shown

by the solid line in Figure 37a. The same data were then fitted to empirical expression $\phi(E) = \phi'_0 E^{\varsigma}$ with $\varsigma = 4.1$ as shown by the dotted line in Figure 37a.

Figure 37a (filled squares, left ordinate) displays an electric field dependence of the photoconductivity sensitivity. The photoconductivity of the composite was also measured as a function of the illumination intensity and the result is presented in Figure 37b. The data can be fitted to a sublinear dependence, $\sigma(I_0) \sim I_0^x$ with a best fit parameter of $x = 0.72$. Assuming that the charge mobility is independent of the illumination intensity, the photocharge generation quantum efficiency can then be expressed as

$$\phi(I_0) = d\, I_0^x \ , \tag{33}$$

where d is a constant. A similar power dependence has been observed in inorganic photorefractive crystals such as barium titanate ($BaTiO_3$)[28] and attributed to the presence of shallow traps (or acceptors). Such a behavior has also been observed in a polymeric composite, although x was much closer to unity ($x = 0.96 \pm 0.02$).[29]

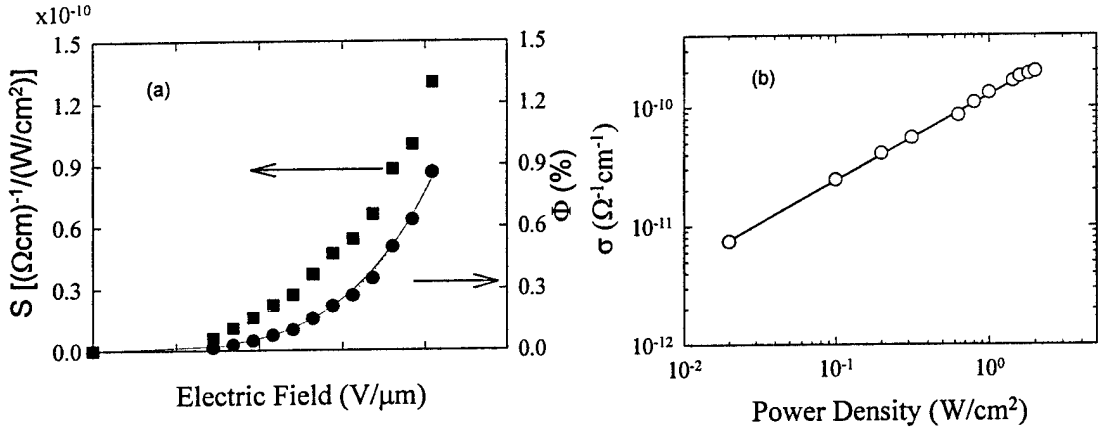

Figure 37 (a) Photoconductivity sensitivity (left ordinate) and photocharge generation quantum efficiency (right ordinate) of a PVK /DEANST/TPY composite as a function of the applied electric field. Solid line: fit of photocharge generation quantum efficiency to the Onsager model (Eq. (20)); Dotted line: fit of quantum efficiency to Eq. (3) with $\varsigma = 4.1$. (b) Dependence of the photoconductivity on the illumination power density on a log-log scale. Solid line: fit to $\phi(I_0) = d\, I_0^x$ with $x = 0.72$.

B. Photorefractive properties

One of the features of the photorefractive effect is the strong electric field dependence of the four-wave mixing diffraction efficiency, as can be seen from Eqs. (17) and (18). The diffraction efficiency for this composite was measured as a function of the external electric field and the dependence is shown in Figure 38a. The diffraction efficiency increases rapidly with the applied electric field and reaches a value of 1.1 % at an external field of 62.5 V/μm. The difference

between this material and permanently poled polymers is that the field dependence of the diffraction efficiency also includes the field dependence of the electrooptic coefficient of the composite, due to its low T_g, as described by Eq. (34):

$$r_{33} = 3r_{31} = -\frac{8\pi f N \beta}{n_0^4}\left[\frac{1}{3}p - \frac{1}{45}p^3 + \frac{2}{945}p^5 - \frac{2}{9450}p^7 + \ldots\right] \qquad (34)$$

where N is the number density of NLO chromophore molecules, β the molecular first hyperpolarizability, n_0 the refractive index, f an appropriate field factor, and $p = \mu_d E/k_B T$ with μ_d being a molecular dipole moment, E the applied electric field, k_B the Boltzman constant and T the temperature. The experimentally measured diffraction efficiency, η_p, was fitted to Eq.(18) (taking into account the field dependence of r_{33} and E_{SC} as given by Eqs. (6) and (8), respectively) giving a best fit value of $b = E_D/E_q = 0.0024$. Therefore, using the calculated drift field, $E_D = 0.105$ V/μm, the limiting space charge field E_q was calculated to be 43.8 V/μm, which corresponds to a trap density of 2.9×10^{16} cm^{-3}. The space charge field was calculated to be E_{SC} = 24.3 V/μm at an external field of 62.5 V/μm. The solid line in Figure 38a shows the fit to Eq. (18). Using the diffraction efficiency value at 62.5 V/μm, the effective EO coefficient (r_{eff}) and

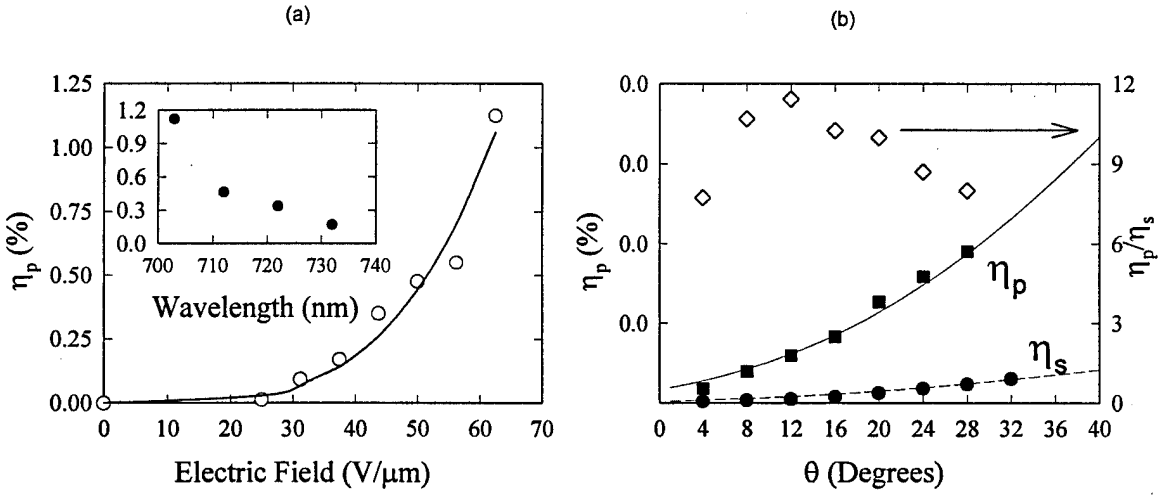

Figure 38 (a) Electric field dependence of the holographic diffraction efficiency. Inset: Dependence of the diffraction efficiency on writing beam wavelength. Filled and open circles: experimental data; Solid line: theoretical fit of the diffraction efficiency to Eq. (18). **(b)** Angular dependence of the four-wave mixing diffraction efficiency for *p*- and *s*-polarized reading beams, respectively. Filled squares and circles are experimental values and solid and dashed lines are theoretically calculated curves. Open diamonds: diffraction anisotropy (η_p / η_s) (right ordinate). The angle between the writing beams outside the material was kept constant at 32°.

r_{33} are calculated to be 1.9 and 4.1 pm/V, respectively, in good agreement with the experimentally determined values (Figure 36). The diffraction efficiency was also measured as a function of writing beam wavelength. The results show that the efficiency follows the absorption profile of the thiapyrylium dye as is seen from Figure 38a (inset).

The second feature of photorefractivity is the diffraction anisotropy in a slanted configuration. We have measured the angular dependence of the diffraction efficiency for both *s*- and *p*-polarized reading beams and the results are shown in Figure 38b (filled squares for *p*- and filled circles for *s*-polarized reading beams, respectively). In the experiment, the angle between the writing beams was kept constant at $\Delta\theta^0 = \theta_2^0 - \theta_1^0 = 32°$. Also shown in the figure are the theoretically (Eq. (18)) calculated dependence of the efficiencies on the incidence angle (solid line for *p*- and dotted line for *s*- polarized reading beams, respectively). The measured anisotropy (η_p/η_s) is shown by the open diamonds (right ordinate). An average value of η_p/η_s=9 ± 1 has been obtained. The relatively large error stems from the slight movement of incidence spot which results in a change in the overlap area between the writing beams. A two-beam coupling (or energy transfer) gain of 7 ± 1 cm^{-1} was obtained at 62.5 V/μm.

The third feature of the photorefractive effect, which distinguishes itself from many other mechanisms that may result in refractive index gratings, is the finite phase shift between the refractive index grating and the interference pattern, as seen in Eqs. (14) and (15). This finite phase shift, or the nonlocal nature of the photorefractive effect, causes an asymmetric energy transfer between the writing beams, a unique process which does not occur in any of the other processes. Therefore, the photorefractive nature of the composite can be further confirmed by the asymmetric energy transfer in two-beam coupling experiments. First, the intensities of the writing beams were monitored as the electric field was turned on and off. An energy transfer is evidenced by the increase in the intensity of Beam 1 and decrease in that of Beam 2. When the electric field was turned off, no intensity changes were observed. Two more experiments were carried out in order to observe the growth of the space charge gratings in the presence of the applied field. The intensity of Beam 1 was monitored while Beam 2 was open and then blocked and the same experiment was repeated for Beam 2; Figure 39 shows the change in the beam intensities. The two-beam coupling gain is calculated using the following equation:[11]

$$\Gamma = \frac{\cos\theta}{L}\left[\ln(\gamma_0\xi) - \ln(\xi + 1 - \gamma_0)\right] \tag{35}$$

where ξ is the ratio of the beam intensities and $\gamma_0 = P/P_0$ is the beam coupling ratio where P_0 is the detected signal without the pump beam and P is the signal with the pump beam on. A two-beam coupling (or energy transfer) gain of 7 ± 1 cm^{-1} was obtained at 62.5 V/μm.

C. Dynamics of the grating formation and erasure

The growth of photorefractive index grating (Eq. (10)) can be rewritten as:

$$E_{SC} = E_{SC}^0\left[1 - \exp(-t/\tau_e)\right] \tag{36}$$

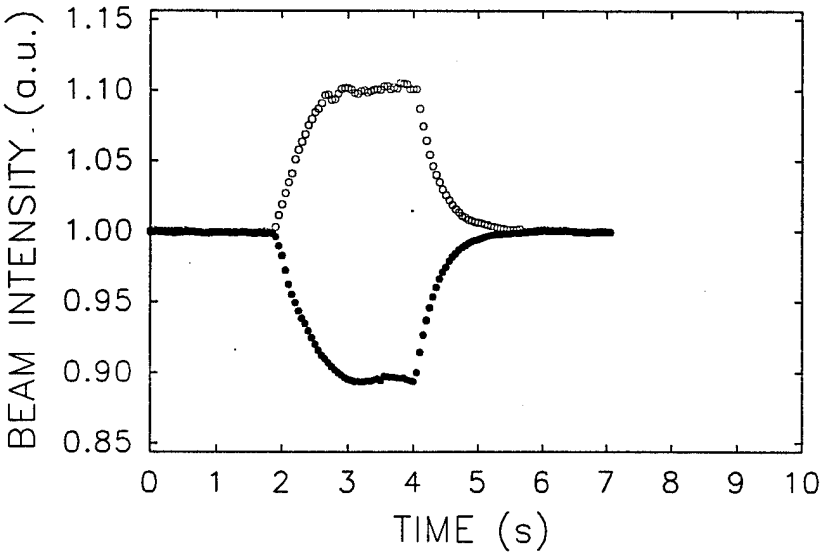

Figure 39 Energy transfer in a two-beam coupling experiment

where E^0_{SC} is the saturation space charge field and τ_e is the space-charge-field buildup constant which is proportional to the material's dielectric relaxation time τ_{di} given by:

$$\tau_e = a\tau_{di}, \qquad \tau_{di} = \frac{\epsilon}{4\pi e\mu N_0} \tag{37}$$

provided that the recombination time is much shorter than the dielectric relaxation time. In Eq. (37), a is a proportionality constant, μ is the photocharge mobility, and N_0 is the number density of photocharges which is dependent on the illumination intensity and photocharge generation quantum efficiency through:

$$N_0 = N_s \frac{\phi(I_0)}{hc/\lambda} \tag{38}$$

where h is the Planck constant, c is the speed of light, and λ is the laser wavelength.

While the applied electric field was kept constant, the writing time constant was measured as a function of the writing beam intensities and the erasure time constant measured as a function of the erasing beam intensities. The results are presented in Figure 40a where, on a log-log scale, the inverse of the writing time constant ($1/\tau_e$) is plotted against the writing beam intensity (filled squares) and that of the erasure time constant ($1/\tau_{er}$) plotted against the erasing beam intensity (open circles). The data were fitted to a model $\tau \sim I_0^y$ with best fit parameters of $y = 0.40$ and $y = 0.33$ for the writing and erasure times, respectively; both are considerably smaller than unity. This sublinear dependence can be explained by the sublinear photoconductivity in the material as

described earlier, although these parameters differ from the power dependence parameter of the photoconductivity where $x = 0.72$ was obtained. As comparison, similar power dependence for the writing time has been observed in a fullerene doped photorefractive polymer with $x = 0.35$,[34] although no photoconductivity data were available in that case.

The dark decay of the space charge grating was measured as follows. First, an electric field of 62.5 V/μm was applied and the writing beam were open, establishing a space charge field. Then all beams were blocked. A weak reading beam was repeatedly open for less than 100 ms at time intervals of ~ 5 s and the diffracted signal was monitored. The grating decay time constant was measured to be about 8 s. This relatively fast dark decay is due to the shallow traps present in the material and could be improved by the addition of deep traps.[35]

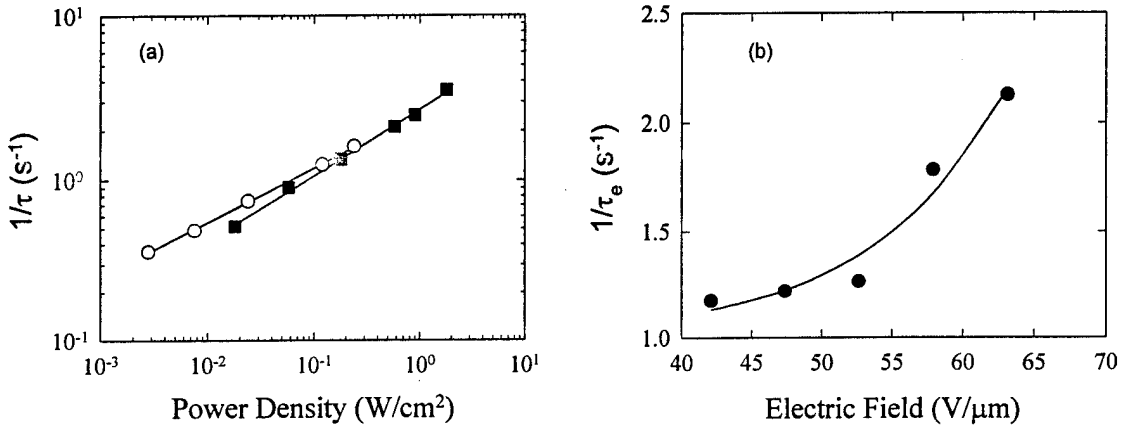

Figure 40 Dynamics of the formation and erasure of the space charge fields. (a) Dependence of writing time on writing beam intensities (filled squares) and that of erasure time on erasing beam intensity (open circles) on a log-log scale. Solid and dotted lines: fitting to $\tau^{-1} \sim I_0^y$ with $y = 0.40$ and 0.33 for the writing and erasure processes, respectively. (b) Dependence of the writing time on the applied electric field. Filled squares: experimental data; Solid line: fit to Eq. (37) taking into account the field dependence of the photocharge generation quantum efficiency and that of the charge mobility.

Eq. (37) also suggests that the writing time is dependent on the applied electric field since the photocharge generation is field dependent (see Eq. (20)). The charge transporting properties of PVK have been studied by many authors;[22,-23, 36-37] the charge mobility is both electric field and temperature dependent and can be described by the empirical expression as in Eq. (23).
The dependence of the writing times on the applied electric field strength was confirmed by the results of a measurement of the writing times at various applied electric fields as depicted in Figure 40b. In this measurement, the writing and reading beam intensities were kept constant while the electric field was varied. Taking into account the field dependence of photocharge generation quantum efficiency (Eq. (20)) and that of the charge mobility (Eq. (23)), the measured data were fitted to Eq. (37) with a best fit curve shown by the solid line.

D. Holographic image recording and retrieval

A driving force behind the research in photorefractive materials is the potential use of these materials in applications such as high volume data storage and information processing, including image amplification, image reconstruction, etc. To simply demonstrate the capability of this material to perform these functions, we have performed image recording and retrieval in the material presented. The setup is similar to that presented in Figure 18. One of the writing beams (Beam 2) was expanded to about 10 mm in diameter using a telescope. The image to be recorded (Figure 41a) was placed in the expanded beam which was then collimated using another identical telescope. The recorded image was then read by a He-Ne reading beam and captured by a photographic camera on a black and white film. The result is presented in Figure 41b.

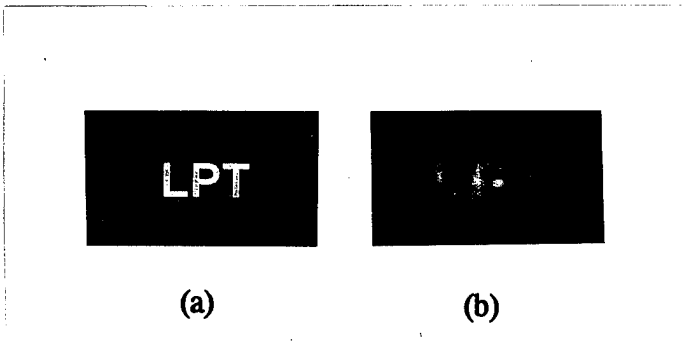

Figure 41 Holographic image recording and retrieval: (a) image recorded; (b) image retrieved.

E. Effect of dye concentration on the photorefractive responses

The effect of the sensitizer dye concentration on the photorefractive responses was studied by varying the dye concentration in the range of 0.1 ~ 0.3 % and measuring the writing times of the space charge gratings. It is clear, from the results presented in Figure 42, that higher concentration of the photosensitizer improves time responses of the photorefractive effect. However, optical density (absorption) of the composite material increases in the same time resulting in a lower value of the energy transfer gain and, perhaps, undesired thermal effects. It is, thus, important to optimize the dye concentration so that PR responses are enhanced, but not at a cost of excessive absorption losses.

F. The trapping effect on the photorefractive responses

In the case of photoconductive polymer composites consisting of an inert polymer matrix doped with charge transporting agents and a photosensitizer, the charge transporting molecules (CTM), such as triaryl amine (TAA), form a connected network throughout the matrix so the transport can ensue by holes hopping from molecule to molecule. The donation of a photogenerated charge (hole) to the charge transporting network can only occur when ionization potential, E_I, of the photosensitizer is larger than that of CTM. For intentionally introduced trapping molecules, their E_I must be smaller than E_I of CTM by more than the Boltzman energy, k_BT, in order for the traps to be effective.

This process can be illustrated on PVK, a photoconductive polymer matrix, and triaryl amine

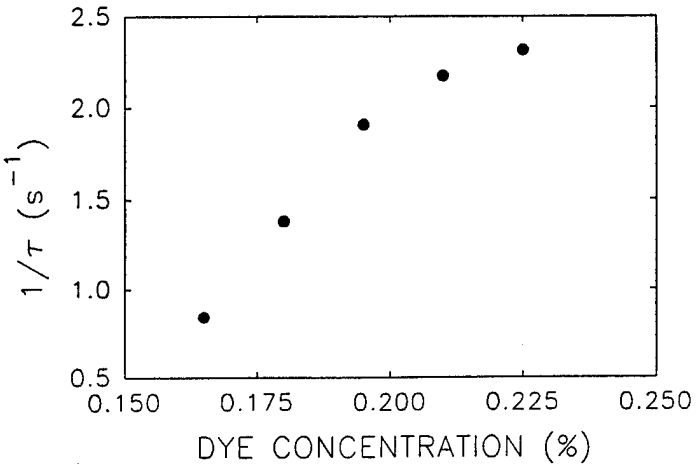

Figure 42 Dependence of the writing time on the sensitizer dye concentration

sample. The ionization potentials of PVK and TAA can be qualitatively determined from the strength of charge transfer complexes with an electron acceptor according to the following equation:[23,36]

$$\upsilon(eV) = aE_I - b \tag{39}$$

where υ is the energy of the lowest energy charge transfer band, E_I is the ionization potential of the donor, and a and b are constants. The results obtained for TAA and PVK are presented in Table II. From these values it appears that the difference in ionization potential is large. Since E_I of TAA is lower by about 0.5 eV, TAA is expected to act as a trap for hole transport in PVK. Thus, it is expected that the addition of a *very small amount of another hole transporting dopant* (such as TAA) with a lower oxidation potential than that of the main hole transporting material will result in the formation of trap sites. The carriers in transit will stop at the site of the molecules with lower oxidation potentials and will be released when a neighboring neutral molecule gains statistically enough thermal energy to release an electron and move it to the site of the trap. This process is illustrated in Figure 43. When the concentration of such a dopant exceeds certain limit (usually about 0.6%), the hole transport process will ensue through both, the dopant and the PVK; if the dopant concentration is close to that of the conducting matrix species, the hole hopping process will proceed exclusively via lower ionization potential dopant molecules.

The trapping effect on the photorefractive responses was studied by measuring the buildup and decay speeds of the space charge gratings in a four-wave mixing experiment using the setup as described in the experimental section of this report. The holographic gratings were written by two laser beams of equal intensity (1 W/cm^2) from an Ar^+ laser pumped Ti:Sapphire laser operating at 703 nm and read by a much weaker (6 mW/cm^2) He-Ne laser beam at 633 nm. All measurements were performed with the same writing beam intensity and external electric field (25 V/μm). The writing process was modeled using Eq. (36). The dark decay was modeled according to $E_{SC} = E_{SC}^0 e^{-t/\tau}$.

Table I Ionization potentials according to Eq. (39).

charge transfer complex	υ, eV	E_I, eV
TAA/TCNE	**1.63**	**7.1**
PVK/TCNE	**2.06**	**7.6**

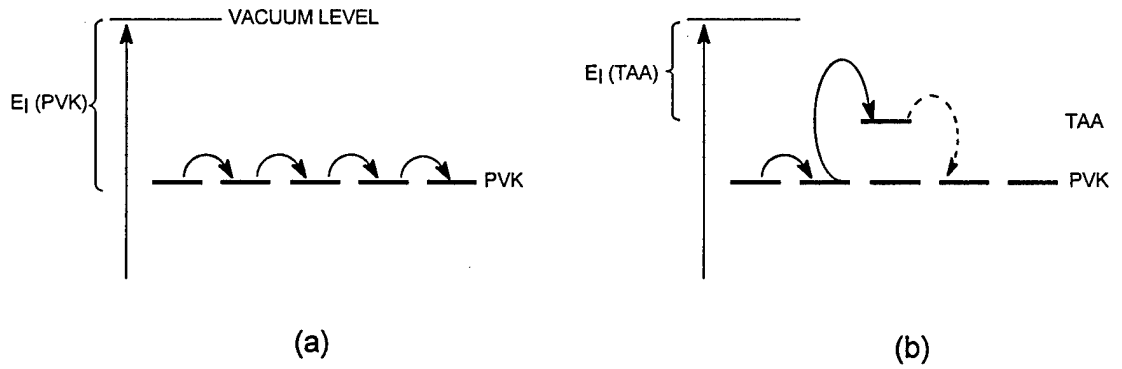

Figure 43 Formation of trapping sites by a low ionization potential molecule (TAA) dispersed in a high ionization potential matrix (PVK): (a) hole hopping without dopant; (b) hole hopping in the presence of a small amount of low ionization potential dopant.

A series of samples with various concentrations of the trapping molecules were prepared and the writing times and dark decay time constants were measured. The results are presented in Figure 44 where the inverse of the writing time and that of the dark decay time constant are plotted against the number density of the trapping molecules on a semi-log scale. It is clearly seen that the writing time and the dark decay time first increase as the concentration of the trapping molecules is increased, reaching a maximum at N_T=7.5x10^{18}cm^{-3}, and then decrease as the concentration of trapping molecules increases further. These two curves both resemble the dependence of the charge mobilities on the trapping number density since the writing time is related to the charge mobility (μ) by $\tau^{-1} = 4\pi e\mu N_0/\epsilon$ where e is the electron charge, N_0 the number density of photocharges and ϵ the material's dielectric constant.

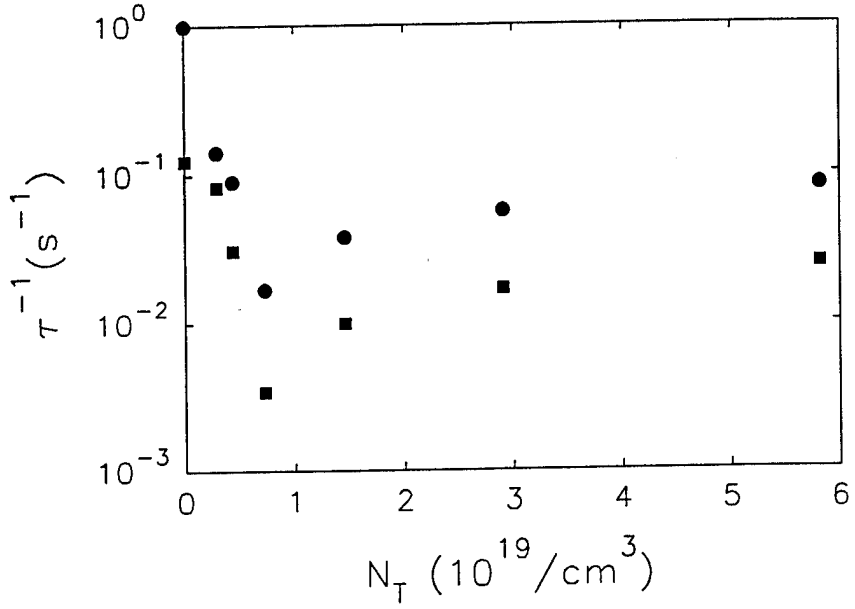

Figure 44 Dependence of the holographic grating writing time (circles) and dark decay time (squares) on the concentration of trapping molecules.

The results of this work indicate that the addition of a small amount of the triphenylmathane molecules, with a lower ionization potential than that of the charge transporting molecule (PVK), greatly reduces the charge mobility and, as a consequence, *increases the dark decay time* of the photorefractive grating. The effect on the response time of the photorefractive gratings is less pronounced, although there is an observable increase of the writing and erasure times. Both the charge mobility and the photorefractive responses show strong dependence on the concentration of the trapping molecules. Therefore, by properly adjusting the concentration of a trapping molecule, the writing time and the dark decay of the space charge gratings can be judiciously controlled. There is a large number of triphenylmethane derivatives and other charge transporting agents with various ionization potentials which can be used as trapping molecules. Therefore, the study of the trapping effect on the photorefractive properties should be extended to incorporate these molecules in order to improve the storage time of the photorefractive polymeric composites.

D.5 Conclusions

In summary, we have studied the electrooptic, photoconductive and photorefractive properties of a novel doped polymeric composite based on charge transporting polymer (PVK) containing several different photocharge generators and NLO chromophores. The composite sensitized with thiapyrylium dye and doped with DEANST as second-order NLO chromophore showed the best photorefractive performance in terms of diffraction efficiency and response rates. The linear electrooptic response is obtained by the application of a strong dc electric field at ambient temperature since the second-order NLO chromophores can be effectively aligned

owing to the low glass transition temperature of the composite. The strong electric field dependence of the four-wave mixing diffraction efficiency and the asymmetric energy transfer between the writing beams confirm the photorefractivity in this composite. The dynamics of the formation and erasure of the holographic gratings show a sublinear dependence of both the writing time on the writing beam intensity and the erasure time on the erasure beam intensity at the same power levels, in good agreement with theoretical predictions. These sublinear dependencies can be explained by the apparent sublinear photoconductivity of the material which is described as a result of the shallow traps inherent to the material. The grating writing time also shows a strong dependence on the external electric field because the photocharge generation quantum efficiency and the charge mobility in the material are both electric field dependent. The potential of this material as an optical data storage and image processing medium has been explored. However, the dark storage time in the studied composite is rather short; the space charge field decays with a time constant $\tau \sim 8$ s. In an attempt to increase this dark storage time, trapping molecules (those with ionization or oxidation potentials lower than that of the charge transporting agent, PVK) have been added to the composite. The results of the trapping effect on the photorefractive responses will be presented elsewhere[36] along with the studies of the effect of the composition on the photorefractive responses.

It should be pointed out that orientational enhancement of photorefractivity, as predicted by a recently developed model for low T_g polymers,[38] was not observed in this composite. No higher order ($2K_G$, $3K_G$, ...) gratings were detected. The measured diffraction anisotropy (9 ± 1) and the lack of higher order gratings imply that the orientational enhancement, if any, is too weak. The fact that the T_g of the composite (53 °C) is still much higher than the operating temperature may serve to explain these observations. Further investigation of this enhancement can be performed by employing a higher level of DEANST doping, which will further reduce the composite's T_g.

There exists great potential for the thiapyrylium dyes being used as sensitizers in photorefractive composites. As mentioned above, the aggregates formed between these dyes and polycarbonate dramatically increase the photocharge generation quantum efficiency. If such aggregates are used in photorefractive composite materials, one would expect a substantial decrease in the response (writing) time and an increase in the achievable space charge field and, consequently, the strength of the material's photorefractive response. Another advantage of using the thiapyrylium dye aggregates is that the absorption maximum is red shifted, enabling photorefractivity in the near IR wavelength region.

The results of photorefractivity studies in composite materials being developed in LPT, Inc. are summarized in Table II. It presents the material parameters as recommended by the protocol presented during the AFOSR Organic Photorefractivity Program Review Meeting at Hanscom Field, MA, June 2, 1992.

Table II. Experimental data obtained in photorefractive Four Wave Mixing studies on PVK based composite materials developed in LPT, Inc.

Composite	ϕ_{max} (%)	η_{max} (%)	τ_r (s)	τ_{er} (s)	I_1, I_2 (W/cm^2)	$n^3 r_{eff}^*$ (pm/V)	L (μm)
TiO_2 PVK DEANST C_{60}	2	0.005	-	-	0.24	4.1	100
PVK DEANST/NPP TPY	-	0.08	< 1	< 0.5	0.5	3.5	100
PVK DEANST BDK	0.4	0.3	2	1.6	0.24	2.5	300
PVK DEANST TPY	0.9	1.25	0.5	0.6	1.8	4.2[a]	120

LEGEND:

ϕ_{max} maximum quantum efficiency of photocharge generation
η_{max} maximum holographic diffraction efficiency
τ_r raise time of the holographic grating to saturation in seconds
τ_{er} erasure time of the holographic grating in seconds
I_1, I_2 illumination intensities in W/cm^2
$n^3 r_{eff}^*$ electrooptic coefficient in pm/V
L thickness of the sample in μm

* Electrooptic coefficients estimated from four-wave mixing diffraction efficiencies using Eqs. 10 to 12.
[a] Electrooptic coefficient measured on thin film at a field of 65V/μm.

2.7.2 Composites based on inert polymer matrices[39,40]

Polycarbonate was chosen as a host polymer because of its excellent compatibility with a variety of charge transporting molecules. The second-order NLO chromophores used were PRODAN and NPP; their selection was based on their wide-band transparency. The absorption maxima of PRODAN and NPP are at 290 nm and 391 nm, respectively, thus minimizing the absorption at the operating wavelengths. Tris-*p*-tolylamine (TTA) was used as a charge transporting agent.

A. General properties

The absorption spectra of NPP and PRODAN in chloroform as well as that of the composites (100 μm thick samples) were recorded on a Shimatzu UV-VIS spectrometer and are shown in Figure 45. The absorption coefficients of the composites at the operation wavelengths are summarized in Table III. It is clear that the chromophores used for this study have very wide transparancy bands and can be used over a wide range of wavelengths for photorefractive applications without considerable absorption resulting from the chromophores themselves.

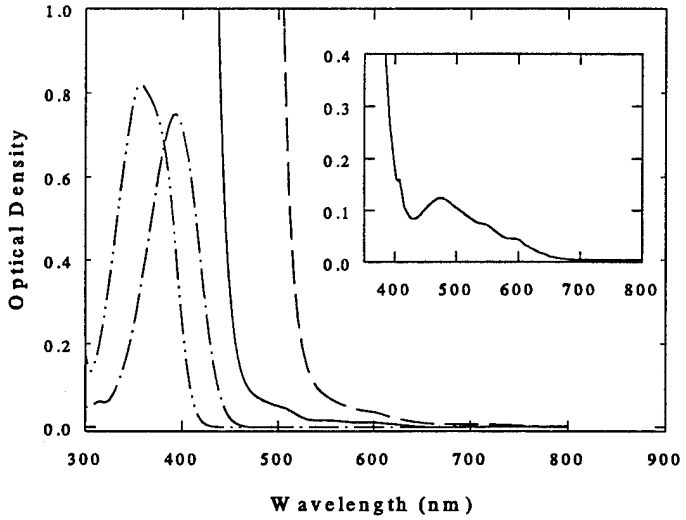

Figure 45 Absorption spectra of the molecules and composites used in the present studies. Dash-dot-dot-dash line: PRODAN in chloroform; Dash-dot-dash line: NPP in chloroform; Solid line: the PRODAN/TTA/PC/C_{60} composite; dashed line: the NPP/TTA/PC/C_{60} composite. Inset: absorption spectrum of the photocharge sensitizer (C_{60}) in toluene.

Table III. Properties of the photorefractive composite materials: glass transition temperature (T_g), absorption coefficients (α), maximum diffraction coefficients (η_{max}), and maximum two-beam coupling gains (Γ_{max}).

Composite	T_g(°C)	λ(nm)	α(cm^{-1})	η_{max} (%) [E, V/μm]	Γ_{max} (cm^{-1}) [E, V/μm]
PRODAN/TTA/PC/C_{60}	67	633	0.1	1.4 [80][a]	13 [70][a]
		515	0.74	0.6 [80][a]	14 [85][a]
		488	12	Not measured	25 [85][a]
NPP/TTA/PC/C_{60}	50	633	0.4	14 [75][b]	20 [42.5][b]
		515	7.6	8.8 [76][b]	Not measured

a. Sample thickness: 140 μm.

b. Sample thickness: 100 μm.

Eq (34) gives the field dependence of the electrooptic coefficient. The experimentally determined electrooptic coefficients were fitted to Eq. (34) and the result is shown in Figure 46(a) (solid lines). The photoconductivity (σ) and the photoconductivity sensitivity (S) of the material are calculated using the experimentally measured photocurrent (I_{ph}) flowing through the film using[30]

$$\sigma = \frac{L}{AV/I_{ph}} \quad and \quad S = \sigma/I_0 \ , \tag{40}$$

respectively. Here L is the sample thickness, A the illumination area (the same as the silver electrode area), V the applied dc voltage, and I_0 the illumination laser power density. A Log-Log plot of the photoconductivity sensitivity versus square root of the applied field is shown in Fig. 46(b).

The photorefractive properties of these composites were evaluated by previously reported four-wave mixing and two-beam coupling experiments.[30-33] Holographic gratings were written at three different wavelengths: 633, 514.5 and 488 nm. Two *s*-polarized writing beams of approximately equal intensities intersect in the sample at incidence angles of 45° and 60° (in air), respectively, creating gratings with a spacing of approximately 3.4, 2.9 or 2.6 μm for the three wavelengths respectively. The reading beam, either from another He-Ne laser at 633 nm with an intensity of 2 mW/cm^2 or from a diode laser at 670 nm with an intensity of 3.5 mW/cm^2, propagates in the direction opposite to one of the writing beams. The diffracted signal is reflected off a beam splitter and detected by a photodiode. The 633 nm writing beam intensities

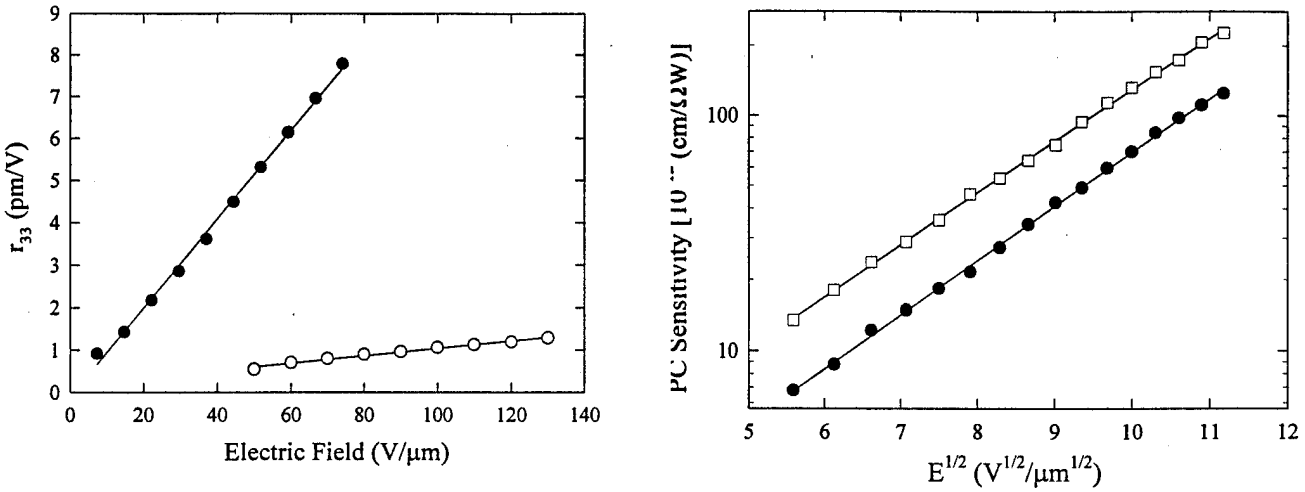

(a) (b)

Figure 46 Electric field dependence of the electrooptic coefficients (a) and photoconductivity sensitivity (b) of the composites. Open circles: the PRODAN/TTA/PC/C_{60} composite; Filled circles: the NPP/TTA/PC/C_{60} composite. Solid lines are linear regressions.

were 220 and 230 mW/cm^2 for beams 1 and 2, respectively. The writing beam intensities at 514.5 and 488 nm were 30 and 32 mW/cm^2, respectively. For two-beam coupling measurements, the intensities of the writing beams were monitored while the applied electric field was turned on and off. The same energy transfer is also observed by noting the increase (or decrease) of one beam's intensity while the other writing beam is open and blocked.

B. Photorefractive properties

Samples for four-wave mixing and two-beam coupling measurements have been prepared with different thicknesses. Since the four-wave mixing diffraction efficiency depends qudratically on the thickness, all diffraction efficiency data in this report have been normalized to a thickness of 100 μm.

1. The PRODAN/TTA/PC/C_{60} composite

The photorefractive properties of the PRODAN/TTA/PC/C_{60} were studied at three wavelengths: 633, 514.5, and 488 nm. The four-wave mixing diffraction efficiency at two different wavelengths (633 and 514.5 nm) and the two-beam coupling gain at all three wavelengths are presented in Figure 47. The writing beam power intensities at 633 nm were 220 and 230 mW/cm^2 for beams 1 and 2, respectively. The corresponding writing beam intensities for the 514.5 and 488 nm wavelengths were 30 and 32 mW/cm^2 for beams 1 and 2, respectively.

FWM diffraction efficiency at 633 nm was measured to be about twice that at 514.5 nm.

The absorption coefficients of this composite are 0.1, 0.74 and 12 cm^{-1} at 633, 514.5 and 488 nm, respectively. As the data in Figure 47(b) show, net two-beam coupling gains have been obtained at all three wavelengths since the TBC gains exceed the absorption. At 633 nm, this occurs at an electric field of 25 V/μm (the lowest field applied). Net TBC gains were obtained at fields above 30 V/μm (at 514.5 nm), above 50 V/μm (at 488 nm).

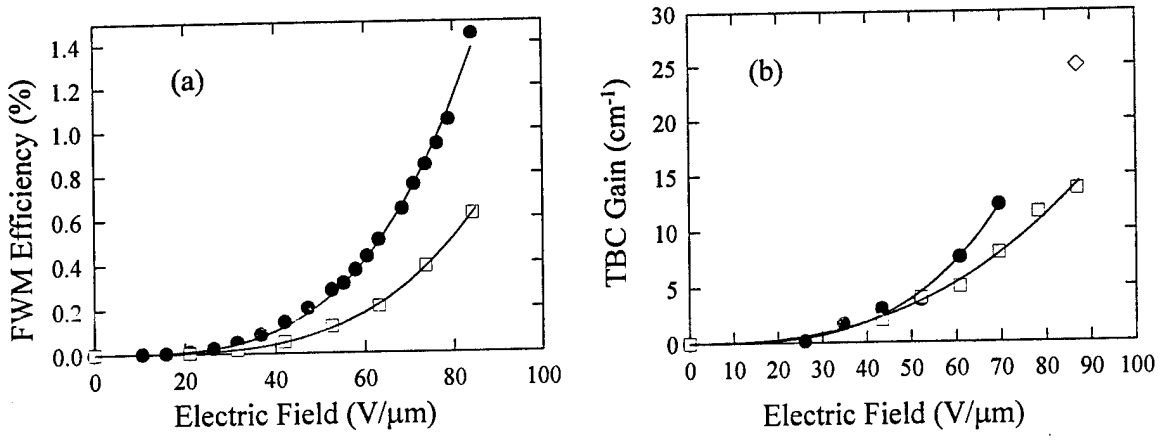

Figure 47 Electric field dependence of the four-wave mixing diffraction efficiencies (a) and two-beam coupling gains (b) for the PRODAN/TTA/PC/C_{60} composite at various wavelengths: 633 nm (filled circles), 514.5 nm (open squares), and 488 nm (open diamond). The solid lines in (a) are a theoretical fit to Eq. (18).

2. The NPP/TTA/PC/C_{60} composite

Because of the strong absorption from NPP at wavelengths below 500 nm, the photorefractive properties of composites containing NPP were studied at 633 and 514.5 nm only. The four-wave diffraction efficiency at two different wavelengths, 633 and 514.5 nm, and the two-beam coupling gain at all three wavelengths are presented in Figure 48. Again, almost the same diffraction efficiency was obtained at 514.5 and 633 nm with much lower writing beam intensities at 514.5 nm. Net TBC gains have been obtained at 633 nm at all fields at which the TBC experiments were carried out.

Photorefractivity is a complex process and the four-wave mixing diffraction efficiency and two-beam coupling gain depend on a variety of parameters such as photoconductivity and electrooptic coefficients. Despite the different power levels used at 514.5 and 633 nm, virtually the same diffraction efficiency and two-beam coupling gains have been obtained at these wavelengths, for both the PRODAN- and NPP-containing composites. This results from two processes. The photocharge generation sensitizer, C_{60}, has an absorption coefficient at 514.5 nm three times higher than that at 633 nm. The higher absorption coefficient at 514.5 nm results in a larger photoconductivity, a stronger space charge field (because of the larger number of charges) and, consequently, a higher diffraction efficiency (if the same writing laser intensity is used). The second process which may contribute to the higher diffraction efficiency at the shorter

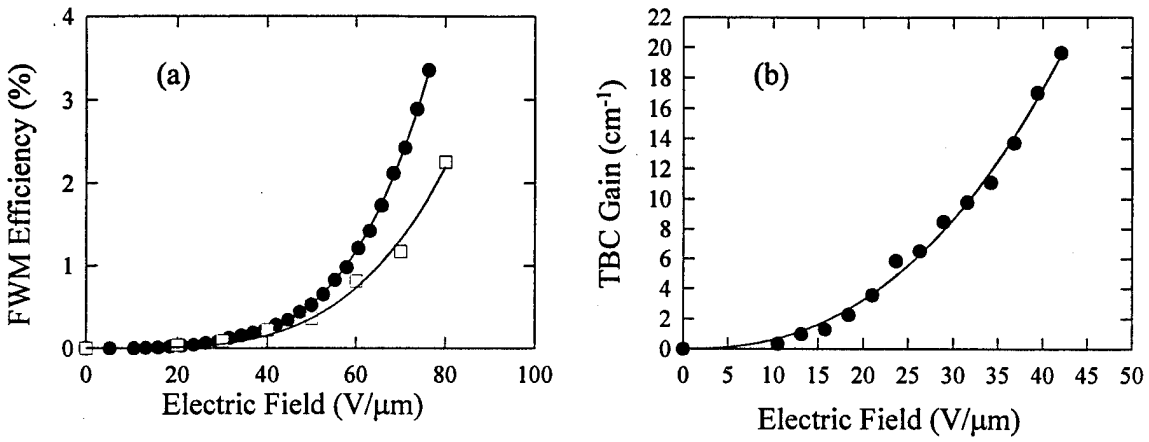

Figure 48 Electric field dependence of the four-wave mixing diffraction efficiencies (a) and two-beam coupling gains (b) for the NPP/TTA/PC/C_{60} composite at two wavelengths: 633 nm (filled circles) and 514.5 nm (open squares). The solid lines in (a) are theoretical fit to Eq. (18).

wavelength is the dispersion of the second-order nonlinearities of the chromophores which results in a higher electrooptic coefficients at wavelengths closer to the absorption peaks of the chromophores.

C. Conclusions

The photorefractive properties of a new series of composite materials have been prepared and tested. The composite photorefractive materials contain an inert polymer binder (polycarbonate) which is doped with three components, each providing a different function necessary for photorefractivity. Charge photogeneration is facilitated by doping a sensitizer, fullerene (C_{60}). The charge transporting and second-order properties are provided by two separate molecules, TTA and either NPP or PRODAN, respectively. Owing to the high bandgap of the NLO chromophores, these composites can be used in a wide range of wavelengths. We have demonstrated, for the first time to our knowledge, photorefractive responses in polymers at a wavelength as short as 488 nm. Diffraction effciencies in excess of 10% (and as much as 20%) were recorded for 150 μm thick composite film containing NPP as a chromophore at 633 nm wavelength. Net two-beam coupling gains above 20 cm^{-1} have been obtained at wavelengths above 500 nm.

These new photorefractive composites exhibit great promise for practical applications because of the high photorefractive figure of merit, high optical quality of the polymer used and its widespread commercial availability. In addition, these materials show photorefractive responses in a wide range of wavelengths that makes them even more attractive for further development as practical photorefractive polymeric composites.

2.7.3. Bi-functional chromophores[41, 42]

Most of the reported polymeric photorefractive materials fall into one of the following three categories: (1) second-order NLO polymers doped with charge transporting agents,[43-49] (2) photoconductive polymers doped with second-order NLO chromophores,[30-33, 50-52] and (3) inert polymer matrices doped with charge transporting agents and second-order NLO chromophores.[39-40, 53] There are inherent problems of phase separation in all of these systems which adversely limits the chromophore concentration and, thus, the value of the achievable electrooptic coefficient. Consequently, the photorefractive efficiencies and figures-of-merit are limited. This problem is further amplified in the third case since the incorporation of CTA may additionally limit the concentration of the second-order chromophores. The ideal solution lies, perhaps, in the design and development of a fourth class of materials known as multifunctional PR polymers[54-56] where all required functions are provided by a single molecule and phase separation can thus be avoided. Although the approach is a sound one, the photorefractive efficiencies reported for such materials developed thus far have been very low for unclear reasons.[54-56]

Another drawback associated with the above described doped systems lies in the competing process between the achievable EO coefficient and the charge mobility. In the case of second-order chromophore doped photoconductive polymers, an increase in chromophore concentration results in lower charge mobilities and, therefore, slower photorefractive responses. In the case of CTA doped second-order NLO polymers, an increase in CTA concentration leads to a decrease in the effective number density of the NLO moiety and, thus, the achievable EO coefficient and, consequently, the photorefractive figure-of-merit. Recently bi-functional chromophores which possess second-order NLO and charge transporting properties have been reported.[41, 42, 57] Combining both second-order NLO and charge transporting properties in a single molecule, an increase in the chromophore concentration will not only increase the achievable EO coefficient, but also increase charge mobility. Therefore, higher photorefractive figure-of-merit and faster response can be simultaneously obtained.

In this section we report the observation of photorefractivity in polymer composites containing bi-functional chromophores, DPANST and DPANS (see Fig. 8 for molecular structures).[41, 42] The second-order NLO effect of the chromophores arises from the conjugated structures terminated by a donor (amine) group and an acceptor (nitro) group, and the charge transporting ability stems from the triphenylamine moiety. The second-order NLO properties and charge transporting abilities are evidenced by the concentration dependence of both the electrooptic responses and the photoconductivity of composites containing these chromophores. These chromophores were incorporated into an inert polymer and sensitized by a photocharge generation compound to form photorefractive composites. The dependence of the four-wave mixing diffraction efficiency, the holographic grating writing rate, and the two-beam coupling gain on the applied electric field all prove the photorefractive character of the developed composite materials.

While most of the publications on photorefractive polymers have focused on the electric field dependence of the above parameters, little attention has been paid to the effect of the concentration of either the second-order NLO chromophore or the CTM on the photorefractive performances. This is partially because of the complicated processes involved in the photorefractive phenomenon as mentioned above. The use of the bi-functional chromophores presented in this paper has permitted us to simultaneously increase or decrease the concentration

of both CTM and second-order chromophores and to establish a quantitative relationship between chromophore concentration and a variety of the photorefractive parameters including EO coefficient, photoconductivity, holographic four-wave mixing (FWM) diffraction efficiency, and grating formation dynamics.

A. Linear optical properties

Figure 49 shows the absorption spectra of the bi-functional chromophores in chloroform solutions. The absorption peaks for DPANST (BF-1) and DPANS (BF-2) are at 435 and 429 nm, respectively. The absorption coefficients of the composites containing these chromophores are summarized in Table IV.

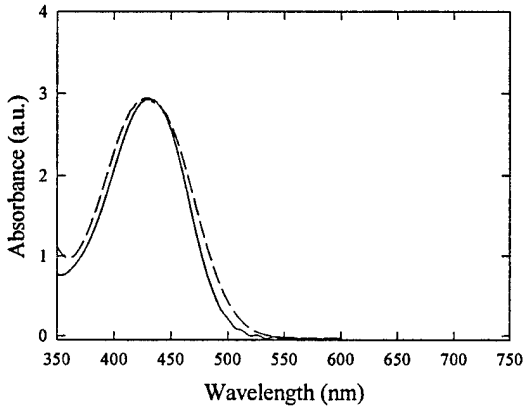

Figure 49 Absorption spectra of the bi-functional chromophores in chloroform. Solid line: DPANST; dashed line: DPANS.

B. Electrooptic coefficients

The electrooptic response of the composites arises from the electric field induced alignment of the chromophores. Because of the low glass transition temperature of the composites, the chromophores can be easily aligned at room temperature by the applied dc electric field. For each of the bi-functional chromophores, we have prepared a series of composites with various chromophore concentrations and performed electrooptic coefficient measurements. Typical electric field dependence of the EO coefficients are presented

Table IV Absorption coefficients of the composites at 633 nm for various chromophore concentrations.

Chromophore Concentration (wt.%)	Absorption coefficients (cm^{-1})		Diff. eff. η (%)		Gain, Γ (cm^{-1})	
	BF-1	BF-2	BF-1	BF-2	BF-1	BF-2
10	11	10	0.1#	0.05		
22	15	12	0.6	0.9		
36	20.7	20*	0.5##	3.8‡	24	26*

* chromophore concentration: 33 wt.%
\# chromophore concentration: 15 wt.%
measured at field of 40 V/μm
‡ measured at field of 60 V/μm

in Figure 50 (a) for each of the composites. Solid lines in Figure 50 (a) show the numerical fit of experimental data to Eq. (34). This equation also suggests a linear dependence of the

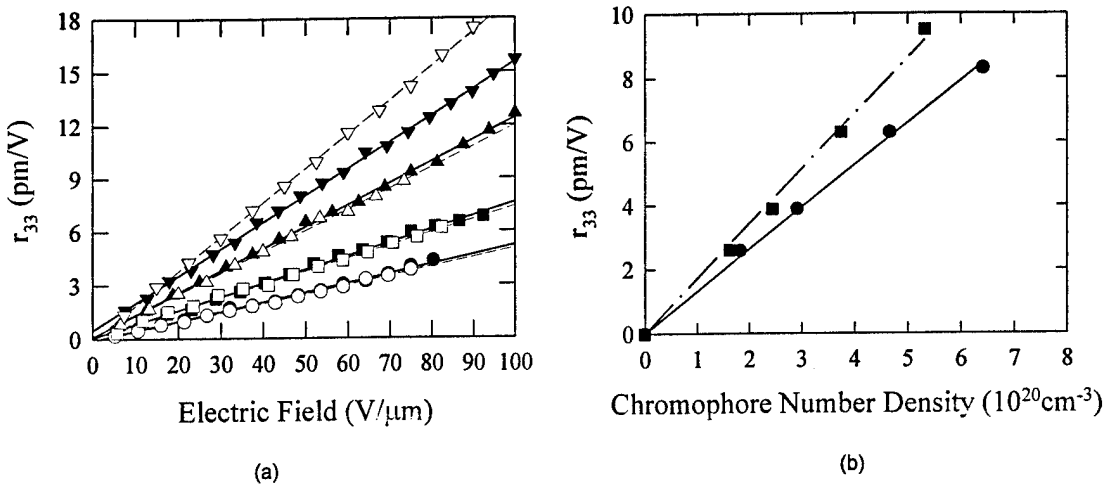

Figure 50 (a) Electric field dependence of the electrooptic coefficients for composites containing various amounts of the chromophores, DPANST (BF-1) or DPANS (BF-2). Filled symbols are for BF-1; circles: 10 %, squares: 15 %, triangles: 22 %; inverse triangles: 34 %. Open symbols are for BF-2; circles: 10 %, squares: 15 %, triangles: 22 %; inverse triangles: 34 %. (b) Dependence of the electrooptic coefficients on the chromophore number density. Circles: BF-1; Squares: BF-2. All data for an electric field of 50 V/μm.

electrooptic coefficient on the number density of the second-order chromophores. Figure 50 (b) displays the concentration dependence of the EO coefficients for BF-1 and BF-2 at an electric field of 50 v/μm. A linear dependence has been obtained for both BF-1 and BF-2 with slopes of 1 and 1.2, respectively. This is in good agreement with the difference in the β values of the two chromophores.

C. Photoconductivity

The photoconductivity sensitivities of composites containing various amounts of the bi-functional chromophores have been measured as a function of the applied electric field. The results are presented in Figure 51 where the photoconductivity sensitivity is plotted against the square root of the electric field on a semi-log scale. A linear dependence has been obtained for each composite. It is seen that the BF-1 series shows a slightly higher photoconductivity than the BF-2 series at equivalent chromophore concentrations by weight. However, when taking into account the molecular weight and chromophore number density, the photoconductivity of BF-1 and BF-2 are very close at the same chromophore number densities. It is not surprising because the two chromophores have almost the same charge transporting structures.

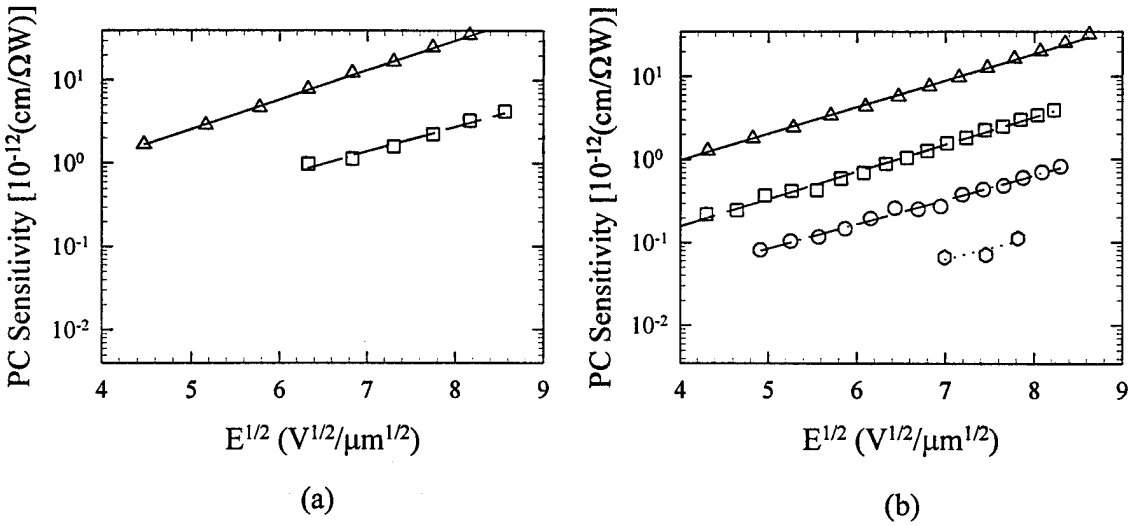

Figure 51 Photoconductivity sensitivity as a function of the applied electric field for composites containing various amounts of DPANST (a) and DPANS (b). S is plotted against the square root of the electric field on a semi-log scale. Circles: 10 %; Hexagons: 15 %; Squares: 22 %; Triangles: 33.7 %.

Photoconductivity in organic/polymeric materials consists of two processes: photogeneration of charge carriers and their subsequent transport through a hopping mechanism. Since the same concentration of charge generation sensitizer (C_{60}) is used for all the composites reported in this paper, and chromophore absorption is negligable, it is safe to assume that the charge generation efficiency is identical for all composites at a given electric field strength and illumination intensity. Therefore, the charge mobility and photoconductivity sensitivity should have the same dependence on the chromophore number density at a given field strength and light intensity. It has been shown[23-25] that the concentration dependence of charge mobility in CTA doped polymers can be expressed as $\mu \propto \rho^2 \exp(-2\rho/\rho_0)$. Therefore, the dependence of photoconductivity sensitivity on the chromophore concentration can be written as

$$S \propto \rho^2 e^{-2\rho/\rho_0}, \tag{41}$$

where ρ_0 is the localization radius. The average distance, ρ, between molecules is calculated from the formula $\rho = (M/Ad)^{1/3}$, where M is the molecular weight, d is the density of the chromophore in the composite, and A is the Avogadro's number (6.02×10^{23}). For example, the average separation distances, ρ, between the chromophores in a sample containing 10 and 33 wt. % of DPANS are, therefore, 19.3 and 12.9 Å, respectively. The data in Figure 51 are replotted in Figure 52 as a function of the chromophore concentration (at an electric field strength of 50 V/μm). An exponential relationship between S/ρ^2 and ρ is observed with ρ_0 = 1.74 and 1.80 Å for BF-1 and BF-2, respectively.

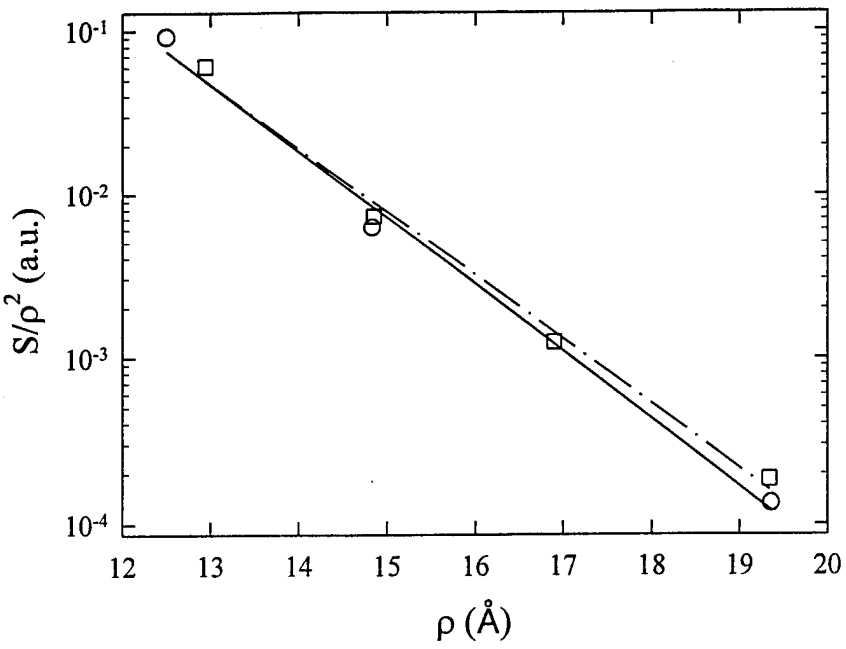

Figure 52 Concentration dependence of the photoconductivity sensitivity. S/ρ^2 is plotted vs ρ on a semi-log scale (where ρ is the average distance between chromophore molecules). All data were taken at an external field strength of 50 V/μm. Circles: BF-1; Squares: BF-2. The lines show numerical fit to Eq. (3) with $\rho_0 = 1.74$ and 1.80 Å for BF-1 and BF-2, respectively.

D. Four-Wave Mixing Diffraction Efficiency

In our experiments, only η_p was measured, although an *s*-polarized beam was used occasionally to check the diffraction anisotropy which was around 9 at electric fields of about 50 V/μm. The electric field dependence of the four-wave mixing diffraction efficiency (η_p) is presented in Figure 53. During the course of our experiments, samples with various thickness ranging from 100 to 150 μm have been prepared and studied. Since the diffraction efficiency is qudratically proportional to the sample thickness [$\eta_p \ll 1$, Eq. 18 (b)], all data in Figure 53 have been normalized to a uniform thickness of 100 μm for comparison. These data were fitted to Eq. (18) and are shown in Figure 53 as solid curves. The data presented in Figure 53 can also be fitted to a field dependence of $\eta_p = aE^x$ and the obtained exponent values (x) ranged from 3.5 to 4.2 with an average value of 3.9.

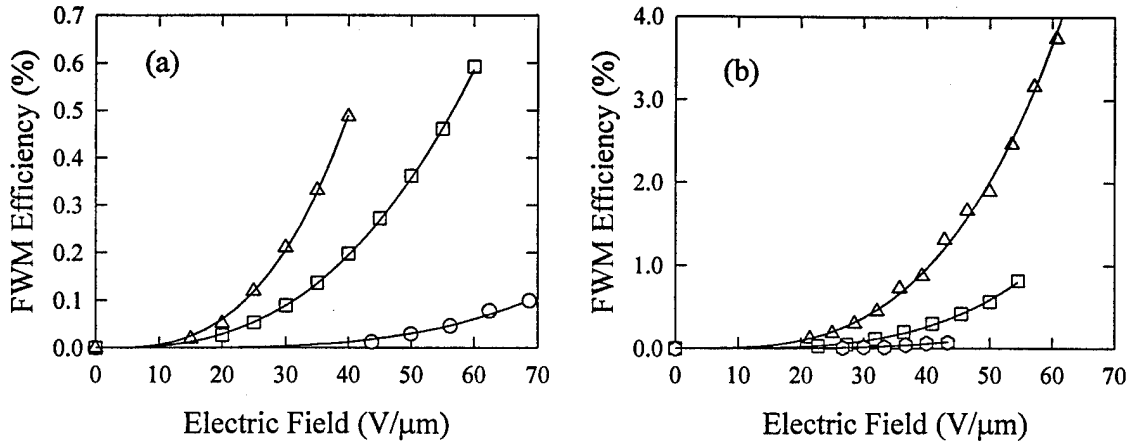

Figure 53 Electric field dependence of the four-wave mixing diffraction efficiency for composites containing various amounts of DPANST (a) and DPANS (b). Hexagons: 10 %; Circles: 15 %; Squares: 22 %; Triangles: 33.7 %.

It is clear that the four-wave mixing diffraction efficiency increases with the chromophore concentration for both BF-1 and BF-2. If one plots the diffraction efficiency versuss the chromophore number density, a relationship in the form of $\eta_p = aN^2$ is obtained with the ratio between the a coefficients $(a)_{DPANST}/(a)_{DPANS} = 2$. This dependence is presented in Figure 54.

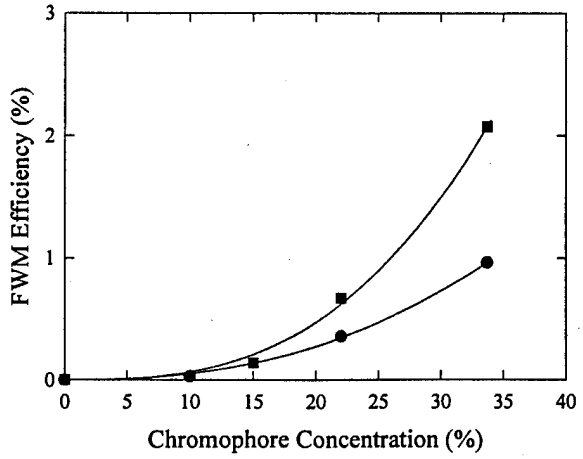

Figure 54 Dependence of four-wave mixing diffraction efficiency on the chromophore number density. Circles: BF-1; Squares: BF-2.

E. Holographic Grating Formation Dynamics

The writing and erasure time constants were measured as described below. Tthe writing beam intensities were maintained at 200 mW/cm^2 and the reading beam intensity at 10 mW/cm^2. With an electric field applied and one of the writing beams (Beam 1) on, the second writing beam (Beam 2) was open for writing and the diffracted signal was monitored. After the saturation of the FWM signal was reached, Beam 2 was blocked, allowing the erasure of the gratings by Beam 1 (since the intensity of the reading beam is much smaller than that of Beam 1, the erasure by the reading beam can be ignored compared to that by Beam 1). The writing and erasure time constants were obtained by numerically fitting the experimental data to Eqs. (10) and (10), respectively where $E^1(t)$ is substituted with $E_{SC}(t)$. Fig. 55 shows the measured rates of holographic grating formation as a function of applied field.

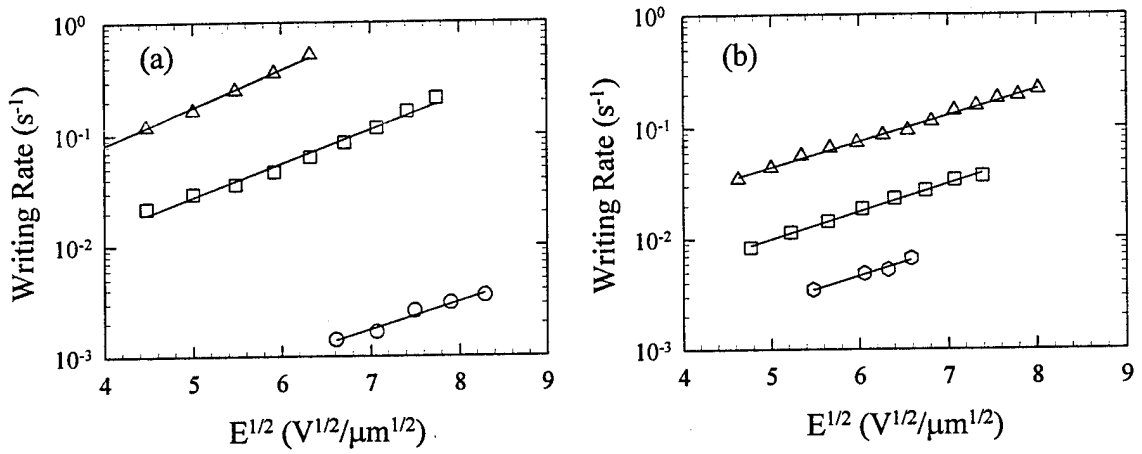

Figure 55 Holographic grating writing rate as a function of the applied electric field for composites containing various amounts of DPANST (a) and DPANS (b). The writing rate is plotted against the square root of the electric field on a semi-log scale. Hexagons: 10 %; Circles: 15 %; Squares: 22 %; Triangles: 33.7 %.

F. Holographic Grating Dark Decay

In order for a material to be used in information storage devices, the material must be able to store images for a certain period of time. Current polymeric photorefractive materials exhibit short storage times which result from both the holographic grating dark decay and the erasure by the reading beam. It has been shown that the holographic grating dark decay speed can be reduced (controlled) by the addition of charge trapping molecules[35] and that the erasure speed can be reduced by the use of weaker reading beams.[58]

The information storage abilities of the composites presented in this paper have been studied. Figure 56 shows typical dark decay curves of the holographic gratings in one of the composites (containing 33.7 wt. % DPANS). After the gratings were written (with a dc field of 50 V/μm applied) the writing beams were turned off and the diffracted signal was monitored. The solid line represents the decay of the readout signal with a reading beam intensity of 10 mW/cm^2. The gratings decay with a time constant of 85 seconds. When the reading beam intensity is reduced

to 1 mW/cm^2, the decay becomes much slower, with a time constant of approximately 300 seconds. This indicates that the decay of the readout signal consists of two processes: the dark decay and the reading beam erasure. The true dark decay of the gratings was determined as follows. After writing, all writing beams and the reading beam were turned off. At an interval of ~ 60 seconds, the reading beam was open for 1 second and the readout signal recorded. The open circles in Fig. 56 show such a measured dark decay curve. This dark decay can be numerically fitted to a double exponential expression, $\exp(-a_1 t/\tau_1 - a_2 t/\tau_2)$, with τ_1=1190 seconds and τ_2=95 seconds. This double exponential decay may be a combined result of the material's inherent dark conductivity and the presence of shallow traps.

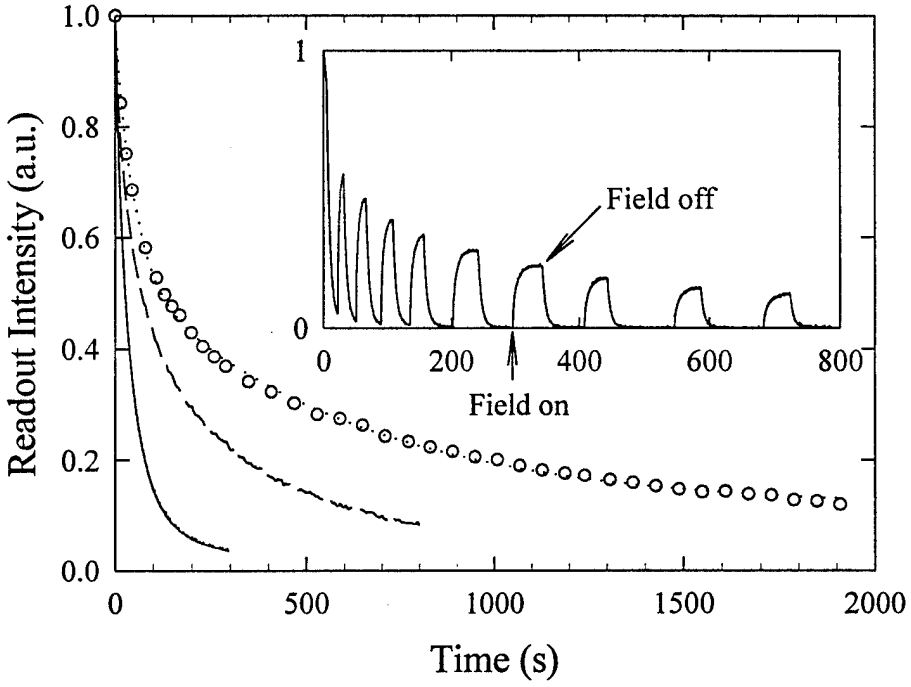

Figure 56 Holographic grating dark decay. Reading beam intensities: 10 mW/cm^2 (solid curve) and 1 mW/cm^2. Open circles: interval reading with an intensity of 1 mW/cm^2 (and numerical fit, dotted line). Inset: grating response to the applied electric field in the presence of a 1 mW/cm^2 reading beam.

The inset of Figure 56 shows the response of the readout signal to the applied electric field in the presence of a 1 mW/cm^2 reading beam. The writing beams were turned off at t=0. The field was turned on and off at points indicated. These results show that a field is needed for for information retrieval (readout), but not for its storage.

G. Two-Beam Coupling

Two beam coupling data provide evidence that light diffraction is attributed to the

photorefractive effect. This experiment is performed be monitoring the intensities of the writing beams as the electric field is turned on and off. In this material, an energy transfer is evidenced by the increase in the intensity of Beam 1 and the decrease in that of Beam 2. When the electric field was turned off, no intensity changes were observed. Two more experiments were carried out in order to observe the growth of the space charge gratings in the presence of the applied field. The intensity of Beam 1 was monitored while Beam 2 was open and then blocked; the same experiment was repeated for Beam 2. The inset of Figure 57 shows a typical change in the beam intensities. With an electric field of 50 V/μm applied, the intensity of Beam 1 (I_1) was monitored as Beam 2 was open at t = 10.0 s and closed at t = 45.0 s. The same procedure was repeated for Beam 2. The two-beam coupling gains were measured as a function of the applied electric field and Figure 57 shows the field dependence of the two-beam coupling gains for two of the composites: BF-2 (33.7wt. % DPANS) and BF-1 (36 wt. % DPANST). A net two-beam coupling gain has been obtained at fields above 60 V/μm for BF-1 (absorption coefficient 20 cm^{-1}) and 40 V/μm for BF-2 (absorption coefficient 12.5 cm^{-2}).

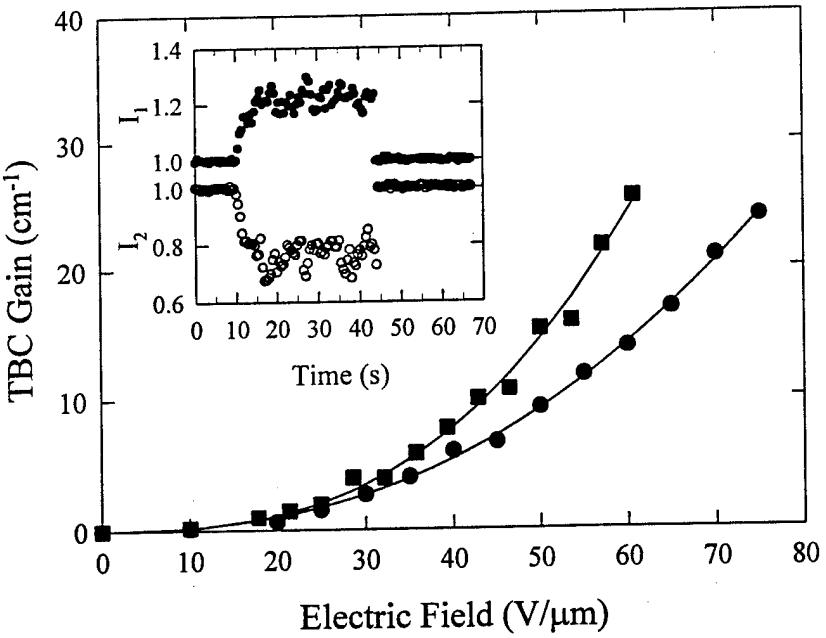

Figure 57 Electric field dependence of the two-beam coupling gains for composites containing 33.7 % of DPANST (circles) and 33.7 % DPANS (squares), respectively. Inset: a typical two-beam coupling curve. With an electric field of 50 V/μm applied, the intensity of beam 1 (I_1) is monitored while beam 2 is open at t=10.0 s and closed at t=45.0 s. The same procedure is repeated for beam 2.

H. Holographic image recording and retrieval

Due to their excellent optical quality, composites containing bi-functional chromophores

were used to record and retrieve holographic images. The recording setup used in this experiment was similar to that described in earlier section for PVK/DEANST/TPY composite. The retrieved images were projected on a screen and captured with the use of photographic camera. They are shown in Figure 58.

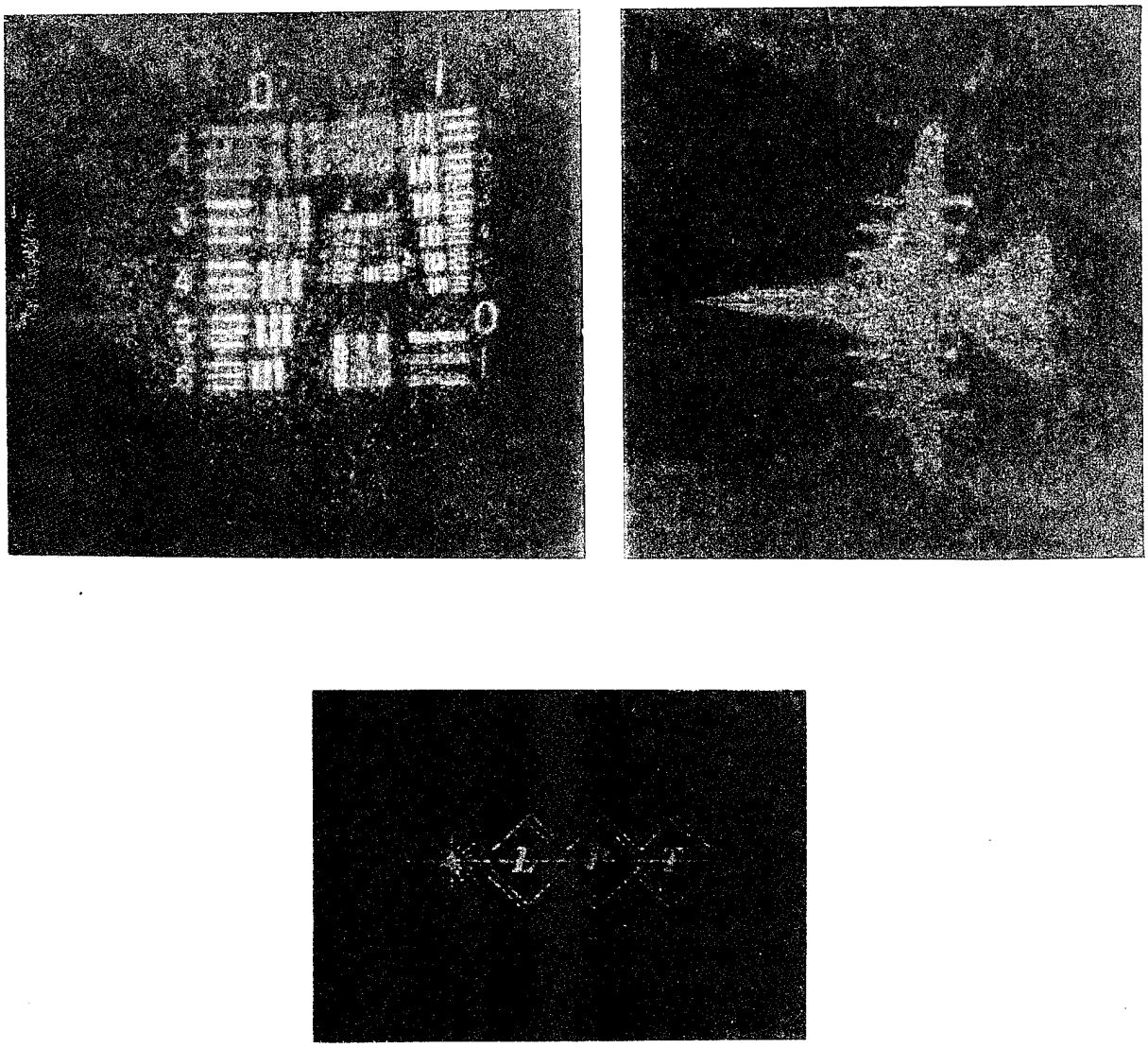

Figure 58 Example of reterieved holographic images using photorefractive composites containing bi-functional chromophores.

I. Discussion

The bi-functional chromophores presented in this paper, DPANST and DPANS, possess second-order NLO and charge transporting properties. The charge transporting abilities of these two chromophores arise from the triphenylamine structure. Due to the similarity of the two chromophores, one would expect similar charge transporting abilities. This is indeed observed in the experiments, as can be seen from the results on the photoconductivity and holographic grating writing rate measurements. The molecular first hyperpolarizability depends on the donor and acceptor strengths as well as on the conjugation length. The first hyperpolarizability of DPANS was measured to be 1.2 times that of DPANST. This difference in the molecular first hyperpolarizability can be attributed to the difference in the conjugation lengths, since both chromophores possess exactly the same donor and acceptor groups. Measurements on the molecular first hyperpolarizabilities of 4-(N, N'-dimethylamino)-(β)-nitrostyrene (DMANST) and 4-(N, N'-dimethylamino)-(β)-nitrostilbene) (DANS) have revealed similar changes.[23] With an increased molecular hyperpolarizability, one obtains a larger EO coefficient, higher photorefractive four-wave mixing diffraction efficiency and larger two-beam coupling gain for BF-2 over BF-2 at equivalent chromophore concentrations.

The EO coefficients reported here contain contributions from the field induced birefringence due to the materials' low T_g. More accurate measurement of EO coefficients can be performed at high modulation frequencies at which the chromophores can only partially respond to the AC component of the applied field and, thus, the contribution from birefringence can be neglected.[38]

The advantage of using bi-functional chromophores in photorefractive materials is that a larger EO coefficient and higher photoconductivity can be simultaneously obtained by using higher chromophore concentrations. Consequently, a higher photorefractive figure-of-merit and faster response can be simultaneously achieved. This is in clear contrast to composite materials wherein photoconductive polymers are doped with second-order NLO chromophores or second-order polymers are doped with charge transporting agents. A higher chromophore concentration in photoconductive polymers results in lower charge mobilities and, therefore, lower photorefractive responses. Similarly, higher CTA concentration in second-order NLO polymers leads to a lower concentration of the NLO moiety, smaller EO coefficient and lower photorefractive figure-of-merit. This dielamma is clearly avoided when a bi-functional chromophore is used. As shown by the results presented in the previous section, both the EO coefficient and photoconductivity increase with higher chromophore concentrations. Consequently, a larger photorefractive figure-of-merit naturally leads to faster responses.

J. Conclusions

We have developed two bi-functional chromophores which possess both the second-order nonlinear optical and charge transporting properties. The chromophores have conjugated structures terminated by an acceptor group ($-NO_2$) and a donor group (triphenylamine) which also serves as a charge transporting agent. Electric field induced second-harmonic generation studies showed relatively large molecular first hyperpolarizabilities. A series of photorefractive composites have been prepared which contain an inert polymer binder (PBMA), a charge generation sensitizer (C_{60}), and various amounts of the two bi-functional chromophores. The electrooptic coefficients and the photoconductivity sensitivity have been determined to be highly dependent on the applied electric field as well as on the chromophore concentrations.

Photorefractive measurements showed that the holographic grating diffraction efficiency increases rapidly with the chromophore number densities in good agreement with the electrooptic coefficient measurement. The dependence of the photoconductivity sensitivity and the holographic grating writing rate on the electric field are also in good agreement with the general field dependence of the charge mobilities. Finally, the field dependence of the two-beam coupling asymmetric energy transfer gains confirm the photorefractive nature of the observed phenomena.

2.7.4. Composites Based On Multifunctional Methacrylate Copolymer[56]

A. Electrooptic and photoconductivity data

Figure 59 displays the electric field dependence of the electrooptic coefficient measured by the reflection technique. The solid curve in Figure 59 shows a fit of the experimental data to Eq. (34). It should be pointed out that the EO coefficients reported in this paper contain contributions from the field induced birefringence due to the low T_g of the material.

The photoconductivity (σ) and the photoconductivity sensitivity (S) of the material are

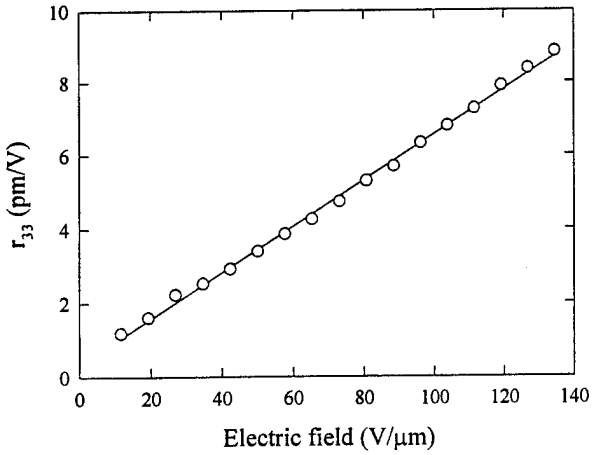

Figure 59 Electric field dependence of the electrooptic coefficient measured by the reflection technique. Open circles: experimental data; solid curve: fit to Eq. (13).

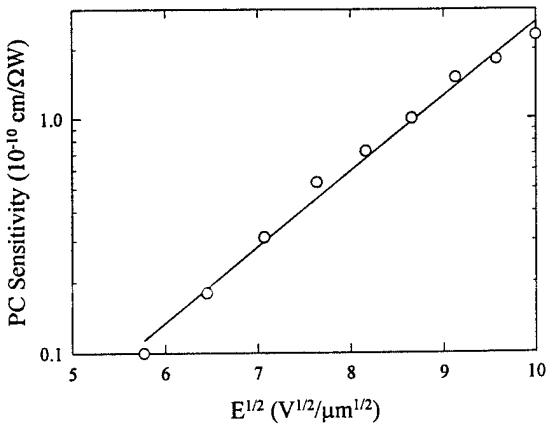

Figure 60 Electric field dependence of the photoconductivity (PC) sensitivity.

calculated using the experimentally measured photocurrent (I_{ph}) flowing through the film. Figure 60 displays an electric field dependence of the photoconductivity sensitivity. The photoconductivity sensitivity is plotted against the square root of the applied dc electric field on a semi-log scale. A linear dependence has been obtained for fields between 30 and 140 V/μm.

B. Photorefractive properties.

Figure 61 presents the electric field dependence of the photorefractive four-wave mixing diffraction efficiency obtained in the material. This field dependence is typical of low T_g materials since the electrooptic coefficient and the space charge field are both electric field dependent as shown by Eqs. (34) and (6). The experimentally measured data were fitted to Eq. (18) and the solid line in Figure 61 shows such a fit.

The most important feature of the photorefractive effect, which distinguishes itself from many other mechanisms that may result in refractive index gratings, is the finite phase shift between the refractive index grating and the interference pattern, as described by Eq. (14). This finite phase shift, or the nonlocal nature of the photorefractive effect, causes an asymmetric energy transfer between the writing beams, a unique process which does not occur in any of the other processes. Therefore, the photorefractive nature of the composite was further confirmed by the asymmetric energy transfer in two-beam coupling experiments. Figure 62 shows electric

field dependence of two beam coupling obtained in this material.

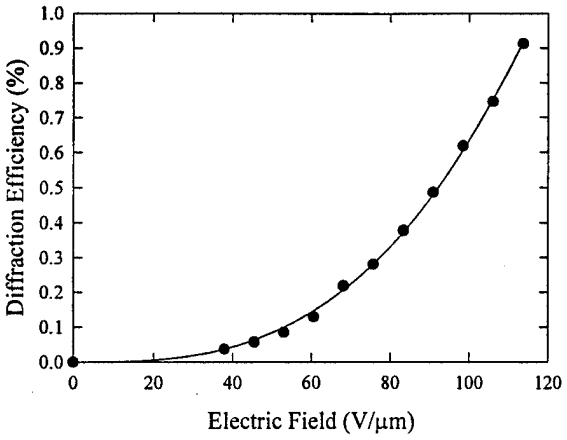

Figure 61 Electric field dependence of the four-wave mixing diffraction efficiency. Filled circles: experimental data; solid curve: fit to Eq. (18).

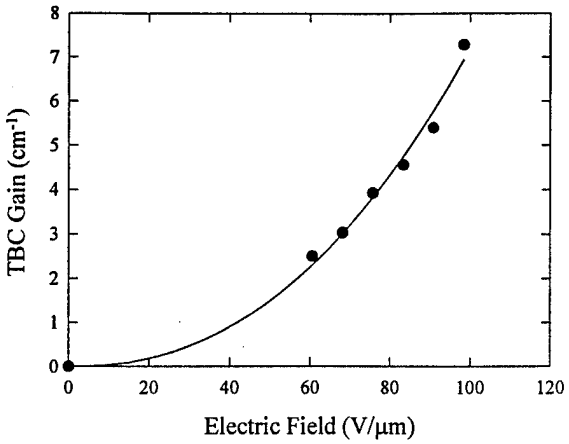

Figure 62 Electric field dependence of the two-beam coupling (TBC) gain.

C. Discussion and conclusion

The polymer presented in this report possesses charge transporting and electrooptic properties arising from the carbazole group and the second-order NLO chromophore, respectively, both covalently attached to the polymer backbone. When doped with a photocharge generation sensitizer, photorefractivity has been observed. Problems associated with phase separation are clearly avoided because of the lack of doped compounds except for a low concentration of the photocharge generation sensitizer. However, the observed photorefractive properties do not seem to compare favorably with those obtained from composite (or guest-host) materials, in terms of the four-wave mixing diffraction efficiency, two-beam coupling gain, as well as the holographic grating writing dynamics.

The dynamics of a holographic grating formation is directly related to the photoconductivity (or charge mobility) of the material. As the results show, the grating writing time constant at a power level of 250 mW/cm^2 and an electric field of 100 V/μm is around 0.5 s. The overall grating writing speed is relatively slow. This may be a result of the low charge mobilities in polymers where the charge transporting agent and second-order chromophores are covalently bound to the polymer backbone, as has been observed in other fully functional photorefractive polymers.[54, 55] Compared with guest-host systems, the molecular motions of the charge transporting agents in fully functional polymers are restricted to very short-range vibrations and rotations at temperatures below the glass transition temperature (T_g). The restricted molecular motions may interrupt the conduction pathway of the charge transporting molecules resulting in

slower photorefractive responses.

In summary, a new low T_g photorefractive polymer has been synthesized and characterized which contains a hole transporting group, a nonlinear optical chromophore and a long aliphatic *n*-octyl methacrylate group to lower the polymer's glass transition temperature. The experimental results demonstrate that the major contribution to the photorefractive effect comes from the space charge field due to the light-induced charge separation with a subsequent effective electric field induced refractive index change.

4.7.5 Photorefractive Sol-Gel Processed Ormosils[59-61]

Although high diffraction efficiencies and beam coupling gains have been obtained in photorefractive polymer composites, their use in practical applications can be limited since the phase separation in these materials, especially at high doping levels, which results in total loss of optical quality is highly probable. Sol-gel processed optically transparent glass and ceramic materials have provided a new generation of the molecular composites extemely useful in the design of optical devices.[62] The low temperature sol-gel processing permits countless varieties of molecules with exceptional optical and chemical properties to be incorporated into the oxide glasses.[63] More recently, the sol-gel processing has been applied to organically modified silanes (ormosils)[61, 62, 63] to produce high optical quality materials possessing the properties of both oxide glass and organic compounds.

We report, for the first time to our knowledge, the development and characterization of a sol-gel processed ormosils exihibiting electrooptic and photoconductive properties. When doped with a photocharge generation sensitizer, thiapyrylium dye or 2,4,7-trinitrofluorenone (TNF)-carbazole charge- transfer complex, the materials shows photorefractivity. Low temperature sol-gel processing technique has been utilized to obtain optical quality films in a wide range of thicknesses, from several to more than 200 μm. The electrooptic coefficient, photoconductivity, four-wave mixing diffraction efficiency, and two-beam coupling gain have been measured. The electric field dependence of the above parameters proves the photorefractive nature of the response.

A. General properties

Sol-gel processed photorefractive ormosils were characterized by measurements of the electrooptic coefficient and photoconductivity. Photoconductivity was measured using a simple photocurrent technique in which a He-Ne laser beam illuminates the sample through the glass substrate. The electrooptic coefficient was measured using a reflection technique. Figure 63 displays an electric field dependence of the photoconductivity sensitivity for composites containing TPY photosensitizer. Figure 64 displays the field dependence of the EO coefficient; the solid line is a fit to Eq. (34).

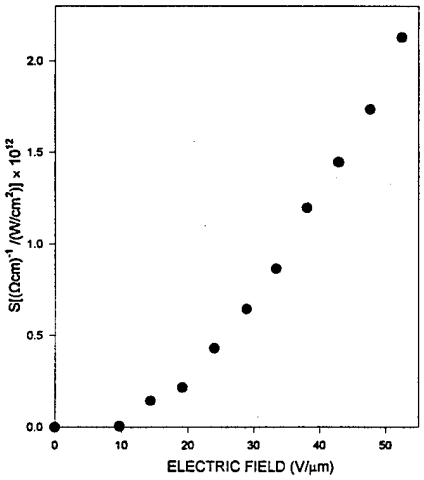

Figure 63 Electric field dependence of photoconductivity sensitivity of TPY dye sensitized photorefractive ormosil.

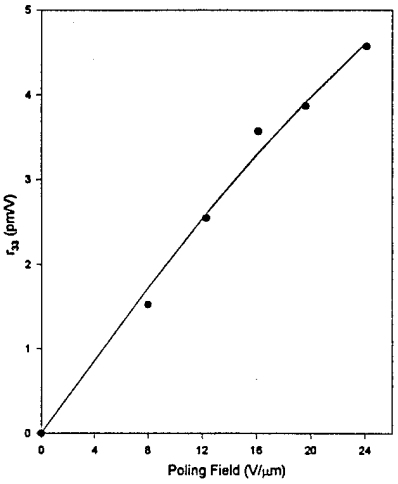

Figure 64 Field dependence of electrooptic coefficient of the photorefractive ormosil.

B. Photorefractive properties

The photorefractive properties of the material were studied by four-wave mixing and two-beam coupling experiments. Holographic gratings are written by two laser beams from a He-Ne laser operating at 633 nm. Two writing beams with an equal intensity of 250 mW/cm^2 intersect in the sample at incidence angles of θ= 45° and θ= 60° (in air), respectively, creating an intensity grating with a spacing of aproximately Λ=3.4 μm. The grating wavevector is oriented at an angle of θ_G = 30.5° with respect to the film surface. The reading beam from another He-Ne laser at 633 nm with an intensity of 10 mW/cm^2 propagates in the direction opposite to one of the writing beams (Beam 2). The diffracted signal propagates in the direction opposite to that of Beam 1, reflected off the beam splitter, and then detected by a photodiode. In a two-beam coupling experiment, the energy transfer between the writing beams is observed by monitoring the intensity of each of the writing beams when an external electric field is applied.

The inset of Figure 65 shows a typical four-wave mixing signal with the writing process fitted to the following equations (derived from Eqs. (9) and (10)):

$$I_s \propto E_{SC}^2 [\, 1 - \exp(-t/\tau)]^2 \qquad \textbf{(42a)}$$

and the erasure fitted to:

$$I_s \propto E_{SC}^2 [\exp(-t/\tau)]^2 \qquad \textbf{(42 b)}$$

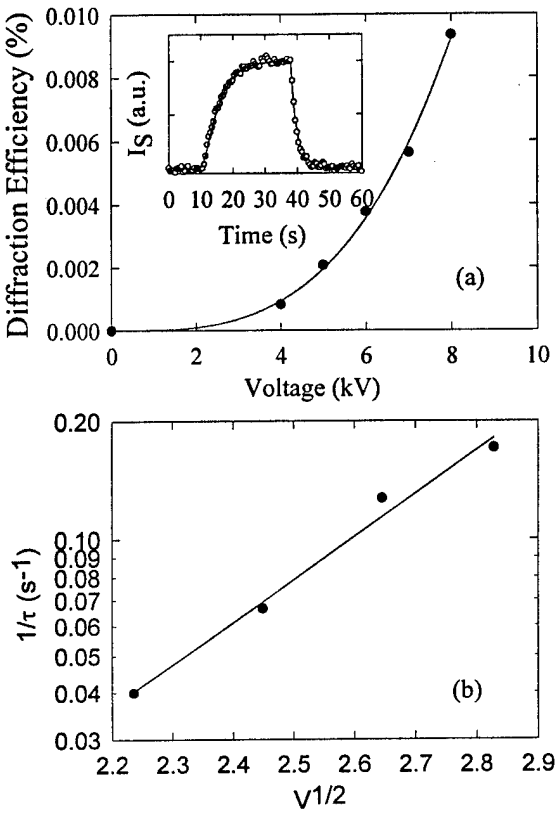

Figure 65 (a) Electric field dependence of the holographic diffraction efficiency. Filled circles: experimental data; solid curve: fit to Eq. (18). Inset: a typical four-wave mixing curve. The writing and erasure processes are fitted to Eqs. 42a and 42b, respectively. (b) Electric field dependence of the grating writing rate. The writing rate is plotted against the square root of the applied field on a semi-log scale.

where E_{SC} is the saturation space charge field and τ is the writing or erasure time constant. The diffraction efficiency was measured as a function of the external electric field and the dependence is shown in Figure 65. The diffraction efficiency increases rapidly with the applied electric field and reaches a value of 0.01 % at an external field of 50 V/μm. It should be pointed out that the field dependence of the diffraction efficiency also includes the field dependence of the composite's electrooptic coefficient.

The holographic grating formation dynamics in the material has been studied by measuring the grating writing and erasure processes and their electric field dependence. The measured field dependence of the writing rate is presented in Figure 65 (b) where the writing rate is plotted against the square root of the electric field on a semi-log scale. The linear dependence is consistent with the field dependence of the charge mobilities as the writing time constant is related with the charge mobility by $\tau \propto 1/\mu$ and $\tau \propto exp(E^{1/2})$.

The presented material can be used in potential information storage applications. We have

measured the dark decay of the holographic gratings. Figure 68 shows the dark decay of

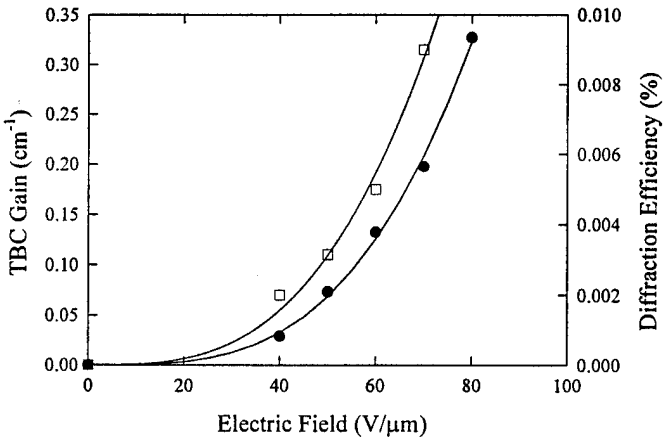

Figure 66 Electric field dependence of diffraction efficiency (solid circles) and two beam coupling gain (open squares) for TNF:CAR sensitized photorefractive ormosil

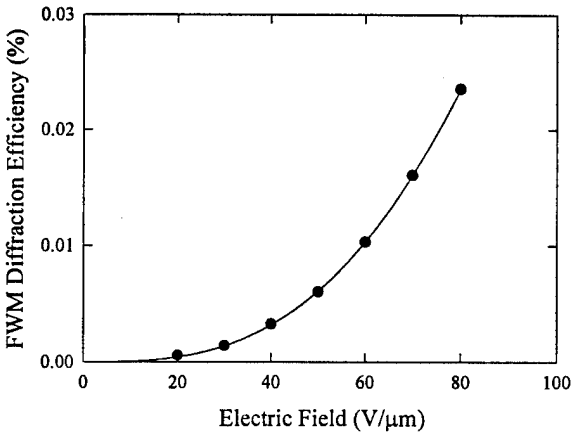

Figure 67 Electric field dependence of holographic diffraction efficiency of TPY dye sensitized photorefractive ormosil

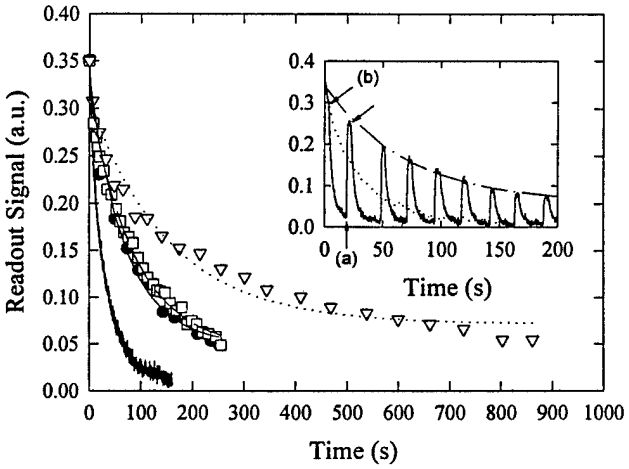

Figure 68 Dark decay of the holographic gratings under various conditions. Solid line: grating decay with the reading beam and electric field on; Open squares: decay with field applied and the reading beam switched on each 10 seconds; Open triangles: decay with both field and reading beam on every for 1 second at a 50 second interval. Inset: grating decay with reading beam on and switching on (at point a) and off (at points b) the applied electric field.

the gratings in the presence of the reading beam, and when the reading beam and the electric field are both turned off. In the presence of the reading beam, which partially erases the gratings, the readout signal quickly decays to zero in about 150 seconds with a time constant of approximately 59 seconds. This decay results from the reading beam erasure in the presence of the electric field. When the field is turned off after the grating was written, the grating decay process becomes slower, as shown by the filled circles in Figure 68. The true dark decay process was determined by turning off the electric field and the reading beam. At an interval of about 50 seconds, the reading beam and the electric field are turned on for 1 second and the readout monitored. The triangles in Figure 68 shows the measured dark decay curve of the holographic gratings with a time constant of 310 seconds.

To prove the photorefractive nature of the observed holographic gratings, we have performed two-beam coupling experiment using two *p*-polarized writing beams with approximately equal intensity. The intensities of each writing beam were monitored while the other beam was switched on and off in the presence of the applied electric field. The results are shown in Figure 66. Clear asymmetric energy transfer has been observed as the intensity of beam 1 increases when beam 2 is switched on, while that of beam 2 decreases when beam 1 is on. However, the decrease of beam 2 intensity seems to be more pronounced than the increase of beam 1. This asymmetric beam intensity change may be a result of a photoinduced absorption of the material.

C. Conclusions

The silica based polymer presented above possesses charge transporting and electrooptic properties arising from the organic side groups: carbazole and the second-order NLO chromophore, respectively, both covalently attached to the polymer backbone to form excellent optical quality inorganic/organic composites. Upon doping a photocharge generation sensitizer, this composite shows a photorefractive response. Because this material (upon sol-gel processing) forms a single phase composite, the problems associated with phase separation are clearly avoided. However, the observed photorefractive responses (four-wave mixing diffraction efficiency and two-beam coupling gain) seem to be relatively low as compared to those obtained from organic guest-host composite materials. The ormosil based photorefractive material, however, possesses a clear advantage over organic polymers because of its superior optical quality, environmental stability and a potential for retaining induced orientation of the poled structures.

In summary, we have synthesized and characterized, for the first time to our knowledge, a sol-gel processed ormosil photorefractive composite which contains a hole transporting group and a nonlinear optical chromophore. The experimental results clearly demonstrate that ormosil-based materials exhibit a photorefractive effect and, if optimized, can be used in various applications due to their excellent optical quality and environmental stability.

2.8 References

1. A. Askin, G.D. Boyd, J.M. Dziedzic, R.G. Smith, A.A. Ballman, J.J. Levinstein and K. Nassau, *Appl. Phys. Lett.* **9**, 72 (1966).
2. F.S. Chen, J.T. LaMacchia and D.B. Fraser, Appl. Phys. Lett. 13, 223, 1968.
3. F.S. Chen, *J. App. Phys.* **40**, 3389 (1969).
4. N.V. Kukhtarev, V.B. Markov, S.G. Odulov, M.S. Soskin and V.L. Vinetskii, *Ferroelectrics* **22**, 949 (1979); *ibid* **22**, 961 (1979).
5. see for example papers in *MRS Bulletin*, March 1994.
6. P. Günter and J.P. Hignard, eds. *"Photorefractive Materials and their Applications I and II"*, Topics in Applied Physics, Vols. **61** & **62** , Springer-Verlag, 1988.
7. M.P. Petrov, S.I. Stepanov and A.V. Khomenko, "*Photorefractive Crystals in Coherent Optical Systems*", Springer-Verlag, 1991.
8. A.M. Glass D. von der Linde and T.J. Negran, *Appl. Phys. Lett.* **19**, 130 (1971).
9. A.M. Glas and D.H. Auston, *Opt. Commun.* **5**, 45 (1972).
10. K. Sutter, J. Hulliger and P. Günter, *Solid State Commun.* **74**, 867 (1990).
11. W.E. Moerner and S.M. Silence, *Chem. Rev.* **94**, 127 (1994).
12. I.C. Khoo, H. Li and Y. Liang, *Opt. Lett.* **19**, 1723 (1994).
13. P. Günter and D.W. Pohl, *"Laser Induced Dynamic Gratings"*, Springer Series in Optical Sciences vol. 50, Springer, 1986.
14. see for example paper of R.A. Mullen in Ref 6.
15. P. Yeh, "*Introduction to Photorefractive Nonlinear Optics*", Wiley Interscience, 1993.
16. M.C. Bashaw, M. Jeganathan and L. Hesselink, *J. Opt. Soc. Am.* **B 11**, 1743 (1994).
17. D. L. Staebler and J. J. Amodei, *Ferroelectrics*, **3**, 107 (1972)
18. J. Feinberg, in "*Optical Phase Conjugation.*" R. A. Fisher, Ed. Academic Press; New York, 1983.
19. H. Kogelnik, *Bell. Sys. Tech. J.*, **48**, 2909 (1969).
20. P. N. Prasad and D. J. Williams, *Introduction to Nonlinear Optical Effects in Molecules and Polymers* (Wiley, New York, 1991).
21. D. S. Chemla and J. Zyss, Eds., *Nonlinear Optical Properties of Organic Molecules and Crystals* (Academic Press, Orlando, 1987)
22. W. D. Gill, "Polymeric photoconductors", in *Photoconductivity and Related Phenomena*, Eds. J. Mort and D. M. Pai (Elsevier, New York, 1976)
23. M. Stolka, J. F. Yanus, and D. M. Pai, *J. Phys. Chem.* **88**, 4707 (1984).
24. P. M. Borsenberger, W. Mey, and A. Chowdry, *J. Appl. Phys.* **49**, 273 (1978).
25. P. M. Borsenberger, *J. Appl. Phys.* **68**, 6263 (1990).
26. J. Schildkraut, *Appl. Opt.*, **29**, 2839, 1990.
27. Teng, C. C.; Man, H. T., *Appl. Phys. Lett.*, **56**, 1734, 1990.
28. Khanarian, G. et al, *Proc. SPIE*, **824**, 72, 1987.
29. Zhang, Y. Ph. D. Dissertation, SUNY at Buffalo, 1992.
30. Y. Zhang, C. A. Spencer, S. Ghosal, M. K. Casstevens and R.Burzynski, *Appl. Phys. Lett.*, **64**, 1908, 1994.
31. Y. Zhang, C. A. Spencer, S. Ghosal, M. K. Casstevens and R. Burzynski, CLEO/IQEC Conference, Baltimore, May 1, 1994.

32. Y. Zhang, S. Ghosal, M. K. Casstevens and R. Burzynski, *SPIE Proceedings*, **2285**, 24-29 (1994).

33. Y. Zhang, C. A. Spencer, S. Ghosal, M. K. Casstevens and R. Burzynski, *J. Appl. Phys.*, **76**, 671 (1994).
34. J. C. Scott, L. Th. Pautmeier, and W. E. Moerner, *J. Opt. Soc. Am.* **B9**, 2059 (1992).
35. Y. Zhang, C. A. Spencer, S. Ghosal, M. K. Casstevens and R. Burzynski, *Polymer Preprints* **35**, 233 (1994).
36. D. M. Pai, J. F. Yanus and M. Stolka, *J. Phys. Chem.*, **88**, 4714 (1984).
37. P.M. Borsenberger, D. A. Weiss in"*Organic Photoreceptors for Imaging Systems*", Marcel Dekker, New York, 1993.
38. W. E. Moerner, S. M. Silence, F. Hache, G. C. Bjorklund, *J. Opt. Soc. Am.*, **B 11**, (1994).
39. R. Burzynski, Y. Zhang, S. Ghosal, M. K. Casstevens, *J. Appl. Phys.*, **78**, 6903 (1995).
40. R. Burzynski, Y. Zang, S. Ghosal, M. K. Casstevens, presented on *ACS National Meeting*, Anaheim, CA, April 1995.
41. Y. Zhang, S. Ghosal and R. Burzynski, *CLEO'95,* Paper **QWE3,** Baltimore, MD, 1995.
42. Y. Zhang, C. A. Spencer, S. Ghosal, M. K. Casstevens and R. Burzynski, *Appl. Phys. Lett.*, **66**, 256, 1995.
43. S. Ducharme, J. C. Scott, R. J. Twieg, and W. E. Moerner, *Phys. Rev. Lett.* **66**, 1864 (1991).
44. W. E. Moerner, C. A. Walsh, J. C. Scott, and R. J. Twieg, *Proc. SPIE* **1560**, 278 (1991).
45. J. S. Schildkraut, *Appl. Phys. Lett.* **58**, 340 (1991).
46. Y. P. Cui, Y. Zhang, P. N. Prasad, J. S. Schildkraut, and D. J. Williams, *Appl. Phys. Lett.* **61**, 2132 (1992).
47. S. M. Silence, C. A. Walsh, J. C. Scott, W. E. Moerner, *Appl. Phys. Lett.* **61**, 2967 (1992).
48. M. J. Sansone, C. C. Teng, A. J. East and M. S. Kwiatek, *Opt. Lett.* **18**, 1400 (1993).
49. M. Liphardt, A. Goonesekera, B. E. Jones, S. Ducharme, J. M. Takacs and L. Zhang, *Science* **263**, 367 (1994).
50. Y. Zhang, Y. P. Cui, and P. N. Prasad, *Phys. Rev.* B**46**, 9900 (1992).
51. S. M. Silence, F. Hache, M. C. J. M. Donckers, C. A. Walsh, D. M. Burland, G. C. Bjorklud, R. J. Twieg, and W. E. Moerner, *Proc. SPIE* **1852**, 253 (1993).
52. S. M. Silence, J. C. Scott, P. K. Jenkner, R. D. Miller, R. J. Twieg, W. E. Moerner, F. Hache, and E. J. Ginsburg, *J. Opt. Soc. Am.* **B10**, 2306 (1993).
53. K. Yokoyama, K. Arishima, T. Shimada and K. Sukegawa, *Jpn. J. Appl. Phys.* **33**, 1029 (1994).
54. (a) B. Kippelen, K. Tamura, N. Peyghambarian, A. B. Padias, and H. K. Hall, Jr., *J. Appl. Phys.* **74**, 3617 (1993); (b) B. Kippelen, K. Tamura, N. Peyghambarian, A. B. Padias, and H. K. Hall, Jr., *Phys. Rev.* B **48**, 10710 (1993).
55. (a) L. P. Yu, W. K. Chan, Z. N. Bao, and S. X. F. Cao, *J. Chem. Soc., Chem. Commun.* 1735 (1992); (b) L. P. Yu, W. K. Chan, Z. N. Bao, and S. X. F. Cao, *Macromolecules* **26**, 2216 (1993); (c) Y. M. Chen, Z. H. Peng, W. K. Chan, and L. P. Yu, *Appl. Phys. Lett.* **64**, 1195 (1994); (d) L. P. Yu, Y. M. Chen, W. K. Chan and Z. H. Peng, *Appl. Phys. Lett.* **64**, 2489 (1994).
56. C. F. Zhao, C.-K. Park, P. N. Prasad, Y. Zhang, S. Ghosal, and R. Burzynski, *Chem. Mater.* **7**, 1237 (1995).

57. J. J. Stankus, S. M. Silence, R. J. Twieg, D. M. Borland, R. D. Miller, J. C. Scott, W. E. Moerner, and G. C. Bjorklund, *Proc. SPIE* **2285**, 204 (1994).
58. S. M. Silence, G. C. Bjorklund and W. E. Moerner, *Opt. Lett.* **19**, 1822 (1994).
59. R. Burzynski, M. K. Casstevens, Y. Zhang, S. Ghosal, *Opt. Eng.*, February 1996. to appear.
60. Y. Zhang, R. Burzynski, S. Ghosal, M. K. Casstevens, *Adv. Mat.*, February 1996 invited review paper, to appear.
61. P. N. Prasad, M. E. Orczyk, B. Swedek, J. J. Zieba, C. -F Zhao, C.-K. Park, R. Burzynski, Y. Zhang, S. Ghossal, M. K. Casstevens, *SPIE Proceedings*, **2527**, paper no. 26, July 11-13, 1995, San Diego, CA.
62. "*Sol-Gel Technology for Thin Films, Fibers, Preforms, Electronics and Specialty Shapes*", L. C. Klein, Ed., Noyes Publ., Park Ridge, N.J., 1988.
63. R. Burzynski, P. N. Prasad in *Sol-Gel Optics. Processing and Applications".* Ed. L. C. Klein, Chapter 19, pp. 417-450, Kulver Academic Publisher, Boston 1994.

3. FINAL DISCUSSION AND RECOMMENDATIONS

Photorefractive materials are thought to be promising media for information storage and processing applications. The ability to reversibly write large amounts of information (digital or analog) in small volumes (as a result of various multiplexing schemes) certainly makes these materials worth developing. Photorefractive crystals have been shown to perform quite well, but they are extremely difficult to process into low-cost practical devices. Organic photorefractive materials, when fully developed, promise several advantages including tunable performance and lower cost.

At the time this contract began, some organic materials were being investigated, but the diffraction efficiencies were very low (on the order of 10^{-5}). It was an open question whether organic materials could deliver sufficient diffraction efficiency required of practical devices. Soon after the contract began, it became clear that they could; several groups working with different composite systems, almost simultaneously, demonstrated diffraction efficiencies in the tens of percent - values that were clearly sufficient for practical devices.

Following our ability to prepare photorefractive materials with sufficiently high diffraction efficiencies, our team focused its attention to developing materials whose properties were more likely to be used in practical devices. In order for a material to perform adequately in a commercial device, it must exhibit several properties. The material must be:

(1) stable for the intended lifetime of the device (negligible aging effects)

(2) compatible with low intensity diode lasers (response time is a concern)

In addition, depending upon the intended application, the stored information must be: (1) capable of being written quickly (high speed information processing) and/or (2) persist for a prolonged length of time (archival storage of information). If a material exhibits only average performance in either or both of these last two categories, there are very few applications for it. With these considerations in mind, LPT turned its attention to developing materials meeting these requirements.

Doped systems are convenient to work with since the components could be switched and their concentrations easily adjusted. It is, of course, desirable to increase the concentration of the active components as high as possible. This approach has the unfortunate consequence of rendering the composite unstable, i.e. the material has a tendency to phase segregate. In an effort to mitigate this effect, LPT successfully designed, synthesized and incorporated multifunctional chromophores, that is, ones that are both electrooptic and charge transporting. This accomplishment is an important step toward the development of more stable systems. Continuing this trend further, LPT also successfully developed fully functional polymers (all functions performed by the polymer or covalently attached side chains). This system, like others developed by other groups, exhibited less than desirable performance indicating the need for further work in this area.

It has become clear that the long term tendency for stored information to be lost (even in the dark) may be the biggest challenge for organic photorefractive materials if they are ever to be used as memory media. LPT successfully demonstrated that a dopant (acting as a charge trap) could be intentionally introduced resulting in longer storage times. This important demonstration was tempered by the realization that writing times would also be increased. It is the opinion of LPT's research staff that some type of activated charge trap is required to solve the

storage problem. Information should be written in the absence of traps (perhaps by suppressing their function), at which point, the traps could be activated (preferably optically).

Recommendations

While LPT's accomplishments under this program are substantial and have resulted in a number of materials that can be used in particular applications, it is recognized that a good deal more needs to be accomplished before these materials are suitable for several others. Some of the problems and possible solutions are discussed above. If these problems can be overcome through the implementation of improved materials or device designs, there are a vast number of applications, perhaps the largest being computer memories and/or graphical (including video) storage. The return on investment would be tremendous.

There needs to be a number of improvements before these materials can compete in the long-term memory market. Incremental advances and improvements are unlikely to deliver these materials. Many of the underlying processes involved in photorefractive materials were studied on crystalline materials. Most of the organic photorefractive technical literature discusses these processes using assumptions developed for crystalline materials. Current work is pointing out that organic materials are different and may have to be treated differently.

It has become clear that the term photorefractivity (loosely used) can encompass a wide variety of unrelated processes. This is perhaps most clear in the area of liquid crystal "photorefractive" materials. While many of the processes or contributions from these nonclassical effects can be used effectively, it is necessary to distinguish between these processes.

LPT has pioneered the development of sol-gel processed ormosil based photorefractive systems. The mechanical, electrical and optical properties of these materials are clearly different from other materials being studied and offer new opportunities to fine-tune the properties of photorefractive materials to meet device requirements.

It is clear that continued advancements in the development of these materials must occur with a clear knowledge of the intended application(s) since a single material will not satisfy all device requirements. Some applications require fast response times and virtually no storage times while others simply require long storage times with only reasonable writing times. The stark differences in performance are reflected in material composition and design

LPT will continue in the development of photorefractive materials in Phase III. Work accomplished in Phase II has given our research and development team an array of materials with which to continue. LPT will attempt to work with a Phase III collaborator(s) to develop these materials targeting practical requirements.

4. APPENDIX A

A. MATERIAL PREPARATION

Many chemicals used to prepare the composites were obtained commercially. Notable exceptions include the bifunctional chromophores, ormosils and $\chi^{(2)}$ chromophores: diethylaminonitrostyrene (DEANST), 6-propionyl-2-dimethylaminonaphthalene (PRODAN), N-(3-hydroxy-4-nitrophenyl)-(L)-prolinol (HNPP), and N-(4-nitrophenyl)-(L)-prolinol (NPP). The syntheses of these compounds were performed at LPT's laboratory and are described in the following pages. Silica glass, SiO_2, was formed by a proprietary catalytic hydrolysis of tetraethylorthosilicate to accommodate subsequent blending of the silica sol solution with the dopants sensitive to hydronium ions. The polymers used were: secondary standard polyvinylcarbazole (PVK), polycarbonate Lexan (PC) and polyacrylonitrile (PAN). A small amount of sensitizers (ie. a mixture of C_{60}/C_{70} fullerenes, thiapyrylium dye, boron diketonate, etc. - see molecular structures in Figure 11) was also used to prepare the composite materials. In another approach to composite preparation, different second order chromophore compounds NPP, HNPP and PRODAN, see Figure A1, were used instead of DEANST or were mixed with DEANST in 1:1 weight ratio in order to decrease the absorption at 633 nm.

The choice of the second order chromophores was based primarily on two factors: (1) processability (solubility) of the chromophore and (2) the value of its molecular first hyperpolarizability, β. In cases where the β value was not known, the magnitude of the induced dipole moment change, $\Delta\mu$, was a determining selection criterion; in the two-level model, it is directly proportional to β, as can be seen from the following relation:[20]

$$\beta(-2\omega;\omega,\omega) \cong \frac{3e^2}{2\hbar m} \frac{\omega_{eg} f \Delta\mu}{(\omega_{eg}^2-\omega^2)(\omega_{eg}^2-4\omega^2)} \qquad \textbf{(A1)}$$

where f is the oscillator's strength related to the transition moment between the ground and charge transfer excited state and ω_{eg} is the frequency of the optical transition. Other factors such as optical transparency in the visible and near IR regions were also considered. Table AI summarizes molecular parameters of the $\chi^{(2)}$ chromophores tested in this work.

It has been found that the preparation conditions of the composite materials play a critical role in achieving the desired optical quality of the final product. For example, small variations in the concentrations of the composite components can often result in nonuniformity of the films or even phase segregation; these are unacceptable features for films being considered for use as optical media. Additional problems have been faced in obtaining adequate concentrations of some of the sensitizers. Fullerenes are particularly troublesome due to their insolubility in common solvents; benzene and toluene are the best solvents although the fullerenes' solubility is still rather low. Fullerene concentrations of about 1 wt.% in the composite films could be achieved; greater concentrations were possible at the cost of the films' optical quality.

Table AI Molecular parameters of the second order chromophores used in the preparation of photorefractive composites.

$\chi^{(2)}$ chromophore	β (10^{30} esu)	β/M (10^{30} esu)	λ_{MAX} (nm)	μ (D)
NPP	76.2	0.34	393	6.0
DEANST	222	1.0	432	7.38
PRODAN	40	0.17	350	4.6
HNPP	73.0	0.31	411	6.0

A.1 Synthesis of 2nd Order NLO Chromophores

a. Synthesis of diethylamine nitrostyrene (DEANST).

Synthesis of the nonlinear optical organic chromophore, diethylamine nitrostyrene, was performed according to the procedure described by Kobayashi et al. wherein p-(N,N-diethylamino)benzaldehyde and nitromethane are reacted in the presence of ammonium acetate. The reaction mixture was stirred for 5 hrs at 100 ^{0}C and then cooled down to about -20 ^{0}C. This product was allowed to crystallize; the red crystals were filtered off and recrystallized several times from ethanol, dried and finally purified by sublimation under vacuum. The chemical structure of DEANST is depicted in Figure A1.

b. Synthesis of PRODAN (6-Propionyl-2-dimethylaminonaphthalene).

The synthesis begins by placing 19 ml hexamethylphosphoric triamide (HMPA) and 20 ml of dry benzene in a 3 neck 200 mL flask equipped with a gas inlet tube. Dimethyl amine gas (3.5 g) was dissolved in the solvent over approx. 2-3 hrs; subsequently, 500 mg of lithium metal ribbon was added and dissolved in this mixture to form a bright red colored lithiated amine solution. After total dissolution of lithium, 3.85 g of 6-propionyl-2-methoxy naphthalene (PROMEN) was added at once. The progress of the reaction was checked by thin film liquid chromatography (tlc). The reaction was complete in 15 hrs after which time the reaction mixture was poured in a crushed ice and water mixture and stirred. A yellow product formed and was extracted with methylene chloride (dried over anhydrous magnesium sulfate). Evaporation of the solvent and recrystallization from ethanol produces brownish flaky crystals of PRODAN. Using toluene as a recrystallizing solvent, white crystals were generated. The ^{1}H-NMR was matched with that obtained from commercial product purchased from Molecular Probes.

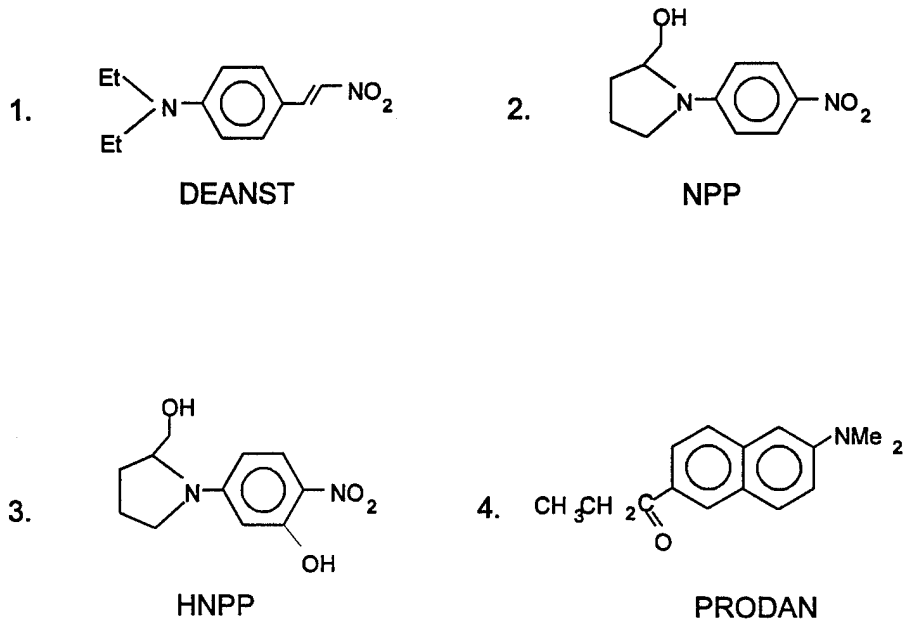

Figure A1 Chemical structures of second order NLO chromophores.

c. Synthesis of PENHCOM

The synthesis of methacrylate backbone copolymers containing charge transporting and second-order NLO side groups is a multistep effort yielding a high purity product. This lengthy synthetic scheme has been described in detail in a recent publication[56].

d. Synthesis of the ormosils

The molecular structures of the ormosils forming sol-gel processed composites are presented in Figure 10 (b). The ormosils were synthesized by reacting triethoxysilylpropylisocyanate separately with 4-(N,N-bis(β-dihydroxyethyl)amino)-4'-nitrostilbene (DHD) and N-(β-hydroxyethyl)carbazole (HCAR) under nitrogen at 100-120 ^{0}C for about 3 hours. Solutions were cooled to room temperature, diluted with dry butanol and stored under nitrogen at 4 ^{0}C.

A.2 Preparation of PVK Based Composite Materials and Film Fabrication

Two routes of preparation were explored. The first method (route 1) involved the use of inorganic/organic matrix components, i.e. SiO_2 and/or titania (TiO_2), organic polymer and a photosensitizer. In the second approach (route 2), sol-gel oxides were not used. This allowed the use of water sensitive (insoluble) organic polymers like PVK or polycarbonate.

The preparation of oxide/polymer/$\chi^{(2)}$ chromophore composite materials was conducted following the general descriptions below. However, due to the solubility differences of the organic materials and oxide precursors, some deviations from the general scheme were introduced to achieve *optimal* processing conditions (time, temperature, etc.) and prevent aggregation and/or precipitation of some composite components.

(route 1) The preparation of titania containing sol-gel composites was conducted as follows: 20 to 25 mg of $\chi^{(2)}$ chromophore was dissolved in 1 gram of 5 wt% PVK/DMF solution and mixed with freshly prepared titanium (IV) butoxide (1 mole) /2,4-pentadione (2 moles) complex abbreviated hereafter as TBAC. The films of this composite material were cast and dried at room temperature followed by an annealing process in a vacuum oven maintained between 60 ^{0}C to 80 ^{0}C. Films were prepared that were very uniform and optically clear with an average thickness of 5 μm per single coating. The addition of up to 30% PVP polymer to this composite permitted the preparation of films as thick as 200 μm in a single coat.

(route 2) This method of preparation resulted in composite materials without sol-gel oxides. This approach, as described below, was used for the preparation of thicker films which are more suitable for evaluation of photorefractive properties. It should be stressed that the photorefractive diffraction efficiency is strongly dependent on the sample thickness (quadratic dependence). Thus, in order to achieve an observable diffracted signal for yet unoptimized materials, the sample's thickness should be about 100 μm or (preferably) more. Therefore, in this approach, concentrated solutions of polymers (10 wt% to 25 wt%) in a mixture of volatile and relatively nonvolatile solvents were used. For example, secondary standard PVK polymer was dissolved in a toluene/cyclohexanone (4:1 volume ratio) mixture and filtered. Next, a second order NLO chromophore (usually 16 wt% to 20 wt%) and photosensitizer (approximately 0.2 wt%) were added to this solution yielding a composite. The presence of a high boiling point solvent helped to achieve smooth surfaces on the dried films. In some instances a plasticizing agent, namely dibutyl phthalate (DBP), was also incorporated in order to facilitate fabrication of sandwiched structures. This was accomplished by bonding two composite films deposited on ITO coated slides. Both films were preheated above the softening point, i.e., glass transition temperature of the composite, and combined by pressing the polymer films against one another. Care was taken to avoid the presence of air bubbles which may cause dielectric breakdown when high electric fields are applied.

The glass substrates used for film deposition were carefully cleaned in an ultrasonic bath, by immersion into a sequence of solutions: a base cleaning solution (KOH in isopropyl alcohol), deionized water, HCl in isopropyl alcohol (this step was skipped for substrates covered with ITO layers), deionized water and, finally, high grade isopropyl alcohol and blow drying with dry air.

a. Preparation of organic polymer/sol-gel oxide/chromophore/photosensitizer composite films.

The preparation of the oxide/polymer/DEANST composite was conducted as follows: hydrolysis of tetraethylorthosilicate (TEOS) was performed using a mild acid catalyst and a 2:1 molar ratio of water to TEOS. An equivalent volume of methanol (MeOH) was introduced into the mixture as a homogenizing agent (mutual solvent). The hydrolysis and condensation reactions were allowed to proceed for 1 day at room temperature. Concurrently, a 10% solution of poly-vinylcarbazole (PVK) polymer in dimethylformamide (DMF) was prepared and combined with the desired amount of hydrolyzed TEOS. Finally, an appropriate amount of DEANST was added to the solution. This composite could be prepared only with a very small concentrations of silica gel, i.e. less than 1% by weight, because of a phase separation that results in an inadequate optical quality composite.

b. Preparation of PVK/PVP/SiO_2-TiO_2/$\chi^{(2)}$ chromophore composite films

Attempts to incorporate PVK polymer into a polymer/silica/$\chi^{(2)}$chromophore composite were undertaken in order to introduce a structure capable of *transporting charge carriers*. PVK polymer is well known for forming charge transfer complexes with a variety of organic compounds, including the fullerenes. However, it is also known for its immiscibility (formation of incompatible blends) with other polymers, both organic and inorganic. For our purpose, small amounts of PVK should be sufficient to provide a transporting path for the charge carriers. The following procedure was used to prepare the composite solution. A small amount (60 mg) of 5 wt% PVK/Benzene solution was mixed with 1 g of cyclopentanone and 1 g of DMF. Next, 2 g of 10 wt% PVP in DMF was added and, finally, 60 mg of prehydrolyzed TMOS (mild organic catalyst, 2:1 molar ratio of H_2O to TMOS). The final composition of the blend was: 1.5 wt% PVK, 88.5 wt% PVP and 10 wt% SiO_2. It was found that the relative amounts of PVP and silica could be varied without sacrificing the films quality. However, films thicker than 4 μm would crack upon drying if the concentration of PVP was reduced below 70% of the composite's mass.

To increase the PVK concentration up to 4 wt%, N-methyl-2-pyrrolidone (NMP) was used as a principal polymer solvent. DEANST or NPP were added as 2nd order chromophores, and fullerenes, up to 2 wt%, as sensitizers. In this approach, 1 g of 25 wt% PVK in NMP was mixed with 15 mg of DEANST (or other $\chi^{(2)}$ chromophores), 1 g of DMF and 80 mg of prehydrolyzed TEOS. A solution of 1 wt% PVK in NMP (1 g) was added to the above mixture and stirred for several minutes. This solution was subsequently used for the film preparation. The films had to be dried quickly in the preheated oven (100°C) to avoid phase separation. If desired, a dilute solution of fullerenes in NMP (approx. 0.3 wt%) could be added without affecting the film's quality.

In another attempt to increase both the PVK concentration and the refractive index of the composite, titanium butoxide, $Ti(OBu)_4$ was cohydrolyzed with TEOS. In this procedure, in order to avoid uncontrollable hydrolysis of the metal alkoxide, $Ti(OBu)_4$ was first "deactivated" by reacting it with a chelating agent, 2,4-pentadione (acac). The prepared mixture of inorganic oxides contained about 10 wt% of TiO_2. This mixture was subsequently used in a preparation of oxide/polymer composites, as described above. The use of this approach allowed the PVK concentration to be increased more than twice, to about 10 wt% without detectable phase segregation.

The films were prepared as follows: after stirring for 15 min at room temperature, the mixture was used in the preparation of films on glass substrates (plain or ITO coated) using either a spin coating method (thin films) or doctor blading method (films of thickness greater than 1 μm). LPT employs a commercial spincoater (Headway) and a custom built "doctor blading" apparatus using a modified microtome. Among several different DEANST concentrations (between 10 wt% to 45 wt%) used in film preparations, we found that a 20 wt% concentration of the chromophore in sol-gel/polymer matrix and 20 wt% to 30 wt% in polymer-only matrix was close to the maximum amount which could be dispersed to form a homogeneous and stable composite material. Higher concentrations than 33 wt% in pure polymer (25 wt% in sol-gel oxide/polymer matrices) usually resulted in crystallization of the DEANST in a time which depends upon the amount of incorporated DEANST. Crystallization occurs within two to three days at the highest concentrations.

c. Preparation of PMMA/SiO_2/HNPP/Squarilium Dye (SQ) composite films.

In order to develop techniques to fabricate sol-gel based photoconductive and electrooptic materials of optical quality, we have incorporated second-order nonlinear NPP molecules (large β value) and a number of organic sensitizers, such as fullerenes and SQ. The SQ dye is of interest because of its very well defined and narrow absorption band centered at 640 nm, very close to the HeNe laser and diode laser wavelengths. Once the film structure has been formed, an external electric field is applied to induce a noncentrosymmetric alignment of large β molecules.

Due to the presence of the labile conjugated π-electron system in SQ (see Figure 4), the dye's molecular structure is not very stable in acidic or basic media, as evidenced by the color (absorption profile) changes. Several attempts to form sol-gel composites using PVP as the host polymer did not succeed, whereas those prepared with PMMA, being a neutral component, showed much improved results.

Several films were cast using a 5 wt% solution of PMMA in cyclopentanone together with prehydrolyzed solution of TMOS (60 wt% of the total mixture), SQ dye as a sensitizer, and a second order chromophore (NPP or HNPP). A slow drying process had a tendency to decompose the dye along with the precipitation of the second order chromophore material. The use of rapid heating at high temperatures decomposed the dye leaving clear films having the color of the second order chromophore material. When the films were carefully dried on room temperature teflon blocks placed in an preheated oven at 70-80^{0}C for 20 minutes just after casting, the two second order chromophore materials gave slightly different results. The phenolic substituted compound (HNPP) was much gentler on the dye molecule in comparison with NPP.

Figure A2 displays the absorption profile of the sample composite; one can clearly see a narrow absorption at 640 nm due to the presence of the dye. This important absorption feature remains after the composite film has been exposed to a DC corona poling field at temperatures of about 130 ^{0}C. However, the films poled at temperatures higher than 140 ^{0}C for a period of several hours do not show this characteristic absorption, which leads us to the conclusion that the dye molecules have either decomposed or otherwise lost some of their conjugated structure.

d. Preparation of PVK/2nd order chromophore/photosensitizer composite films.

As described above, PVK polymer was dissolved in a toluene/cyclohexanone (4:1 volume ratio) solvent mixture. DEANST and NPP molecules were used as the 2nd order NLO chromophores and thiapyrylium or borondiketonate dyes as photosensitizers to yield the following material composition: PVK 71 wt%, DEANST 29 wt%; the concentration of the photosensitizer was less than 0.1 wt%.

The solution, filtered through 0.45 μm pore size disc filters prior to use, was cast on ITO coated slides. Approximately 1.5 to 2 ml of the solution was needed to cover 1" by 3" rectangular slide. Freshly cast films were placed on teflon blocks, covered with a crystallization dish and left for 12 hours at room temperature. The films were then transferred to a preheated

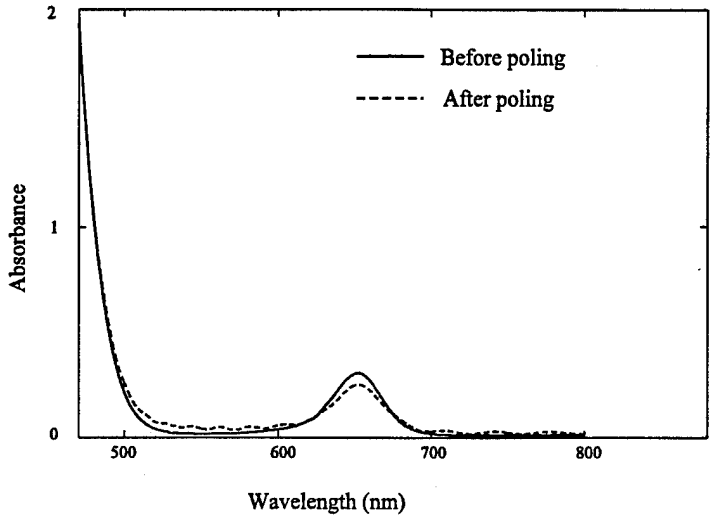

Figure A.2 Absorption profiles of SiO_2/polymer/HNPP/SQ dye composite film: a. before (solid line), and b. after electric field poling (dashed line).

(60 to 80^{0}C) vacuum oven and further dried for 4 to 6 hrs at 10^{-1} to 10^{-2} Torr vacuum. This procedure resulted in films having thicknesses ranging from 50 to 175 μm depending upon the amount of solution used in the preparation. The films dried in such a manner were subsequently used to form sandwiched structures.

A.3. Preparation of Polycarbonate/2nd order NLO Chromophore/Photosensitizer/Charge Transporting Agent Composite Films

Bisphenyl-A-polycarbonate (PC), TTA, and the chromophores (either NPP or PRODAN) were dissolved in dichloromethane at desired concentrations and stirred. A charge generation sensitizer, C_{60}, was dissolved in toluene. The C_{60} solution and a solution containing PC, TTA and chromophore were mixed and heated to 100 °C to facilitate solvent evaporation. The resulting solid materials were then sandwiched between indium-tin-oxide (ITO) covered glass substrates at elevated temperatures where the materials soften. The final composites contained 50 wt. % of polycarbonate, 30 wt. % of TTA, 20 wt. % of chromophores and 0.25 wt. % of C_{60}.

A.4 Preparation of PBMA/Bi-Functional Chromophore Photorefractive Composites

The electrooptic coefficient and photoconductivity measurements were performed on thin, between 2 and 10 μm, films. C_{60} was dissolved in toluene at a concentration of 0.1 wt. % followed by the addition of DPANST (or DPANS) and PBMA at desired concentrations. The final solutions were spin coated on indium-tin-oxide (ITO) covered glass substrates. All samples reported in this paper have a C_{60} concentration of (0.25 ± 0.02) wt. %. All films were dried under vacuum for 24 hrs at 55 °C to remove residual solvents. A set of gold electrodes was then deposited on top of the composite film by vacuum evaporation. The film thicknesses were measured using a profilometer.

For photorefractive four-wave mixing and two-beam coupling experiments, samples with

thickness around 125 μm were prepared as follows. First, all ingredients were dissolved in toluene at the desired concentrations. The solutions were then heated for solvent evaporation. The resulting solids were sandwiched between ITO covered glass substrates at elevated temperatures at which the composites soften. Sample thickness was controlled to be around 125 μm with the use of Teflon® spacers and measured using a profilometer. Because of the low glass transition temperature of the composites, the chromophores can be easily aligned at room temperature by the application of an electric field. Since a strong dc field is already required for the charge generation process, no poling was performed prior to measurements. For simplicity, we denote the composites containing DPANST and DPANS as BF-1 and BF-2, respectively.

A.5 Preparation of PENHCOM Based Photorefractive Composites

Samples used for EO and photoconductivity measurements were prepared by spin coating from solutions onto indium-tin-oxide (ITO) covered glass substrates. All films were dried at 100°C for at least 24 hours to facilitate solvent evaporation. A thin layer of gold electrode was then deposited on the top of the polymer film by vacuum evaporation.

The photorefractive properties of the polymer were studied on thick films prepared as follows: C_{60} and PENHCOM were dissolved in toluene at concentrations of 0.05 and 15 wt. %, respectively; the solutions were mixed in a proportion to yield solid samples containing 0.2 wt. % of C_{60} and 99.8 wt. % of PENHCOM. The solution mixture was then heated to 100 °C until the solvent evaporated. The resulting solid was sandwiched between ITO covered glass substrates at an elevated temperature at which the polymer softens. The sample thickness was controlled to be around 100 μm with the help of Teflon® spacers. Samples prepared in this manner are of excellent optical quality and transparent for wavelengths above 600 nm.

A.6 Preparation of Ormosil Based Photorefractive Materials

Butanol solutions of the ormosils were mixed in a 3:1 (HCAR:DHD) molar ratio and hydrolyzed (50 °C bath, 30 min.) using water (3:1 H_2O:Si molar ratio) and formic acid as a catalyst. Solutions of TNF or thiapyrylium dye were added to hydrolyzed ormosils at room temperature. Films 2-3 μm thick were deposited on indium-tin-oxide (ITO) coated glass substrates by spin coating filtered ormosil solutions (0.2 μm pore size Teflon membrane). Thicker films (80-150 μm thick) were prepared by casting approximately 0.7 mL of filtered ormosil solution on a microscope slide having a 1 cm wide strip ITO electrode. The films were dried at room temperature for 3 days and, then, in a vacuum oven at 80 °C for 24 hours. A thin semitransparent gold electrode was deposited on the top of thick films and used for four wave and two wave mixing experiments. A set of thicker, circular silver electrodes was deposited on the thin films and used for the measurements of photoconductive and electrooptic properties.